Technical University of Łódź

Interdisciplinary Doctoral School

Doctoral Dissertation

Numerical modeling and sensitivity of aerodynamic characteristics to shape and material properties of paraglider

Paulina Maślanka

Supervisor: prof. dr hab. inż. Ryszard Korycki

Łódź, 2023

AUTHOR'S DECLARATION

I hereby declare that this dissertation entitled "Numerical modeling and sensitivity of aerodynamic characteristics to shape and material properties of paraglider" was written by me during the realization of my doctoral study at the Interdisciplinary Doctoral School of Lodz University of Technology from the period of 2019 to 2023 under the supervision of prof. dr hab. inż. Ryszard Korycki. The dissertation was developed from my own research work and has not previously been submitted in any application for a higher degree. All citations and data sources are fully acknowledged through references.

Paulina Maślanka		
Name of the doctoral candidate	Signature	Date

ABSTRACT

Paragliders are devices intended for gliding; typically, their wings are of an elliptical outline (in the orthogonal projection). They are made of upper and lower panels, and ribs, which are woven fabric materials connected by seams. Therefore, the wings do not have any rigid elements applied. The other basic elements of the paraglider are: lines, risers, harness.

The topic regarding development of the paragliders is an interesting field from the point of view of science, i.e. materials engineering, aerodynamics and flight mechanics. The dissertation is focused on numerical modeling and sensitivity of aerodynamic characteristics to shape and material properties of a paraglider.

The laboratory tests were performed on 10 different woven fabrics in the sense of material composition, as well as general, structural and mechanical characteristics.

The analyze of paraglider/parachute fabrics shows that they are characterized by good relation of strength to the surface mass and low air permeability. All the considered samples are PA 6.6 fabrics coated with polyurethane resins or silicone/polyurethane. Based on the SEM records, the paraglider/ parachute fabrics are manufactured using multifilament yarns and are characterized by rip-stop weave. The functional groups characteristic for the analyzed samples were indicated by the Fourier Transform Infrared Spectroscopy.

Three of the analyzed fabrics were selected to be subjected to the UV, thermal and mechanical ageing.

The greatest influence on mechanical properties has ageing caused by the UV radiation. No significant influence of freezing on the mechanical properties of the considered samples is observed. The flexing damage has the greatest influence on the air permeability change among all considered aging factors.
The obtained laboratory results could be introduced to the further steps of the research.

In the next steps a multistage algorithm was introduced; it concerned the numerical analysis in the terms of CFD (Computational Fluid Dynamics) and FEM (Finite Element Method) Structural calculations performed on a model of a traditional recreational paraglider wing in the sequence: (1) study of the initial influence of air permeability on aerodynamic characteristics with applying of the *porous media* tool; (2) recalculating of the flow over paraglider after applying the more accurate permeability results, i.e. with the consideration of the actual pressure drop acting on the material during the flight;

(3) study of the stress, strain and deformation in the materials covering paraglider; (4) determining the impact of deformation on the aerodynamic characteristics of paraglider.

Based on the obtained CFD results it can be concluded that air permeability increase has an impact on the paraglider's aerodynamic characteristics decrease. The best characteristics presented paraglider covered with an air-impermeable material.

The pressure distribution acting on the paraglider covering materials was obtained based on the CFD calculations and the value of the assumed load factor. Deformation and strain in the considered materials decrease with increasing of tensile strength of a material and/or decreasing of pressure acting on a material.

Safety factors of the considered materials not subjected to degradation range between around 4 – 6. However, the structural calculations show that the values of the factor can significantly decrease, when materials subjected to ageing are analyzed.

The CFD re-calculations shows, that the deformation caused by pressure acting on a material has a significant influence on the decrease on the aerodynamic characteristics of a paraglider.

The multistage optimization allowed to determine the influence of material properties on the aerodynamic characteristics of paraglider and can be a useful tool to select the covering materials advantageous to the considered constructions and assumptions.

The next section of the dissertation is focused on introducing a single cover paraglider model. Model of the paraglider wing covered only with the upper brits has a significant importance from the view of packing volume and mass of the final product. The aerodynamic characteristics and material behavior on the proposed geometry are advantageous.

The last part describes initial calculations estimating the safety factors of seams and lines, as well as the heat transfer through the harness. The topics are introduced as fields for the future development.

Each element of the paragliding system is characterized by different behaviors, which require separate physical and mathematical descriptions. Assembling all the parts creates a complex model, which has completely different characteristics than those resulting from partial models. The construction, description and solution of this model is a very complex problem, far beyond the scope of doctoral dissertation.

MODELOWANIE NUMERYCZNE ORAZ WRAŻLIWOŚĆ CHARAKTERYSTYK AERODYNAMICZNYCH NA KSZTAŁT I WŁAŚCIWOŚCI MATERIAŁOWE PARALOTNI

STRESZCZENIE

Paralotnie to urządzenia przeznaczone do szybowania; ich skrzydła mają obrys eliptyczny w rzucie prostopadłym. Skrzydła składają się z górnych i dolnych brytów oraz żeber, które są materiałami tkanymi połączonymi szwami. W związku z tym paralotnie definiowane są jako obiekty latające bez elementów usztywniających. Pozostałe podstawowe elementy paralotni to: linki, taśmy nośne oraz uprząż.

Rozwój paralotni jest interesujący z punktu widzenia nauki, tj. inżynierii materiałowej, aerodynamiki i mechaniki lotu. Tematem rozprawy doktorskiej jest modelowanie numeryczne oraz wrażliwość charakterystyk aerodynamicznych na kształt i właściwości materiałowe paralotni.

Badania laboratoryjne przeprowadzono na 10 różnych tkaninach paralotniowych pod względem składu materiałowego oraz właściwości ogólnych, strukturalnych i mechanicznych.

Z analizy tkanin paralotniowych/spadochronowych wynika, że charakteryzują się one dobrym stosunkiem wytrzymałości do masy powierzchniowej oraz niską przepuszczalnością powietrza. Wszystkie rozpatrywane próbki to tkaniny PA 6.6 powlekane żywicami poliuretanowymi lub silikonem/poliuretanem. Na podstawie zapisów SEM można stwierdzić, że tkaniny są wykonane z przędz multifilamentowych i charakteryzują się splotem typu rip-stop. Grupy funkcyjne charakterystyczne dla analizowanych próbek zostały wskazane za pomocą spektroskopii w podczerwieni z transformacją Fouriera.

Spośród analizowanych tkanin wybrano trzy, które poddano starzeniu UV, termicznemu i mechanicznemu (wielokrotne zginanie).

Największy wpływ na właściwości mechaniczne ma starzenie spowodowane promieniowaniem UV. Nie obserwuje się istotnego wpływu mrożenia na właściwości mechaniczne badanych próbek. Wielokrotne zginanie ma największy wpływ na zmianę przepuszczalności powietrza spośród wszystkich rozpatrywanych czynników starzeniowych.

Uzyskane wyniki laboratoryjne zostały wykorzystane w dalszych etapach badań.

W kolejnych krokach wprowadzony został algorytm wielostopniowy; dotyczył on analizy numerycznej w ujęciu CFD (Computational Fluid Dynamics) i obliczeń strukturalnych MES (Metoda Elementów Skończonych) wykonanych na modelu tradycyjnego skrzydła paralotni rekreacyjnej w kolejności: (1) badanie wstępnego wpływu przepuszczalności powietrza

na charakterystyki aerodynamiczne z zastosowaniem narzędzia porous media; (2) ponowne obliczenie opływu paralotni po zastosowaniu dokładniejszych wyników przepuszczalności, tj. z uwzględnieniem rzeczywistego spadku ciśnienia działającego na materiał podczas lotu; (3) badanie naprężeń i odkształceń w materiałach pokrycia paralotni; (4) określenie wpływu odkształcenia na właściwości aerodynamiczne paralotni.

Na podstawie uzyskanych wyników CFD można stwierdzić, że wzrost przepuszczalności powietrza ma wpływ na pogorszenie właściwości aerodynamicznych paralotni. Najlepsze właściwości prezentowała paralotnia pokryta materiałem nieprzepuszczającym powietrza.

Rozkład ciśnienia działającego na materiały poszycia paralotni uzyskano na podstawie obliczeń CFD oraz wartości przyjętego współczynnika obciążenia. W rozpatrywanych materiałach odkształcenie maleje wraz ze wzrostem wytrzymałości materiału na rozciąganie i/lub spadkiem ciśnienia działającego na materiał.

Współczynniki bezpieczeństwa rozpatrywanych materiałów nie ulegających degradacji wahają się w granicach 4 – 6. Jednak obliczenia strukturalne pokazują, że wartości tego współczynnika mogą znacznie się zmniejszyć, gdy analizuje się materiały poddane starzeniu.

Z obliczeń CFD wynika, że odkształcenie spowodowane ciśnieniem działającym na materiał ma istotny wpływ na pogorszenie właściwości aerodynamicznych paralotni.

Wielostopniowa optymalizacja pozwoliła określić wpływ właściwości materiału na charakterystyki aerodynamiczne paralotni i dzięki temu może być użytecznym narzędziem do doboru materiałów pokryciowych korzystnych dla rozważanych konstrukcji i założeń.

Kolejny rozdział rozprawy koncentruje się na przedstawieniu modelu paralotni jednopowłokowej. Model skrzydła paralotni pokrytego jedynie górnymi brytami ma istotne znaczenie z punktu widzenia pakowności i masy finalnego produktu. Właściwości aerodynamiczne i zachowanie materiału dla proponowanej geometrii są korzystne.

W ostatniej części opisano wstępne obliczenia szacujące zachowanie się i współczynniki bezpieczeństwa szwów i linek, jak również transport ciepła przez uprząż. Te tematy zostały wprowadzane jako elementy do rozważań w przyszłej pracy naukowej.

Każdy element globalnego układu paralotni charakteryzuje się odmiennymi zachowaniami, które wymagają osobnego opisu fizycznego i matematycznego. Złożenie wszystkich części tworzy globalny model, który ma zupełnie inne cechy niż te, które wynikają bezpośrednio z modeli cząstkowych. Budowa, opis i rozwiązanie całkowitego modelu jest bardzo złożonym problemem, daleko wykraczającym poza zakres rozprawy doktorskiej.

List of mathematical and physical symbols

λ	-	Aspect ratio of the wing [-];
l	-	Wingspan [m];
S	-	Wing surface [m^2];
V	-	Volume of an area bounded by a closed surface A [m^3];
ρ	-	Fluid density [kg/m^3];
$\vec{v}$	-	Velocity vector [m/s];
$\vec{p}$	-	Surface stress vector [Pa];
$\vec{F}_m$	-	Vector of body forces [N/m^2];
c_v	-	Specific heat [$\frac{J}{kg \cdot K}$];
T	-	Temperature [K];
$\dot{q}_n dA$	-	Heat flux density related to specified surface [$\frac{J}{m^2 \cdot s}$];
$\dot{q}_m \rho dV$	-	Heat flux density related to specified volume [$\frac{J}{m^3 \cdot s}$].
n	-	Iteration (subsequent) [-]
F_{ext}	-	Applied force [N]
F_{int}	-	Computed internal force [N]
F_{res}	-	Residual force [N]
Δu	-	Displacement increment [m]
K	-	Stiffness matrix [Pa]
F	-	Aerodynamic force [N]
c	-	Dimensionless aerodynamic coefficient, the value of which depends on the geometry, its position to the air streams and velocity [-]
L	-	Lift force [N]
c_L	-	Lift coefficient [-]
D	-	Drag force [N]
c_D	-	Drag coefficient [-]
A	-	Angle of attack [^{o}]
C_0	-	Dimension of the middle chord [m];
C_j	-	Dimension of a chord of subsequent rib [m];
y_j	-	Distance of a subsequent rib from the symmetry plane [m];
R	-	Wing deflection radius [m];

$1/\beta$	-	Porous resistance [l/m^2];
Δp	-	Pressure drop [Pa];
t_m	-	Thickness of the material (overestimated in relation to the actual one, in order to be able to use the *Porous Media* tool, t_m=2mm);
μ	-	Dynamic viscosity of air [17.89·10^{-6} Pa·s]
v_m	-	Flow velocity through the material [m/s]
dE^*_{ab}	-	Difference between two colors in L*a*b* color space [-];
Δa	-	Deviation from the color of the reference sample in the axis of red – green [-];
Δb	-	Deviation from the color of the reference sample in the axis of yellow – blue [-];
ΔB	-	Deviation in brightness parameter from the color of the reference sample [-];
E	-	Young's modulus [Pa];
Σ	-	Uniaxial stress [Pa];
E	-	Proportional deformation [-];
Φf	-	Face value [-];
$\Phi f_1 CD$	-	Face value (central-differencing scheme) [-];
$\Phi f_1 SOU$	-	Face value (second-order upwind scheme) [-]
l_f	-	Load factor [-]
Q	-	Weight [N/kg]
m	-	Mass [kg]
g	-	Gravitational acceleration [9.81 m/s^2]
η	-	Mitigation coefficient [-]
W	-	Updraft velocity [m/s]
$f_{sew1,\,2}$	-	forces on the seams (per unit length) [N/m]
$l_{sew1,\,2}$	-	lengths of the corresponding seams/joints [m]
N_{av}	-	average load acting on the single line [N]

Table of contents

1. Research aim

The aim of the research was to develop a numerical model and perform analysis of the influence of material characteristics on selected aerodynamic characteristics.

2. Research postulate

Numerical modeling is an effective and versatile tool for obtaining the distribution of state variables resulting from the sensitivity analysis of selected aerodynamic characteristics due to the shape and material properties of the paraglider.

3. Introduction

Paragliding is a relatively recently developed form of recreation and sports; in its present form it was created in the 1970s and immediately gained many supporters. Therefore, the structures were constantly improved - both in terms of safety and efficiency in flight.

A paraglider is defined as a device intended for gliding, with a wing with no rigid elements applied (the exception are synthetic lines and PVC foil stiffening on the leading edge). The basic elements of the paraglider are: wing, lines, risers, harness.

From a scientific point of view, this field is an interesting topic both in terms of materials engineering, as well as aerodynamics and flight mechanics. This gives great opportunities for optimizing and improving the paraglider's technological parameters.

However, the existing paraglider structures are manufactured in the specialized factories and have repeatable structural shape and covering materials. Some new trends are implemented in limited range. Thus, innovative solutions should be introduced to improve the aerodynamic characteristics and covering material properties of paraglider wing, based on numerical modeling, material science and flight mechanics.

The dissertation is focused on numerical modeling and sensitivity of aerodynamic characteristics to shape and material properties of a paraglider. The problem is complex and interdisciplinary; thus, only the wing, which is the most important part of the whole paraglider, was analyzed carefully. The remaining, i.e. seams, lines and harness were studied in the sense of introducing topics for the future development.

Typically, the wing of a paraglider has an elliptical outline (in the orthogonal projection). It is made of upper and lower panels, and internal partitions of the shape of airfoils, i.e. ribs. Both, the panels and ribs are woven fabric materials connected by seams. The spaces between adjacent ribs are called cells. The upper and lower covers do not connect completely on the leading edge, so it is possible to draw air into the cells by entering vents and create

overpressure in the wing. The air spreads evenly between the cells as holes are made in the ribs.

The lines are attached to the wing on its lower surface in three/four rows. The lines are connecting into the risers. Such construction is connected with the harness worn by the pilot below the wing.

The following factors have an impact on the aerodynamic characteristics of the wing: (1) shape, i.e. outline and airfoil; (2) air permeability of the covering woven structures; (3) deformation of the material in flight; (4) pressure distribution; (5) air streamlines; (6) mass of the system.

Moreover, a safety factor in accordance to strength of materials and overloads created during the flight is also very important issue. Regardless of no relation of this factor to the aerodynamic characteristics of a paraglider wing, it should be studied.

Neglecting some elements of the system under consideration is a simplification often used during applying the numerical modeling methods. Thus, in the below described numerical calculations regarding the flow over paraglider wing and structural considerations, the following were neglected: lines, risers and pilot wearing a harness. No research focused on the global paraglider system was found; each element of the system is characterized by different behaviors, which require separate physical and mathematical descriptions. Thus, the global analysis was assessed to be too extensive for the doctoral dissertation.

The remaining elements cause creating additional drag force. Thus, the actual c_l/c_d ratio in flight is, in fact, lower than the one obtained in the numerical calculation. However, the obtained values of lift force give an overview of possibility of the wing to lift the system of known mass. Generally, paragliders are designed with assumptions of the sizes of wings in accordance with the mass of the pilot and type of paraglider. Thus, the bigger wing is dedicated to the pilots of higher mass or heavier system (e.g. with a motor drive).

The below analysis were based on a geometry of recreational wing for a pilot of a weight of 70 kg (size S) and was focused on a multistage optimization of an algorithm allowing to determine the influence of material properties on the aerodynamic characteristics of paraglider, as well as the most advantageous selection of the covering materials to the considered constructions.

In the first part of the optimization process, the laboratory tests were performed on 10 different woven fabrics in order to: (1) obtain the general properties of the woven

fabrics, i.e. mass, thickness, strength; (2) analyze the characteristics and type of correlations impacting on the present functional groups with the use of Fourier Transform Infrared Spectroscopy (FTIR); (3) identify structural characteristics of the woven structures under consideration with the use of Scanning Electron Microscope (SEM); (4) describe the influence of UV, thermal and mechanical ageing on the air permeability with different pressure drops applied and mechanical properties.

In the next steps the numerical calculations were applied. The initial influence of air permeability on aerodynamic characteristics was studied. It was based on the Computational Fluid Dynamics (CFD) with the application of the finite volume method. In order to apply air permeability influence, a *porous media* tool was applied on the walls covering paraglider wing. When a *porous media* tool is applied, porous resistance parameter is assigned to materials, that present air permeability greater than zero.

However, after obtaining the initial results it was noticed that maximal pressure acting on a paraglider material in the normal flight conditions is around 200 Pa; whereas the calculations referred to air permeability tested with the pressure drop equal to 2000 Pa.

The pressure drop applied in laboratory testing should not have a large impact on the porous resistance parameter. However, it was decided to perform the CFD calculations based on air permeability property tested with pressure drop of 200 Pa to obtain the results of porosity influence on aerodynamic characteristics of a paraglider wing the most accurate.

Next, the structural numerical calculations, using the finite elements method (FEM) were performed. The following were applied to the analysis: (1) pressure distributions obtained in the CFD numerical calculations multiplied by a maximal overload that can be reached; (2) mechanical properties of the analyzed samples evaluated in the laboratory testing. Thus, this step was focused on the influence of the air permeability and mechanical properties of materials on the structural behavior of a paraglider wing.

The deformations of wing were determined using the ANSYS Structural program. The geometry was introduced in order to analyze the influence of both – air permeability and mechanical properties of the studied materials – on aerodynamic characteristics of the paraglider wing.

The above described methodology was developed in order to possibly support the paragliders manufacturers in the selection of materials that would be the most advantageous for the new models of wings referring to the studied geometry. However, the proposed algorithm can be transformed into an automatized and simple optimization tool.

The next step of the research part was the study of a single cover paraglider. Applying such a structure has a significant importance from the view of packing volume and mass of the final product. Therefore, expected surfaces, masses and volumes of the covering fabrics of a traditional paraglider and the new type of a paraglider were calculated. Moreover, the CFD and FEM numerical calculations were applied for this type of paraglider wing.

In the last section of the research part, fields for the future development were shown and thus, initial calculations were performed and described.

The seams are the basic connecting elements of paraglider wing. Thus, the correct estimation of seams is necessary to create the safe structure during the flight. The seam rupture is a complex issue to be considered. It has a perpendicular direction to an actual force acting on it caused by pressure distribution acting on a paraglider wing and its materials. An accurate method was chosen in order to calculate the value of force transmitted through the seams connecting paraglider materials and thus, a safety index was designated. Moreover, influence of seams type and configuration on the air permeability was determined.

The paraglider lines are the most important control element of the global structure i.e. the basic tool of the paraglider pilot. It is evident, that their arrangement as the connecting and control element should be briefly analyzed. Estimation of the force acting on a single paraglider line in the attachment point was performed, which allowed to calculate the safety factors.

In the last part of the section regarding field for future development, the heat transport through the harness was numerically calculated by implementing the program in the MATLAB environment. The calculations were simplified and regarded only two layers of harness, i.e. a polyurethane foam and polyester woven fabric.

Summarizing, the innovative solutions were developed and introduced to improve and optimize the aerodynamic characteristics and covering material properties of paraglider wing, based on numerical modeling, material science and flight mechanics. Consequently, the parameters determining the aerodynamic characteristics of paraglider wing were introduced and analyzed in respect of the flight dynamics. Additionally, the remaining parts of the paraglider system were discussed as fields for the future development.

4. General construction of paraglider

Paraglider is defined as a gliding wing made of woven fabrics without stiffening rods.

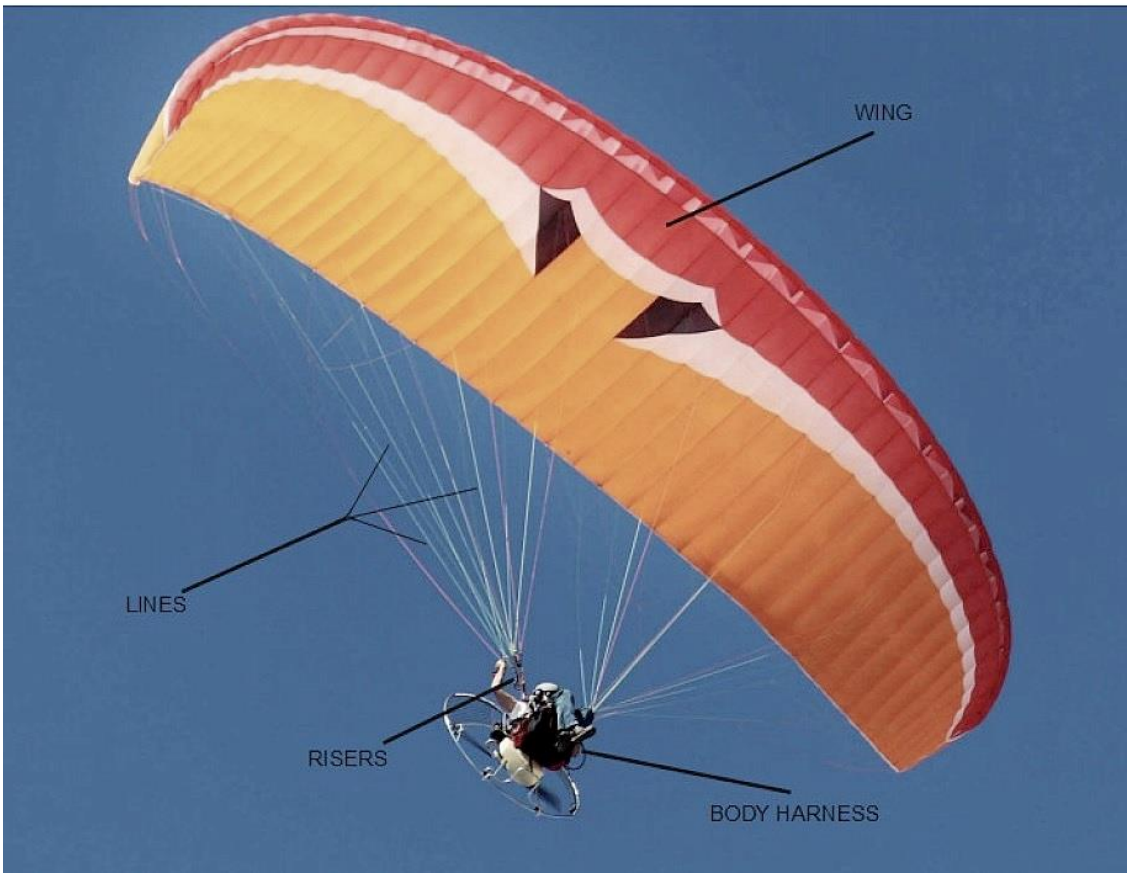

a

b

Figure 1. Paragliding system: a – including all elements (based on [2]); b – body harness (based on [3])

The aerodynamic shape is possible to be maintained due to advantageous pressure distribution; the air entering vents on the leading edge creates overpressure inside the wing [1].

The following main parts create the paragliding system, Figure 1.: wing, lines, risers, body harness.

5. Literature review – state of the art

5.1.Modeling of paragliding system

The proper structural design depends on the intended application of the paraglider. The most common type are free-flying and powered wings. The expanding market and the increase in user expectations require new applications (size, airfoil type, shape of the whole construction and other design solutions).

After determining the assumptions, in the next step, a shape meeting them is designed. Computer programs such as CAD type allow to accurately create a 3D model.

The creation of the solid design is carried in accordance to the following scheme [1]: (1) Design of the airfoil; (2) Applying holes to the ribs, causing the inside air to distribute evenly; (3) Duplication of airfoils; (4) Reducing the size of the airfoils towards the wing side edge; (5) Design of the deflection of the wing – radius size; (6) rotation of the profiles so that they line up properly with the deflection; (7) Selection of support points (attachment points of lines to the wing); (8) Applying supports different than the ribs (e.g. type V); (9) Design of the top and bottom covers (brits); (10) Arrangement of lines connecting the wing with the risers.

The above description is a simplified one. There are many factors, that influence the performance of paraglider and safety in flight, that a designer should be aware of.

The use of a great number of ribs (of an airfoil shape) stiffens the wing, by improving its shape and therefore - performance; however, it reduces the safety in flight. This is due to the extended time of pressure the overpressure equalization in the wing. Manufacturers found a solution that minimizes this problem - the so-called V-supports, Figure 2. They significantly stiffen the wing, only slightly disturbing the process of pressure equalization inside.

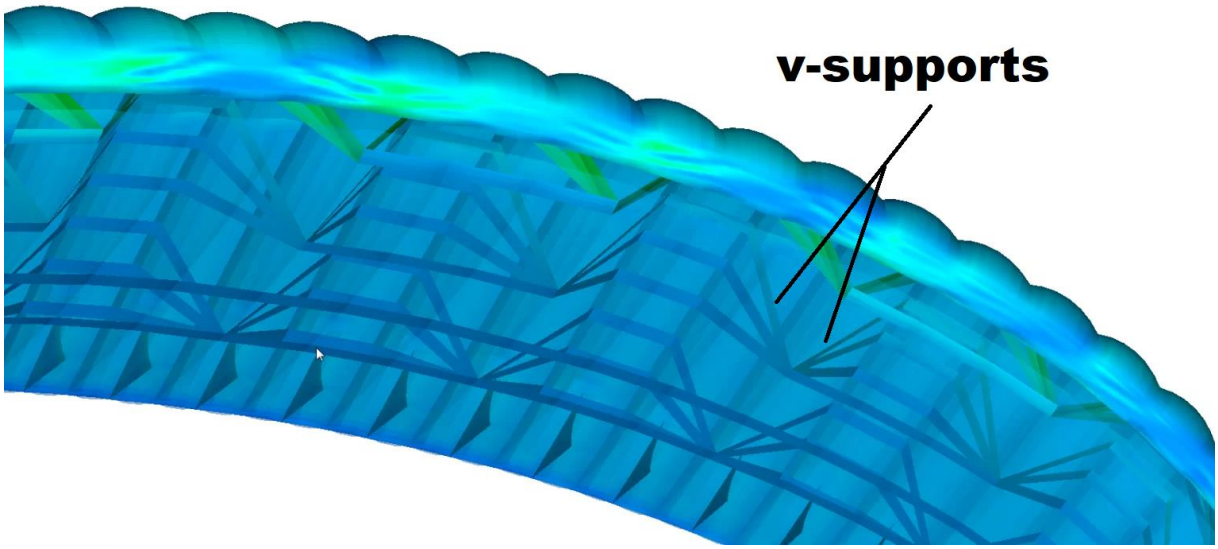

Figure 2. Use and arrangement of the v-supports (based on [4])

Aspect ratio is one of the most important dimensions of the wing, which determines the performance and expected purpose of the paraglider; it is determined by the ratio of the squared span to the area of the wing, according to the formula [5]:

$$\lambda = \frac{l^2}{S} \tag{1}$$

The higher the parameter λ, the better the performance of the paraglider. It is assumed that paragliders with an aspect ratio of about 6 and more are classified as those intended for sports. However, the aspect ratio should not be greatly increased. This is due to the fact that paragliders by definition do not have any stiffeners. Therefore, when the aspect ratio exceeds the limit, the paragliders inflate worse, deform more easily where turbulences in flight occur and are very dangerous.

The lines are a very advanced element of the paraglider. They carry loads, help to maintain the shape of the paraglider and stabilize the flight. However, minimizing their number and diameters allows better aerodynamic performance (reduction of the drag force). Therefore, the following elements are subjected to the optimization procedures[1, 6]: (1) branches (lines attached to the wing, connect to the main lines, then to the risers); (2) adjusting the diameter of the lines depending on the value of the loads they carry.

A row of brake lines is connected to trailing edge. They connect into main lines on the left and right side of the wing, then are attached to the risers.

Supporting lines are attached to the bottom of the wing in rows, Figure 3: A - the closest to the leading edge; B or B and C - between the leading and trailing edges; C or D - the nearest to the trailing edge.

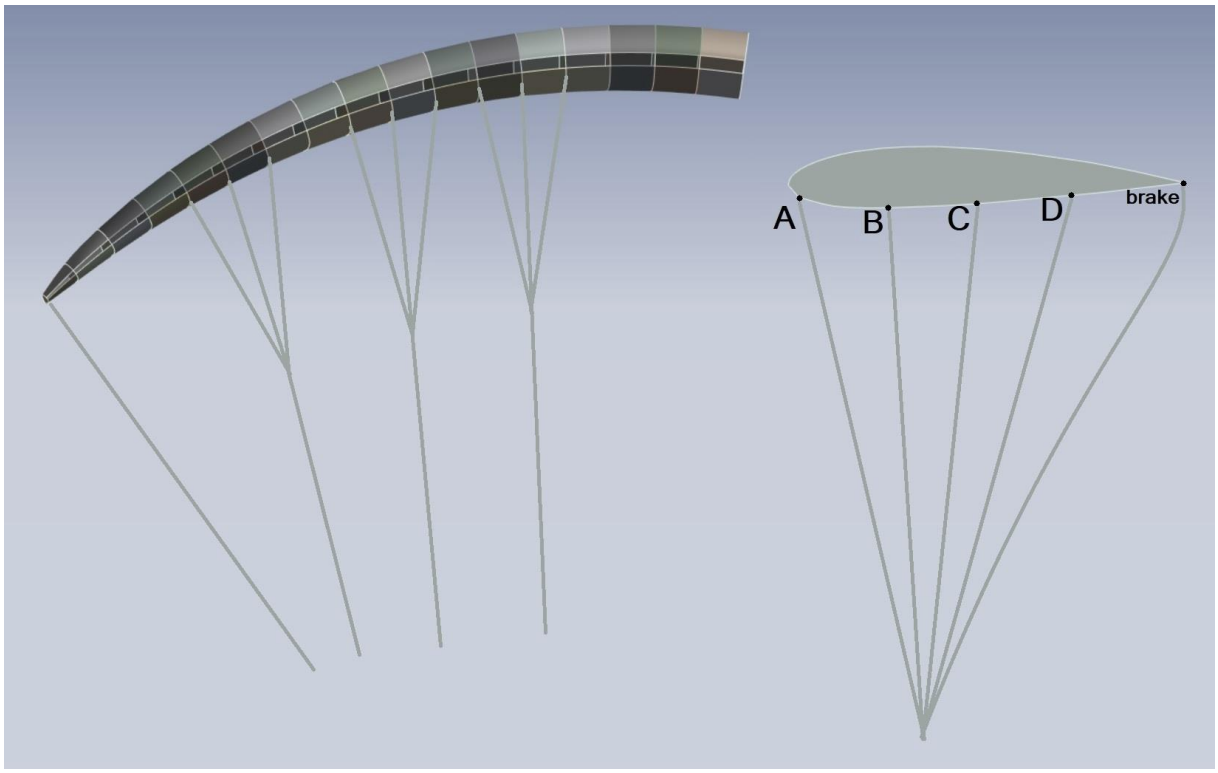

Figure 3. Lines general arrangement

Lines attached to the wing, connect to the main lines, then to the risers. The risers are connected to the harness which is worn by the pilot. Both, pilot and harness, influence the increasement of the drag force. Thus, some of the harnesses models have an aerodynamic shape.

In the next step, a physical prototype can be produced or a computational mesh can be created and then examined in another program in terms of aerodynamic/structural analysis.

Most of the available numerical researches do not include the influence of lines or harness to the aerodynamic characteristics in order to simplify cases and reduce the time of calculations. However, by knowing the basic principles of aerodynamics, some behaviors in flight can be predicted. There is also a possibility to study the influence of e.g. pilot wearing a harness using wind tunnels. Thus, according to [7], drag force created due to pilot wearing a cocoon type harness is around 40 N.

5.2.Numerical modeling

The characteristics obtained by numerical calculations are of great importance for the preparation of highly efficient prototypes and device optimization. They allow omitting many stages of traditional design (laboratory testing of successive prototypes with modified geometry, change of materials etc.), which significantly saves time and costs [8].

Numerical methods rely on the use of finite numbers in a finite sequence of operations. The following methods can be distinguished [8]: (1) finite volume method, (2) finite difference method, (3) finite elements method.

Commercial software available on the market have an extensive working environment of various calculation possibilities, as well as the preparation of geometry, computational mesh and postprocessing of the calculations results. However, a problem should be carefully analyzed by the user who has to perform many tasks and make a number of decisions. Thus, in most of the available software, three basic stages of work are distinguished to be conducted by users [8, 9, 10]: (1) pre-processing (preparation for calculations, including creating geometry, creating computational mesh etc.); (2) solving (solution of a problem); (3) post-processing (validation of results, visualization and complementary numerical postprocessing).

As mentioned above, the pre-processing stage includes creating of geometry and preparation of computational mesh.

The geometry creation consists in introducing the tested model into a virtual computing area. This can be done by import (e.g. from commonly used CAD software). However, it should be analyzed whether it is possible to cleanse the geometry by removing elements from the object that would affect the stability of calculations [8, 11].

The accuracy of the solution is mainly affected by the density of the computational mesh - the density of mesh elements is particularly important in places with large parameter gradients. Therefore, as far as possible to predict these places, it is recommended to adjust the size of the mesh elements at the design stage.

However, the more elements, the larger the size of the matrix, and thus the longer the solution time. In extreme cases, this can significantly slow down calculations or even make them impossible. Therefore, in practice, different mesh densities are most often used. In places that are critical due to flow, geometry or physical conditions, the mesh is densed. In places where rapid changes in state parameters are not expected, the mesh may be sparser and the elements themselves larger [8, 12].

The dissertation uses two types of numerical calculations: the Computational Fluid Dynamics based on the finite volume method and the Structural Calculations based on the finite elements method.

The flow is present in many different fields, related to e.g. human life activities, technologies, etc. The flow of gas or liquid affects the aerodynamic characteristics of aircraft/gliding objects (including paragliders), as well as the efficiency of turbines, engines, etc.

Computational Fluid Dynamics (CFD) is therefore one of the most dynamically developing disciplines of computer-aided design. The finite volume method allows the use of non-orthogonal, non-uniform computational meshes. It assumes that the fulfillment of mass, momentum and energy balances for each elementary cell is tantamount to the fulfillment of these balances in the entire considered space. Thus, non-linear differential equations that describe the conservation of mass, momentum and energy are numerically solved [9]:

$$\iiint_V \frac{\partial_\rho}{\partial_t} dV + \iint_A \rho v_n dA = 0$$

$$\frac{d}{dt}\iiint_V \rho \vec{v} dV = \iint_A \vec{p}_n dA + \iiint_V \vec{F}_m \rho dV \tag{2}$$

$$\frac{d}{dt}\iiint_V \rho(c_w T + \frac{v^2}{2})d = \iint_A \vec{p}_n \cdot \vec{v}\, dA + \iiint_V \rho \vec{F}_m \cdot \vec{v}\, dV + \iint_A \dot{q}_n dA + \iiint_V \dot{q}_m \rho dV$$

Conservation equations for mass, momentum or energy, after appropriate transformations, have the form of an algebraic equations (which can be calculated numerically). However, since the number of the design parameters is very large, the iterative procedure is repeated until the convergence is reached.

The Finite Element Method (FEM) uses both – linear and non-linear partial differential equations to be solved in the following iterations. The principle of this method is to solve governing equations concerning the following: (1) assuming the local equilibriums; (2) strain-displacement relations; (3) predicting material's response to external factors acting on it, i.e. constitutive equations. All the equations are solved with the assumption of before defined boundary conditions based on the real physical conditions [8, 10].

The solution presented below is based on the Newton-Raphson method. This method is implemented when the force-displacement curve is nonlinear. First, the system is stationary.

Next, consecutive iterations of displacements and forces are implemented until the convergence is achieved.

The Newton-Raphson procedure can be described by the following formulas [10], which regard displacement increment and residual force:

$$\Delta u^n = (F_{ext} - F_{int}^n)/K^n$$
$$F_{res}^n = F_{ext} - F_{int}^n \quad (3)$$

The convergence is achieved when the residual force in the current step of calculations is not greater than the assumed difference between the applied and calculated force. Thus, the residual value satisfy the convergence criteria.

The advantages of the numerical methods include [8, 9, 10]: (1) visualization of the obtained results and clear information about variables related to the behavior of the object; (2) easily make geometrical changes on the virtual model and analyze the impact of these changes on the obtained results/operation of the object (paraglider sensitivity to these changes); (3) omitting problems related to creating real conditions (i.e. very high velocities, high/low temperatures, large loads acting on materials) in research centers/laboratories.

5.3.Basics of lift force creation

Many years of research concerning not only the paraglider's wing, but various flying objects, allowed to conclude that the generation of the lift and other aerodynamic forces depend on [1, 5]: (1) Geometry and surface of the body and its position in relation to the air streams; (2) the speed of the body movement; (3) air density.

The aerodynamic force is determined by the formula [5]:

$$F = c \cdot S \cdot \frac{\rho \cdot v^2}{2} \quad (4)$$

The resultant aerodynamic force can be decomposed into two components D (drag) and L (lift) as follows [5]:

$$L = c_L \cdot S \cdot \frac{\rho \cdot v^2}{2}$$
$$D = c_D \cdot S \cdot \frac{\rho \cdot v^2}{2} \quad (5)$$

As mentioned above, the paraglider's wing-section has an elliptical outline. Thus, the geometry of the wing depends on both - the parameters of the base airfoil, as well as on the parameters of the outline (e.g. span to width ratio).

In the air, it is important that the wing is subjected to a large aerodynamic force, but directed as close as possible to the perpendicular to the direction of flight (Figure 4.)

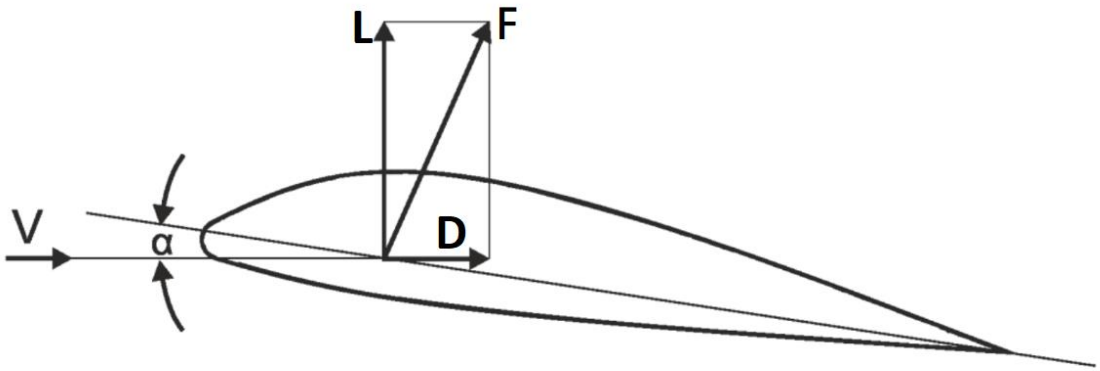

Figure 4. The resultant aerodynamic force acting on a flying object (based on [5])

The-advantageous for the flight is the so called lift force L (directed perpendicular to the flight speed, facing "up"). The disadvantageous is the drag force D, directed parallel and opposite to the flight speed. Thus, when the aerodynamic force F is less deflected from the perpendicular to the direction of flight, the greater the lift to drag ratio the more efficient the wing.

The lift on the airfoil of a paraglider (as well as on any other wing) is created by a favorable distribution of pressures, i.e. there is a pressure drop created at the upper surface. Thus, the air particles move faster along the it than along the lower surface.

This is in accordance with Bernoulli's law [1, 5] and the principles of conservation of energy. Namely, potential energy (related to pressure), is converted into kinetic (increase in flow velocity).

If the initial phase of flight is considered, the air streams cannot meet at the trailing edge at the same time, because those moving along the upper surface have a longer path to cover. Therefore, on the trailing edge a vortex of air streams coming from the lower surface of the airfoil is created. Such a vortex is called a starting vortex (Figure 5.)

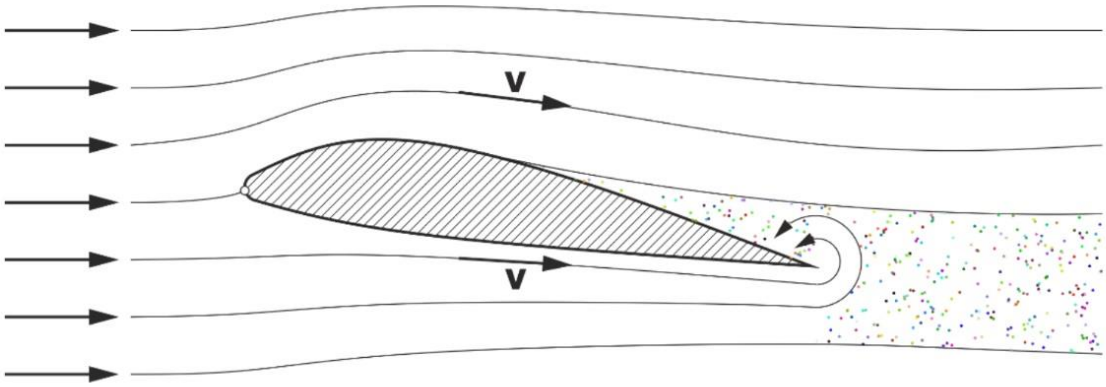

Figure 5. The creation of starting vortex (based on [5])

As, according to the laws of aerodynamics, vortices are always created in pairs [5], next to the starting vortex, a circulation is also created (Figure 6.). Its velocity is added to the velocity of the air flowing over the upper surface and subtracted from the air flowing over the lower surface.

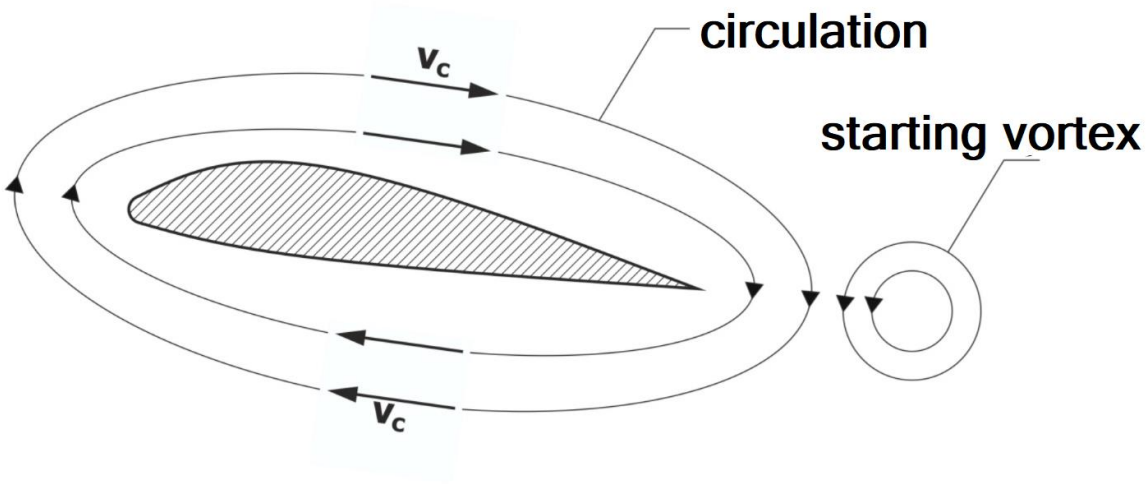

Figure 6. The creation of circulation vortex (based on [5])

In this way, the air streams flowing over the upper and lower surfaces meet at the trailing edge, and the circulation movement does not disappear (Figure 7.). It is concluded that the airfoil shape automatically causes a starting vortex, and thus - air circulation. This creates an advantageous difference in speed and pressure distribution - positive pressure on the lower surface and negative pressure on the upper surface of the wing.

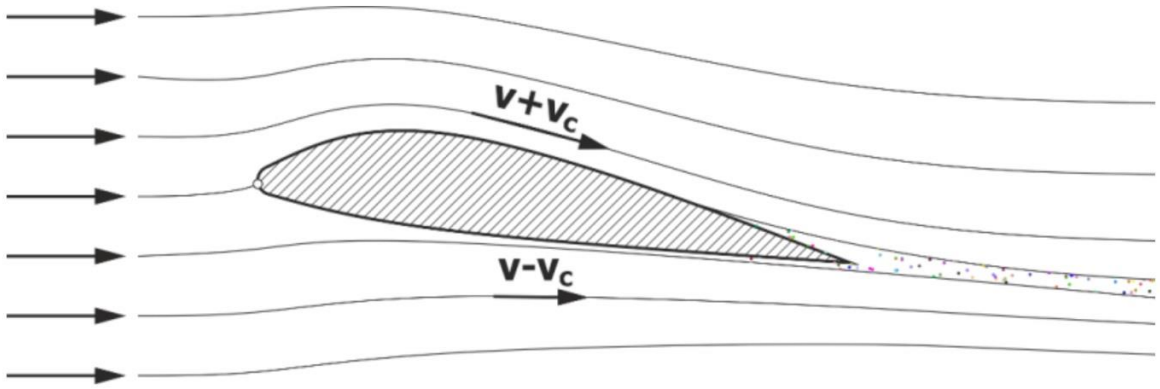

Figure 7. Air streams velocity distribution over the flying object (based on [5])

5.4.Researches on paragliders

Analysis of state variables related to the paragliding system has been performed insignificant number of authors. In their research, they focused mainly on selected issues of aerodynamics. However, no studies that correlate flight mechanics with materials engineering were found in available literature.

Babinsky, 1999 [13] performed analysis of paraglider mock-up in a low speed wind tunnel. The factors under studies were forces, pressure and deformation of the paraglider profile.

In general, the performance of a paraglider depends not only on the aerodynamic properties of the wing. Virgılio, 2004 [14] published the drag coefficient of a pilot wearing a harness. However, the published coefficients are for only one take-off angle and one speed.

Zhu, Cao, 2012 [15] used a finite volume method in order to analyze the influence of airfoil shape, especially the leading edge and the air vents configuration, on aerodynamic characteristics of a paraglider. The studies showed that the arc-anhedral angle created by overpressure acting on brits from the inside insignificantly affect the decrease of the lift and increase of the drag force.

The same authors continued and expanded the research on geometry influence on performance a flight of a paraglider [16]. The main aim was to analyze the leading edge cut, the arc-anhedral size change and the airfoil shape with the use of the CFD method.

Hanke, Schenk, 2014 [17] measured the shape of the paraglider in flight using stereoscopic cameras. Their experiments focused on determining the global geometry of external contours rather than local deformations.

Bofadossi, Savorgnan, 2016 [18] studied the behavior of pressure equalization inside the paraglider wing. Paragliders models with and without inlets were implemented to experimental and computational analysis in the Xfoil program. The experimental and numerical results were assessed as convergent.

Belloc et al., 2016 [19] used the finite volume method to solve the Reynolds averaged Navier-Stokes equations for the 2D flow on a paraglider open airfoil. The material was assumed to be smooth, rigid and impermeable. The parametric study performed concerns the position and the width of the air inlet at the leading edge. It is shown that the aerodynamic coefficients can be easily deduced from the pressure coefficients of the baseline airfoil without solving the internal flow.

Different air inlet configurations are introduced by Abdelqodus and Kursakov, 2018 [20] to the profile, and there effects on the aerodynamic performance are compared to the initial and optimized airfoils. The Reynolds averaged Navier-Stokes equations are solved for the flow field around the closed and open airfoils for the smooth, rigid and impermeable material. Results are focused on lift and drag coefficients for performance analysis and the internal pressure coefficient which can be critical regarding the risk of collapse.

Lolies et al., 2019 [21] presented a new model to compute paraglider cloth dynamics. Despite strong bias due to under-resolved boundary layers, numerical results of the cloth deformations are in an acceptable agreement with wind tunnel measurements on a small and simple wing geometry.

Kulhanek, 2019 [22] performed experimental and numerical studies of the pilot wearing harness influence on the drag coefficient increasement to the paragliding system. The drag coefficient of the pilot suspended in the harness was measured in a low-speed wind tunnel; whereas the aerodynamic characteristics of a paraglider were analyzed in the CFD environment. Performing experimental tests on the wing in a full scale was not possible in the accessible research center.

An in-situ measurement system was designed and applied by Benedetti, Gurgel Veras, 2020 [23]. The main principle of this system was to determine pressure acting on the paraglider brits (difference of pressure on both sides of a surface), when the wings were dynamically filled with air. It was noticed that a recirculation vortex was created due to applying inlets on the leading edge, as well relatively low speed of a paraglider. The results were found to be effective, when the stall phenomena and inflation parametrization.

He et al., 2021 [24] performed tests of single paraglider cells in a wind tunnel in configurations - deformable paraglider cell and a rigid cell mock-up. The analysis was performed in order to improve the shape and inlets arrangement aiming to increase the aerodynamic characteristics of the tested object. Improving the geometry and applying the appropriate angle of attack (higher than a few degrees) affect the full inflation of the paraglider cell.

The aerodynamic performance and flight stability of a 2-dimensional paraglider are optimized using a combination of response surface methodology and a multi-objective genetic algorithm coupled with the unsteady Reynolds-averaged Navier-Stokes equations, cf. Min Je Kim et al., 2022 [25]. Authors show an improvement of the aerodynamic performance and stability of the optimized 3D wing, consistent with the results from the 2D structures.

The studies on wing type parachutes cannot be taken directly as referring to the research regarding paragliding; however, they can inspire the methods, as the nature of the problem is similar.

For example, Geiger et al., 1990 [26] and Matos et al. 1998 [27] conducted experiments on real objects. In the first case, the parachute in a real scale was measured in the Langley Wind Tunnel. The other case considered a flight experiment. The author described deformations and damages on the leading edge when changing the angle during high-speed flight. However, these experiments were carried out on high-speed parachutes. Also, the analysis discussing the aerodynamics of wing parachutes, in which the author analyzed and estimated the aerodynamic characteristics was performed, cf. Lingard, 1995 [28].

A simplified parachute cell mock-up was studied by Uddin, Mashud (2010) [29] in order to evaluate the deformation and internal pressure. Pohl (2011) [30] compared rigid and deformable cells in order to assess different configurations of the applied geometry and arrangements of inlets.

Ovchinnikov, Petrov and Ganiev, 2021 [31] performed an extensive research regarding gliding parachutes. The authors analyzed the influence of different aspects of the wing geometry on the aerodynamic characteristics of the parachute. The analysis also included the cargo transportation issue. Authors claim that the air permeability influence can be neglected due to the properties of materials. Thus, the material porosity influence was not included to the research

6. Material air permeability influence on the aerodynamic characteristics of a paraglider – method of conversion air permeability parameter into porous resistance

The below described method and research from this section is based on the author's publications [32, 33]; it is an introduction to the further numerical analysis contained in the doctoral dissertation.

6.1.Geometry creation

The geometry was based on an existing paraglider wing. In order to recreate the shape of the paraglider, information on parameters such as wing area, span and deflection radius after filling with air were collected. The paraglider manufacturers do not introduce information regarding the airfoil shape. Therefore, the author performed measurements necessary to define dimensionless coordinates of it.

The dimensionless coordinates in the XY plane were described by x_i, z_i coordinates, where the subscript "i" referred to the consecutive coordinate in the plane.

With all the data it was possible to define equations and then create a program generating all the coordinates, that described 3D geometry of the considered wing. The equations were listed below.

From the formula for the coordinates of the ellipse, the following relationship was obtained between the y_j coordinate of a subsequent rib (when the paraglider is projected from the top view, Figure 8.) and its chord C_j:

$$\frac{C_j^2}{C_0^2} + \frac{y_j^2}{l^2} = 1$$
$$C_j = C_0\sqrt{1 - \frac{y_j^2}{l^2}} \tag{6}$$

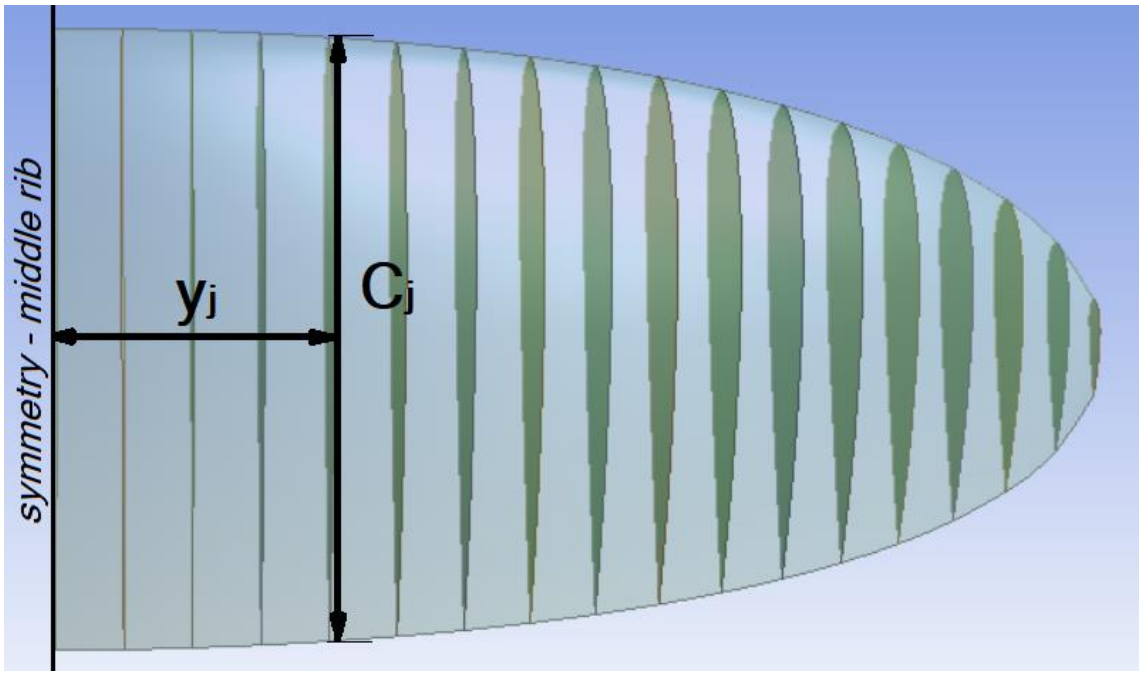

Figure 8. Paraglider geometry parameters
(subscript "j" applies to consecutive ribs in the XY plane)

Based on the above described parameters, formulas of functions of the coordinates of the points forming the paraglider in the three-dimensional XYZ space were derived:

$$\begin{aligned} x_{i,j} &= x_i C_j + 0.5(C_0 - C_j) \\ y_{i,j} &= \left(R + z_i C_j\right) sin\frac{y_j}{R} \\ z_{i,j} &= \left(R + z_i C_j\right) cos\frac{y_j}{R} - R \end{aligned} \tag{7}$$

Based on the dependencies presented above, the 3D coordinates forming the following ribs of half of the wing were generated and then introduced to the ANSYS Design Modeler program.

First, the points were used to form the spline lines and then the faces of the shape of subsequent ribs. It was the basis to create the wing body using the *Skin/Loft* tool, Figure 9. In order to apply a *porous media* tool (for simulations of permeable materials), a thickness of the covering materials of the wing should be introduced. However, it was not possible to apply an actual thickness, as it was too small to be correctly processed by the program. Therefore, a conventional value of thickness of t = 2 mm was applied.

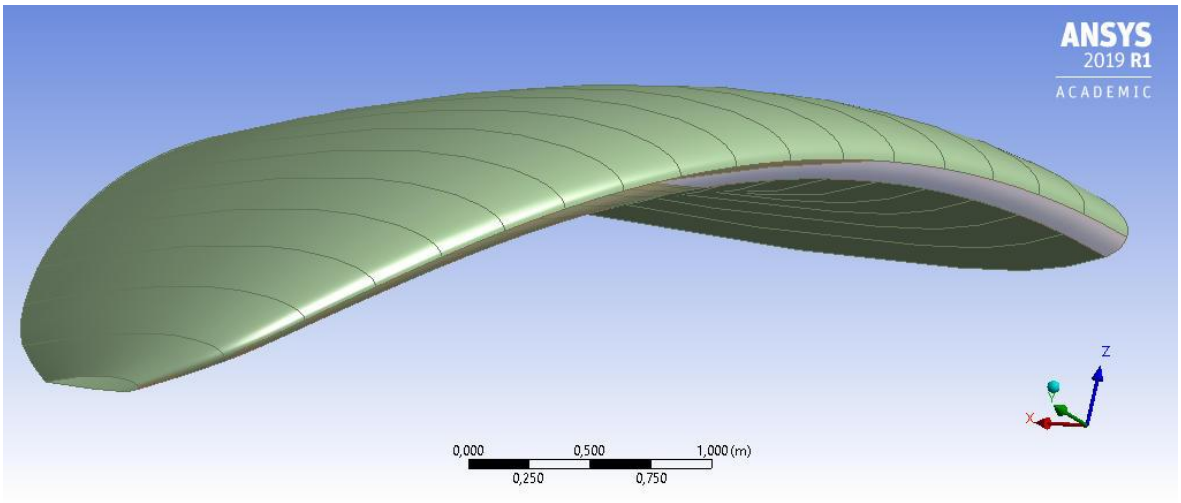

Figure 9. The created paraglider wing model

A calculation area of a shape of cuboid was created around the half of the wing. Its dimensions were significantly greater than the dimensions of the modeled paraglider (20 m in front of the wing and 40 m in other directions); this was necessary to apply a *pressure far field* boundary condition in the further steps of the analysis. The dimensions of the control area have been significantly enlarged to avoid the impact of internal disturbances on the outer surfaces. The calculation area was presented in the Figure 10. below.

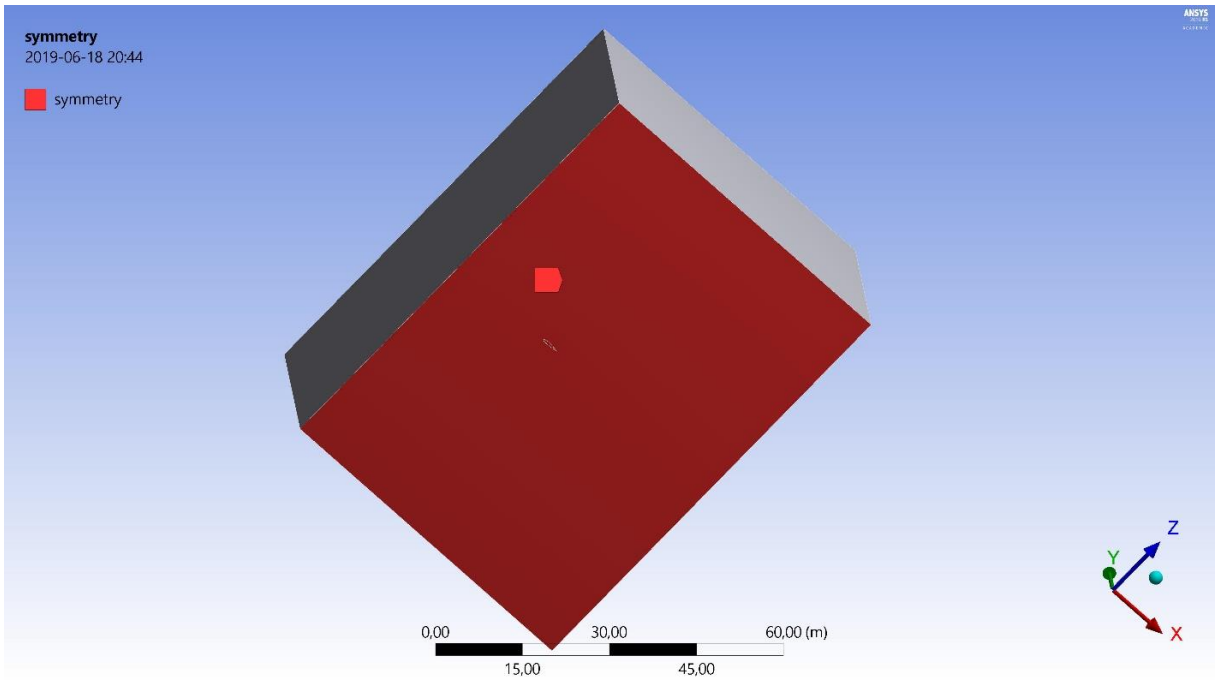

Figure 10. Calculation area of the considered paraglider with the Symmetry boundary condition applied

6.2.Preprocessing

As mentioned above a *pressure far field* condition was given to 5 walls of the cuboid surrounding the paraglider (except the wall forming the symmetry plane of the paraglider). This boundary condition describes an undisturbed flow assumption on the selected walls. Therefore, it conventionally was meeting the below:

$$p=p_{\infty};\ v=v_{\infty};\ T=T_{\infty} \tag{8}$$

The undisturbed flow was assumed to be described by conditions as follows: (1) Pressure of 101325 Pa; (2) Temperature of 26.85 °C; (3) Velocity of 45 km/h; (5) Angle of attack of 6°.

A *Symmetry* boundary condition was given to the remaining wall, Figure 10 above.

The walls forming the paraglider wing were described by the *Wall* (when theoretical impermeable material was considered) or the *Interior* boundary condition (when air permeable materials were studied). It was necessary to introduce the *Porous media* tool, used in order to perform simulations of flow through air permeable materials.

The *Porous media* was characterized by porous resistance (1/β) parameter, related to the permeability of air through the cells. The parameter was derived from the formula for the pressure gradient, i.e. its drop over distance [9]:

$$\begin{aligned} \nabla p &= \frac{-\mu}{\beta} \cdot v_m \\ \frac{\Delta p}{t_m} &= \frac{-\mu}{\beta} \cdot v_m \\ \frac{1}{\beta} &= \frac{-\Delta p}{t_m \cdot \mu \cdot v_m} \end{aligned} \tag{9}$$

The velocity of flow through the material is equivalent to the air permeability parameter, which can be explained by the units conversion:

$$[\frac{l}{m^2 \cdot s}] = [\frac{mm}{s}] = 0.001[\frac{m}{s}] \tag{10}$$

According to the above formulas and exemplary air permeabilities of materials (declared by a fabric manufacturer), in the table below corresponding porous resistance values were compiled).

Table 1. Porous resistance parameter values for the corresponding air permeability

Material	**Air permeability** $[\frac{l}{m^2 \cdot s}]$, pressure drop 2000 Pa	**v_m [m/s]**	**1/β [1/m^2]**
Theoretical	0	-	- *)
a	0.05	0,00005	$1.118 \cdot 10^{15}$
b (aged)	3.33	0,00333	$1.677 \cdot 10^{13}$

*) Wall boundary condition

Finite volume mesh was generated according to general convention of creating the meshes; i.e. smaller elements of the mesh were created near the analyzed object and gradually increased, when coming forward the walls representing the pressure far field boundary condition.

For smaller elements, there is much greater accuracy and smaller calculation errors. Especially with a large gradient of state variables. The smaller the element, the smaller the calculation inaccuracies. No great changes of the state variables in elements distant from the wing were expected. Therefore, the size of the element can be enlarged there. Make polyhedral tool was applied to the unstructured elements of the mesh, which created the calculation area, Figure 11.. This caused increasing of the quality of the final mesh and decreasing of time of the calculation.

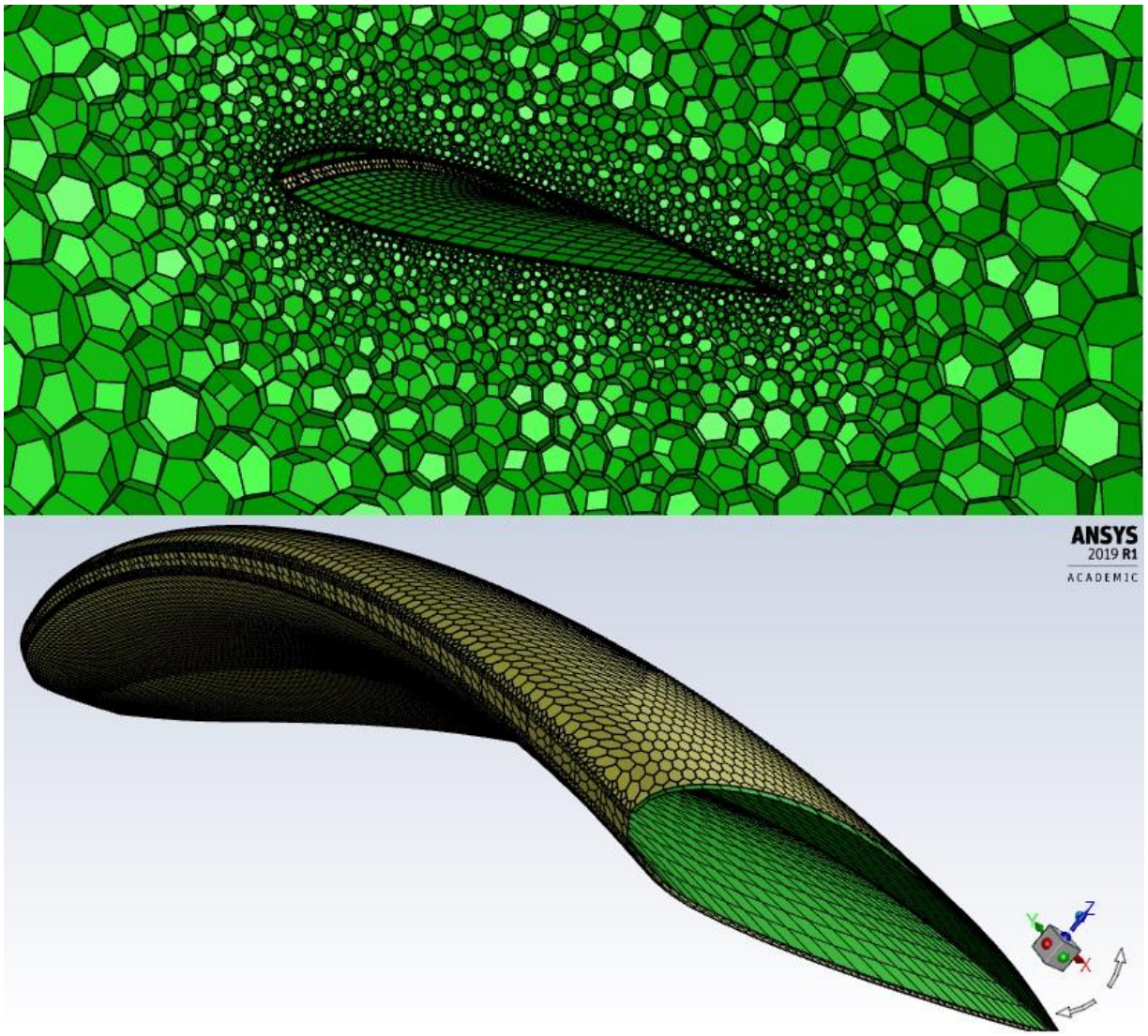

Figure 11. Generated calculation mesh

According to the manual of the ANSYS Fluent program [9], the *Realizable k-ε* model was the most appropriate turbulence model for the applied mesh. It is used for meshes in which the discretizing elements of the boundary layer, i.e. those located in the immediate vicinity of the tested object, are relatively large (in the case under consideration, the use of the *Make Polyhedra* tool resulted in the enlargement of the discretizing elements of the first layer).

However, the initial calculation results obtained with the use of the *Realizable k-ε* model definitely differed from the predicted ones. Therefore, the turbulence model was changed to the *Spalart-Allmaras*, which gave the expected field of air parameters.

Spalart-Allmaras is a one-equation model based on the transport equation. Due to computational savings, it enables the use of meshes with large elements.

It was specifically designed for aerospace applications, where boundary layer flows are present (e.g. airfoils, aircraft wings, missiles).

6.3.Exemplary results

The first considered case was theoretical and concerned a wing covered by an impermeable fabric. Paraglider made of air impermeable material was characterized by the best aerodynamic properties. The c_l/c_d ratio was equal to 13.1687, whereas pressure inside of the wing was 101415.83 Pa. However, paraglider made of the material with the lowest air permeability (0.05 $\frac{l}{m^2 \cdot s}$) presented only slightly worse aerodynamic characteristics; its c_l/c_d ratio was equal to 12.7708.

The mean pressure inside the wing covered with a material after ageing of air permeability of 3.33 $\frac{l}{m^2 \cdot s}$ (tested with the pressure drop of 2000 Pa) was much lower than for the remaining cases and it was equal to 101398 Pa, Figure 12b. According to the results obtained during the numerical calculation, its c_l/c_d ratio was only equal to 4.0655.

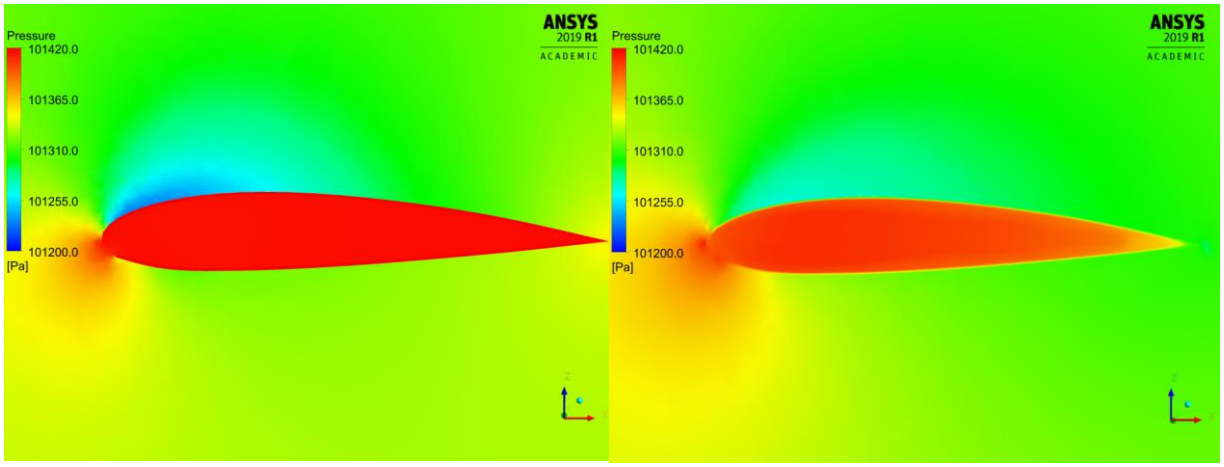

a b

Figure 12. Pressure distribution over a paraglider made of: a – air impermeable material; b – degraded material of air permeability of 3.33 $\frac{l}{m^2 \cdot s}$ tested with pressure drop of 2000 Pa

Based on the Figure 12 it can be concluded, that when a paraglider was covered with an impermeable material, the pressure inside the wing was evenly distributed. It secures maintaining an aerodynamic shape of the paraglider, as well as creating an advantageous forces distribution. Whereas, when the material was impermeable, the air permeating through the material, caused decrease of the pressure and its uneven distribution. This affected in disturbance of creating of negative pressure at the upper surface of the wing, and thus – the decrease of the c_l/c_d ratio.

7. Materials and experimental methods

Good quality of paraglider fabric is indicated by its very low mass, as well as resistance to mechanical loads, i.e. tension (stability of dimensions during usage of a paraglider in flight) and bending (caused by folding and unfolding of the paraglider during its life cycle). Moreover, air-permeability parameter should be tending towards zero, as it enables a wing to reach aerodynamic shape by overpressure inside of it. As a final product is exposed to open air conditions (i.e. solar radiation, precipitation), UV resistance is also required.

The even yarns made of Nylon (PA 6.6) filaments are used in order to weaving Rip-stop type fabrics. Rip-stop is a reinforcing technique, that enables to increase strength of the fabric (especially the resistance to tearing) in relation to its surface mass. In this method of weaving, thicker reinforcing threads are implemented at regular intervals (creating characteristic squares).

Polyamide 6.6 is a synthetic polymer intended for the production of synthetic fibers characterized by high tensile strength and susceptibility to dyeing. It is a crystalline material with a melting point of approx. 255ºC. Compared to other PA6s, it has lower moisture absorption. Due to very good properties (mainly mechanical), polymer has many areas of application [34].

During a finishing process, the woven fabrics are dyed and covered with an impregnating layer that gives them required properties (i.e. air impermeability, resistance to UV radiation, greater stiffness). The impregnation layers are usually based on polyurethane resins or silicones.

The section dedicated to wing analysis includes study of 10 different paraglider/parachute fabrics, as well as their influence on the aerodynamic characteristics and general behavior of a paraglider.

The analyzed materials and their characteristics were listed in the Table 2. Samples no. 1 – 8 are paraglider fabrics; whereas samples no. 9 – 10 are parachute fabrics. Due to confidential character, the author was obliged not to publish companies names nor the trades names of the samples.

Table 2. Basic characteristics of the analyzed materials.

Sample	Mass (g/m^2)	Thickness (mm)	Number of threads/ 1 dm		Max force during elongation (daN/5cm)		Elongation at break (%)	
			warp	weft	warp	weft	warp	weft
1	34	0.05	560	580	34	32	21	20
2	42	0.07	460	500	47	46	30	30
3	32	0.05	420	460	25	33	24	25
4	26	0.05	420	580	25	22	24	22
5	38	0.09	420	480	38	33	25	25
6	38	0.09	420	460	27	28	21	23
7	29	0.04	420	460	25	33	24	25
8	26	0.04	420	480	25	22	24	23
9	36	0.05	520	520	40	40	26	26
10	42	0.08	510	500	42	42	27	27

All the studied samples, except from sample no. 9, were characterized by a standard rip-stop weave. The remaining sample was manufactured using a special hexagonal ripstop, which probably causes increased dimensional stability when stretched in different directions.

Based on the Table 2., the analyzed samples surface mass ranged between 26 g/m^2 – 42 g/m^2 and thickness ranged between 0.04 mm – 0.09 mm. Increasing values of masses and thicknesses of the samples was usually associated with increasing of breaking forces.

The obtained maximal forces during elongation were the highest when the parachute fabrics (samples no. 9-10) and one of paraglider fabrics (sample no. 2) were considered; their values ranged between 40 daN – 47 daN.

The resistance to tensile of the paraglider fabrics were decreased compared to the parachute fabrics. The highest values of breaking force were obtained for samples no. 1, 5 and 6 (around 35 daN). Whereas the lowest values were presented by samples no. 4 and 8.

The Table 2. does not include the air-permeability parameter which was analyzed and described in the subsequent Section 7.1. Considering generally, air permeability of all the studied samples was tending towards zero.

The exact characteristic of functional groups were studied in Section 7.2, the SEM analysis of the samples was introduced in Section 7.3. Moreover, influence of ageing (i.e. UV radiation, high temperatures, freezing process on color change, air permeability and tensile strength) were also analyzed in the subsequent sections 8.1 – 8.3.

Unless otherwise indicated, the samples analysis in the current and following sections were performed in the normal climate conditions i.e. at temperature T = 20 °C; pressure p = 1013.25 hPa; and relative humidity RH = 65%.

7.1.Air permeability characteristics

The air permeability parameter of the considered samples was tested using FX 3300 digital device. The determination of it was based on the EN ISO 9237:1995 standard [35], where the pressure equal to 100 Pa is usually applied. However, paraglider fabrics' manufacturers describe the air permeability with a pressure drop of 2000 Pa. Moreover, parachute fabrics characteristics are divided into types and characterized with a special PIA-C 44378 [36] standard, where the pressure drop equal to 125 Pa is applied.

In order to obtain precise results of the air-permeability parameter, in the below analysis, the following pressure drops were applied: 100 Pa, 125 Pa, 200 Pa, 1500 Pa, 2000 Pa and 2500 Pa. The obtained results were compiled in the Table 3 and Figure 10.

Table 3. Air permeability results [37]

Sample	**Air permeability ($\frac{l}{m^2 \cdot s}$)**					
	100 Pa	**125 Pa**	**200 Pa**	**1500 Pa**	**2000 Pa**	**2500 Pa**
1	0.00	0.00	0.00	0.00	0.03	0.02
2	0.00	0.00	0.00	0.00	0.05	0.07
3	0.00	0.00	0.00	0.00	0.00	0.00
4	0.00	0.00	0.00	0.00	0.05	0.06
5	0.00	0.00	0.00	0.00	0.00	0.00
6	0.00	0.00	0.00	0.00	0.00	0.00
7	0.00	0.00	0.00	0.00	0.06	0.08
8	0.00	0.00	0.00	0.00	0.00	0.00
9	0.00	0.00	0.00	1.72	2.30	2.44
10	0.00	0.00	0.00	0.00	0.06	0.08

Based on the results compiled in the Table 4 and Figure 13, the obtained air permeability values of all the analyzed samples were equal to zero, when pressure drops of 100 Pa, 200 Pa and 125 Pa were applied. Moreover, the samples no. 3, 5, 6 and 8 were impermeable with all applied pressure drops. The remaining fabrics no. 1, 2, 4, 7 and 10 reached values

greater than 0 ($\frac{l}{m^2 \cdot s}$) when pressure drops between 2000 Pa – 2500 Pa were applied. However, the obtained values were 0.02 ($\frac{l}{m^2 \cdot s}$) – 0.08 ($\frac{l}{m^2 \cdot s}$).

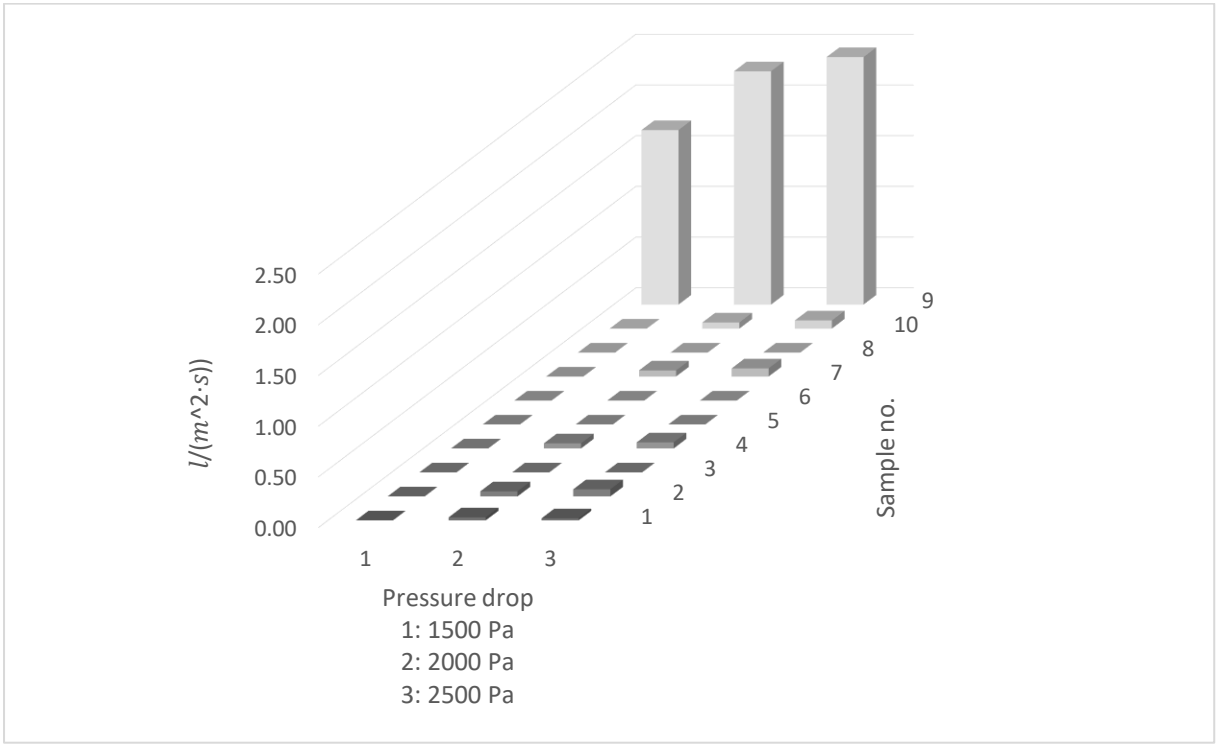

Figure 13. Obtained air permeability values of the tested samples with pressure drops: 1 – 1500 Pa, 2 – 2000 Pa, 3 – 2500 Pa

Material no. 9 presented the greatest air permeability values, which were between 1.72 ($\frac{l}{m^2 \cdot s}$) – 2.44 ($\frac{l}{m^2 \cdot s}$) (with applied pressured drops 1500 Pa – 2500 Pa). It defined this fabric as infinitely more permeable than the remaining samples. However, it should be mentioned, that this sample is still characterized by a very low air permeability parameter.

7.2.Fourier Transform Infrared Spectroscopy (FTIR) [37]

The literature introduces a wide range of investigations connected with the FTIR Spectroscopy; however, the impregnated textiles are not often discussed in the available sources [38]. The combination of different impregnation and base materials can have a significant influence on the mechanical properties, as well as testing methods of the final product [38-43].

FTIR was applied to analyze the characteristics and type of correlations impacting on the present functional groups. Therefore, a detailed discussion was focused on the distinguishing properties of the samples under research. The below analysis is based on research that has been previously published by the author [37].

Fourier Transform Infrared spectra were recorded by Nicolet 8700 spectrophotometer (Thermo Fischer Scientific Instruments, Waltham, MA, USA), equipped with a diamond adapter (Smart Orbit ATR sampling accessory). The research program included the preparation and analysis of 128 spectra in the range from 3800 cm^{-1} to 800 cm^{-1}.

Figures below present the FTIR spectra of the investigated fabrics, where Figure 14. describes the samples no. 3 – 8 and Figure 15. describes samples no. 1 – 2 and no. 9 – 10. Such a division was implemented, as the spectra of samples no. 1, 2, 9, 10 significantly differed from the records obtained for the remaining fabrics.

It can be observed that the discussed materials differ in the content of characteristic chemical groups [40].

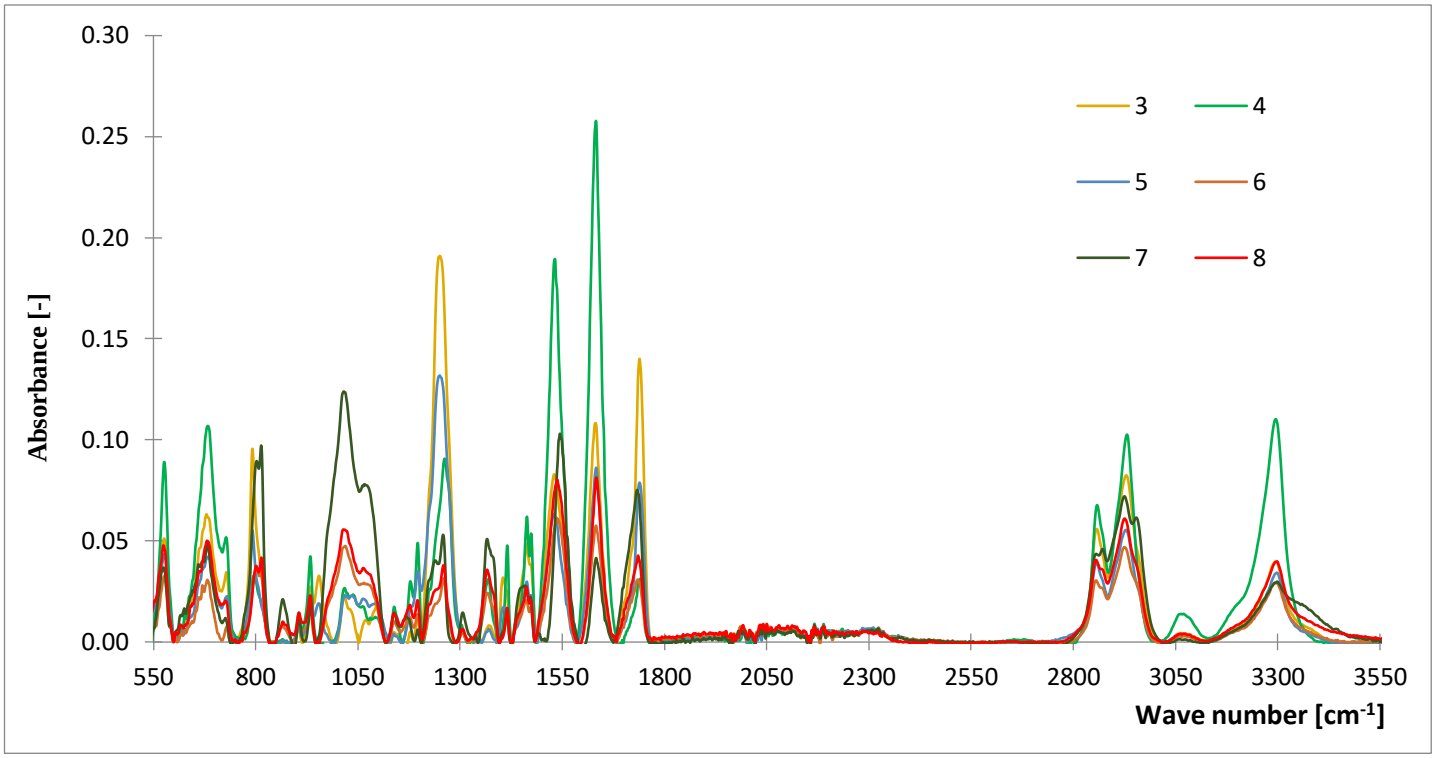

Figure 14. The FTIR spectra of the analyzed samples (3 – 8)

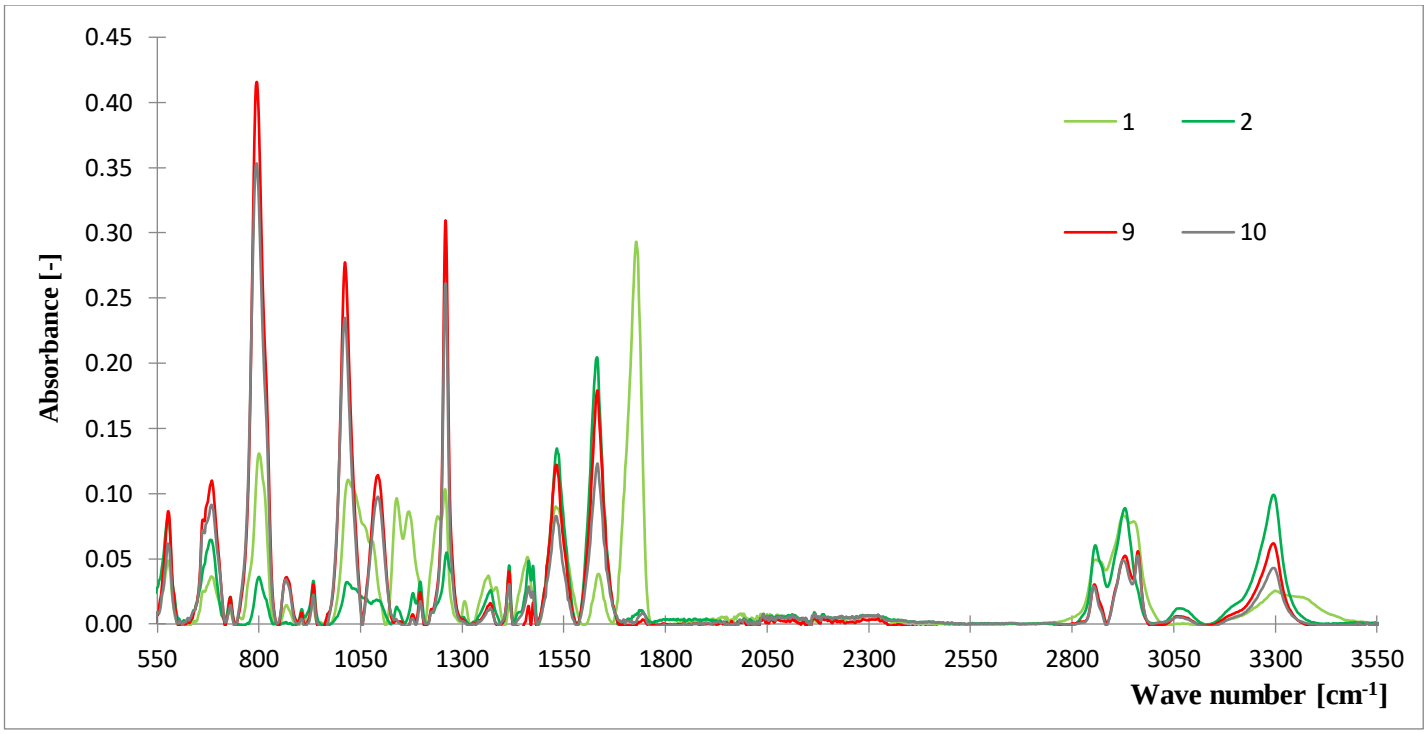

Figure 15. The FTIR spectra of the analyzed samples (no. 1 – 2, 9 – 10).

The absorption ranges referring to the characteristic bonds were compiled in the Table 4. below.

Table 4. Characteristic functional groups registered by FTIR analysis of the analyzed samples [based on 38-43]

Peak assignments and type of vibration	**Wave number [cm^{-1}]**
ν O-H w s	3300-3330
ν_s (C–H), ν(=C–H$_{vw}$)	3100–3050
stretching in Si-CH3	2960
ν_{as} ν CH3s s	2935
ν_{as} ν CH2s s	2852
ν (C=O)	1735–1690
ν(C=C) in aromatic rings	1680–1550
ν NC=O m vs	1631
δ N–H w s	1537
d N–H, ν C–N	1515
δ CH2vw w	1455
sv (C=C) aromatic	1441
m NCO in phase/CH2	1334-1333
ν C–N – w	1276
m (O=)C–O–C stretch/Urethane C–O stretch	1250-1248
ν_m(–C–O) or d_m(–CH$_2$–), $\nu_{w, m, vw}$(–C–H, –CH$_3$);	1285/1244
CH3 deformation in Si-CH3	1260-1250
ν C-O	1183-1153
ν C-O	1153-1123
ν*a* C–N–C	1155-1145
ν C–OH vs vs, , ν(–C–H)	1058-1056
ν (O–C–O, *va* C–O–C), ν(C–C), $\nu_{m,vw}$(–C–O),	1091–1020
ν Si-O-Si	1074–1005
ν C=C	958
ν OC–C s s, *w* νs C–N–C	871-865
−CH3 rocking and Si-C stretching in Si-CH3	796–789
ν, *sν* C–N	765-760
ν CH2	731-727
γ N–H – m	686
δ NC=O – w	576

Abbreviations: *ν* – stretching vibrations; *d* – deformation vibrations; *s* – symmetric; *as* – asymmetric; *st* – strong; *w* – weak; *vw* – very weak; *m* – medium; *sν* – skeletal vibration; *a* – axial.

Based on the above Figures 14. and 15., as well as the Table 4., it was noticed that the fabric no. 1 was characterized by a few peaks that were distinguishing only this sample. There were observed some peculiar to Polyamide 66 C–O stretching vibrations and to the axial stretching of the C-N-C bond; it was related to a presence of a broad band at 1183 cm^{-1} – 1153 cm^{-1} with a peak at 1169 cm^{-1} and 1153 cm^{-1} – 1123 cm^{-1} with a peak of 1138 cm^{-1} [41]. There was also registered

an increased content of C=O group in the discussed fabric compared to the other materials (based on the peak at 1735 cm^{-1} – 1690 cm^{-1}) [39].

Both the samples 9 and 10 also distinguished among the remaining. A high intensity of the following peaks was registered and therefore the highest content of the assigned bonds: at 796 cm^{-1} – 789 cm^{-1} -CH3 stretching of Si-C in Si-CH3, at 1074 cm^{-1} – 1005 cm^{-1} stretching of Si-O -Si, at 1260 cm^{-1} – 1250 cm^{-1} stretching of CH3 in Si-CH3.Vibrations peculiar to the CH, CH2, CH3 groups were noticed between 3100 cm^{-1} – 2852 cm^{-1} and to N-H group between 3300 cm^{-1} – 3330 cm^{-1} [42, 43].

The spectra obtained during the Fourier Transform Infrared, enabled to indicate samples of the expected highest mechanical properties; the highest peaks are often correlated with the functional groups responsible for mechanical strength.

Based on the records, the highest peak around the groups C=O and C-O, was noticeable only for the material no. 1. Sample no. 5 was characterized by the smallest number of O-C-O, C-O-C, C-OH and C-H groups. However, the samples expected to present the greatest strength properties, were fabrics no. 9 and 10; it was caused by the presence of the Si-C and -Si-CH3 functional groups.

The considered groups are formed by chemical bondings, which also influence the mechanical properties, when a final product is considered (in this case paraglider/parachute fabric).

It can be concluded that some specific types of bonds were noticed. The Nitrogen (coordination bonds) or Silicon (polarized covalent bonds) are included to these; also, polarized hydrogen bonds, which were created at the ends of chemical groups and interact with remaining components (as oxygen) were listed.

7.3.Scanning Electron Microscope records

Prisma^{TM} E Scanning Electron Microscope was used in order to record pictures of magnitudes equal to 120x (Figure 16), 200x (Figure 17a) 500x (Figures 17b and 19). In order to analyze woven structure of the considered fabrics, also a magnitude of 40x was applied. The pictures of the lower magnitude were not placed in this Section; however, some observations based on them were described below.

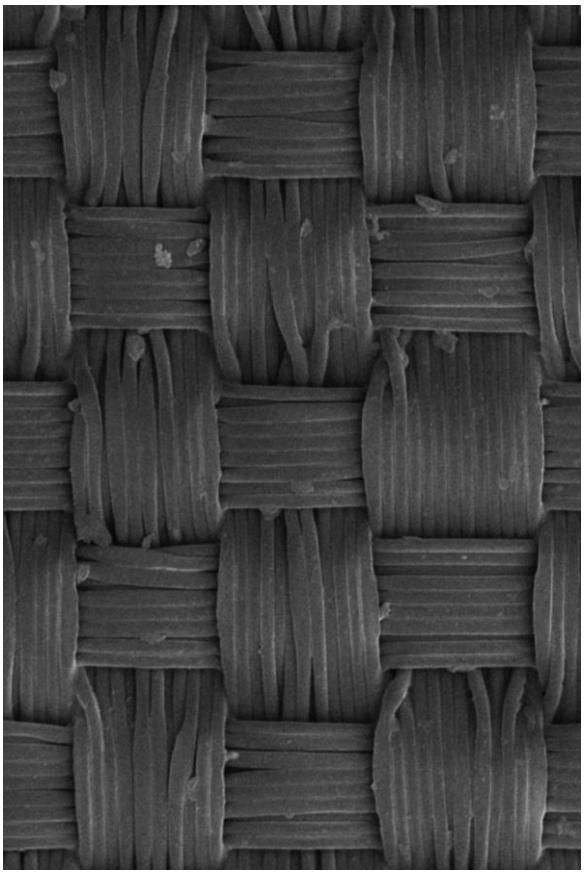

Sample 1

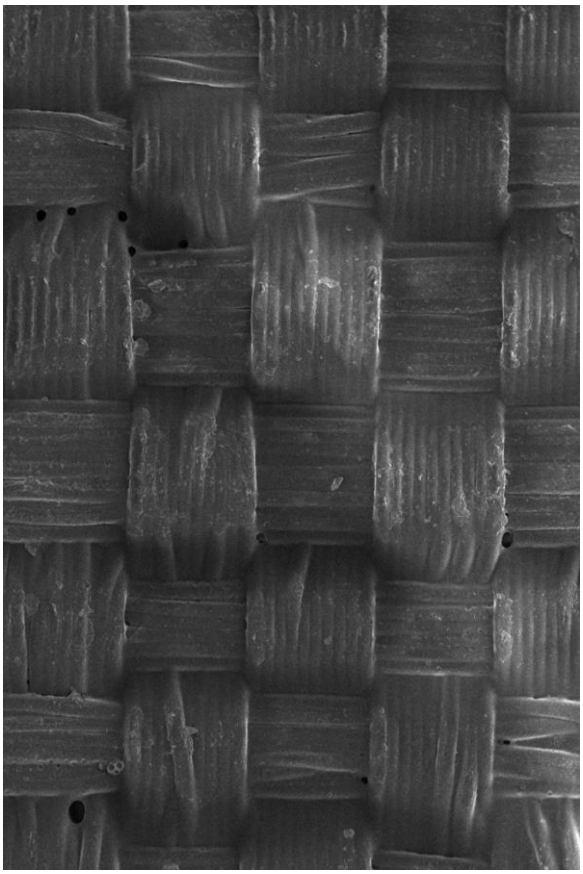

Sample 2

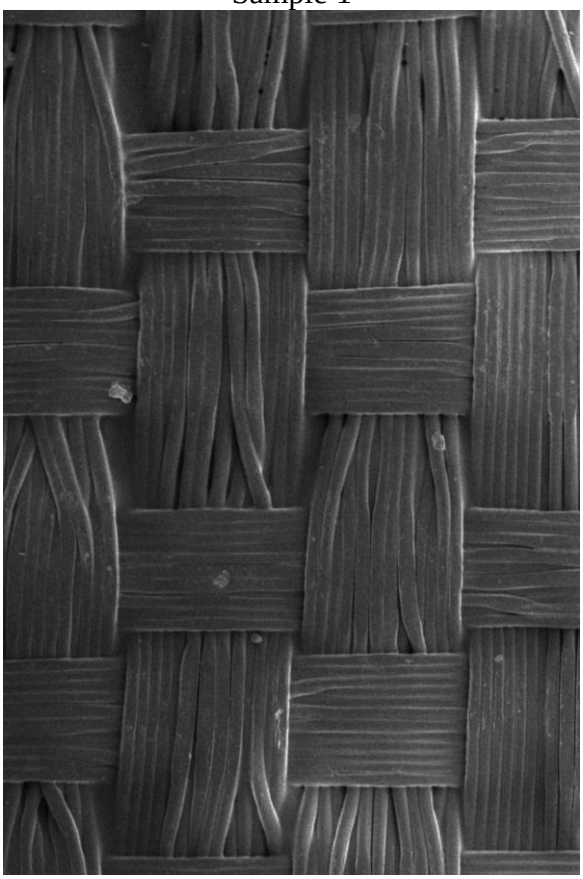

Sample 3

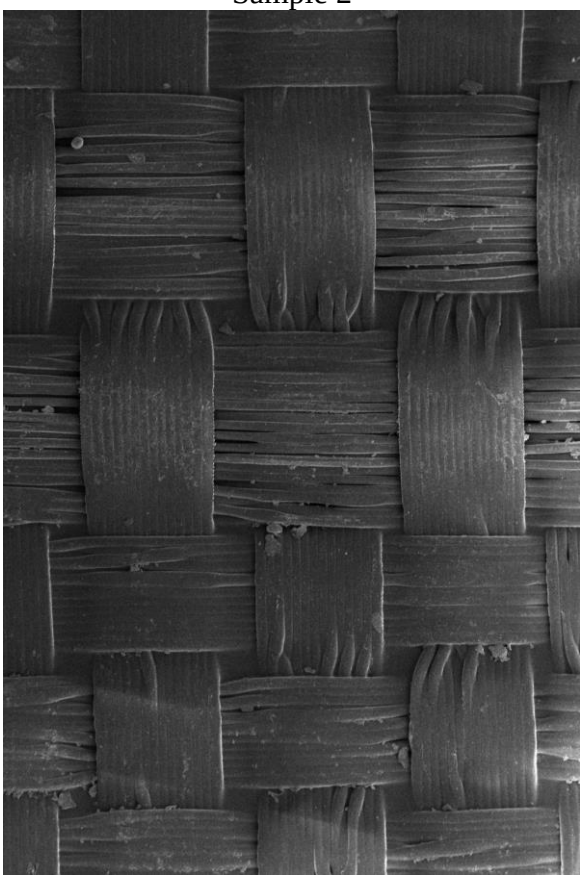

Sample 4

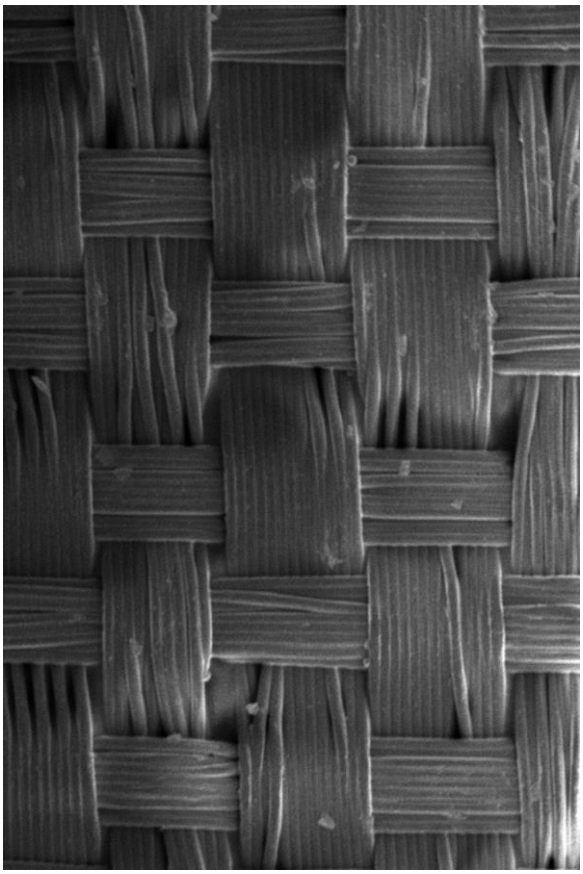

Sample 5

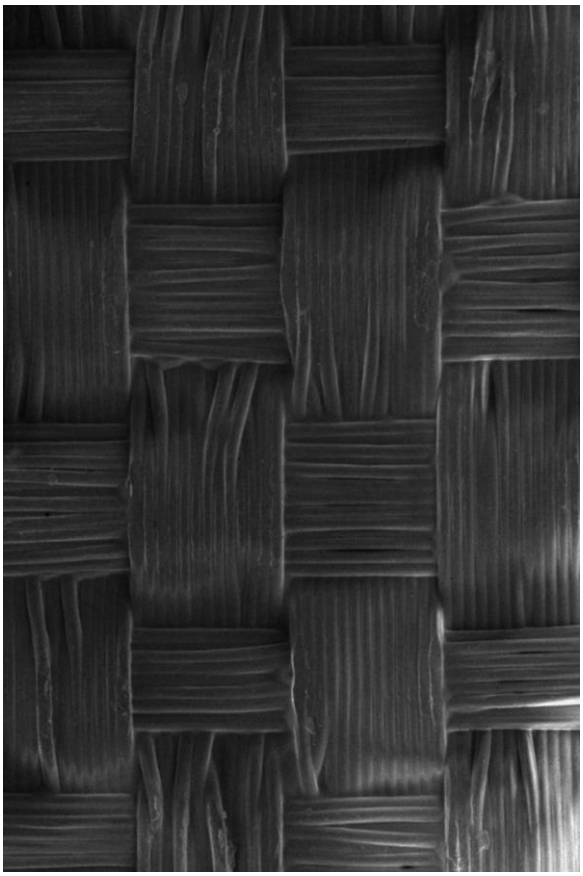

Sample 6

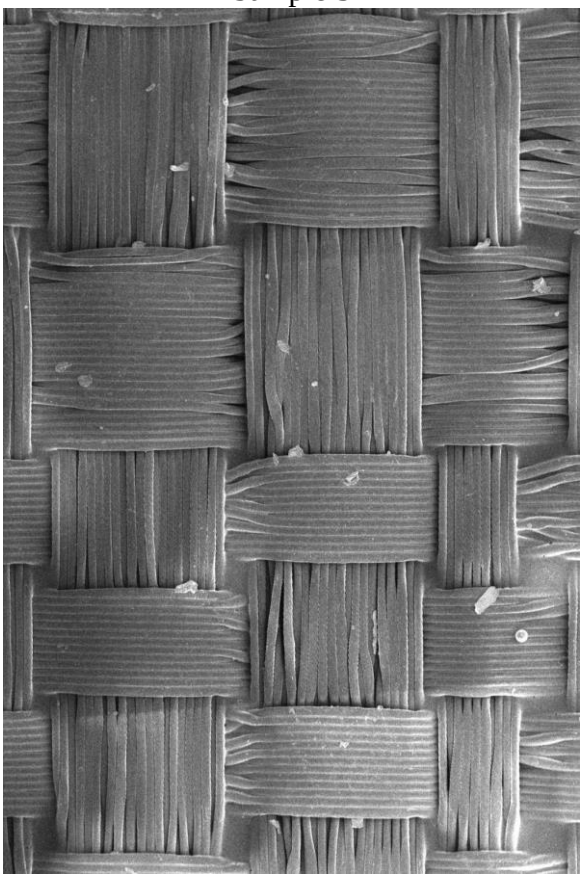

Sample 7

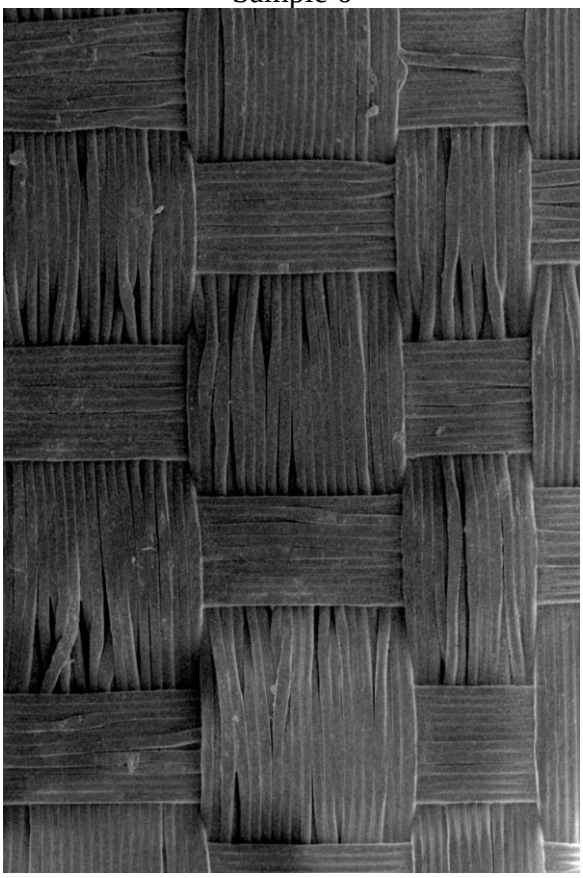

Sample 8

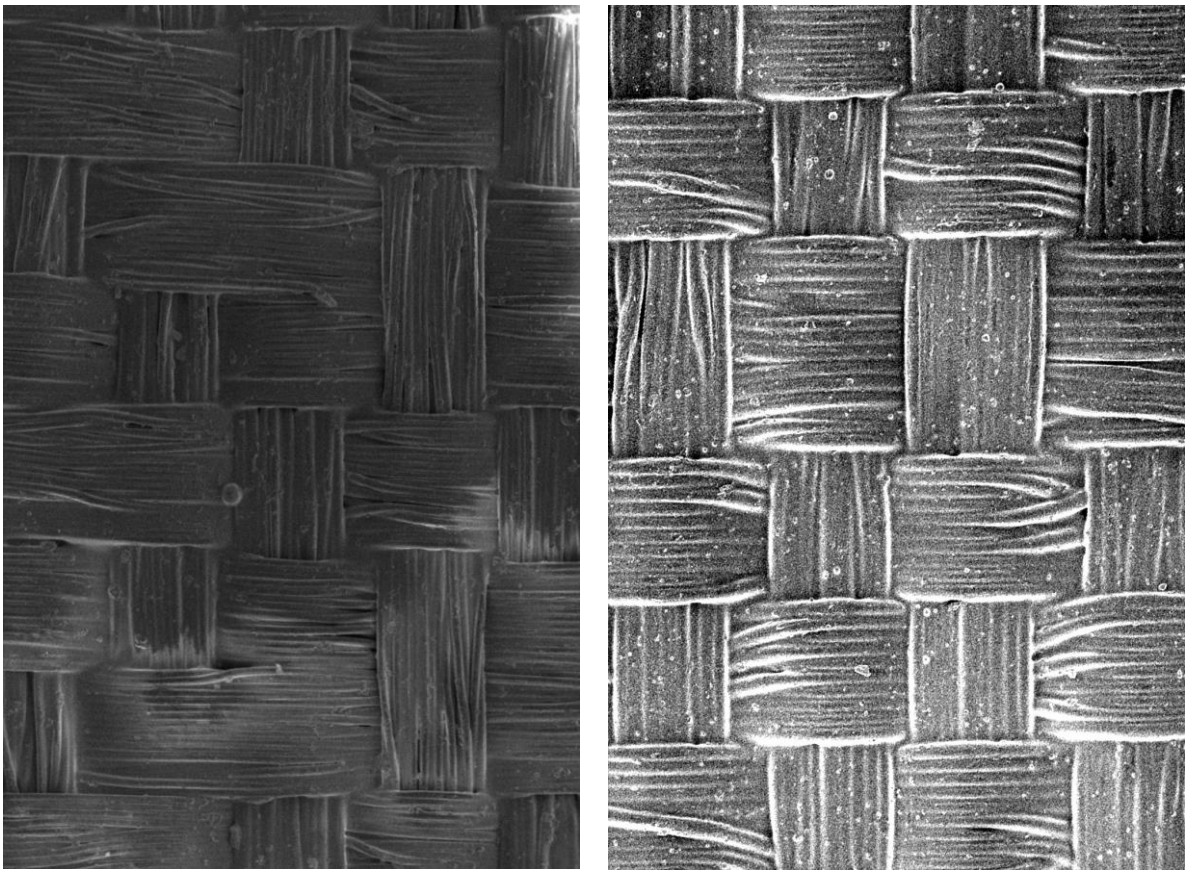

Sample 9 Sample 10

Figure 16. Scanning Electron Microscope records of the considered samples

According to the SEM records presented in the Figure 16, all the considered woven fabrics were manufactured using multifilament yarns. No twist of the yarns was observed. Depending on the type, surface mass and weave of fabric, the diameter of the filaments and yarns differ, what will be discussed further in this section.

There is a high correlation between structural characteristics of yarns and woven fabrics, which has been studied widely by many researchers. The most important studies in this area were performed by Peirce, Dastoor, Kemp or Olofsson etc.; they created models containing formulas, which correlated both – structural and mechanical properties of yarns and fabrics [44, 45].

All the filaments that can be seen in the Figure 16 were significantly flattered. This is a result of high values of weave factor and yarn extension, low crimp factor, as well as no/insignificant twist of the yarns. The fabrics had probably been also calendared during the manufacturing process. Both, tight weave and calendaring, result in achieving required final parameters of the fabric, which is mainly air-permeability tending towards zero. High density of threads per width result in the increased mechanical properties. Whereas

calendaring flatters final product, which enables better packing properties (when a paraglider is considered, it would be decreased volume of a wing).

Fabrics weaves were studied with the magnitude of 40x, however the records compiled in the Figure 16 also present some characteristic elements of it. Every sample is characterized by thicker and thinner yarns. The thicker yarns represent the previously mentioned reinforcement characteristic for the ripstop weave. Based on the obtained pictures and organoleptic analyzes, it was noticed that all the considered fabrics presented traditional ripstop of squares pattern; the exception was sample 9, where the reinforcement creates hexagonal pattern. In the Figure 13 – sample 9, a fragment of the weave, where reinforcement creates corner of the hexagon can be observed; 2 connected reinforcing warp threads separates: one following the plain weave, one connecting with the adjacent thread, forming twill weave (right bottom corner of the discussed SEM record). In each considered case, reinforcement contained of two thicker threads/1 edge (of the square or hexagon). The exact number of thinner threads/1 edge was compiled in the Table 5.

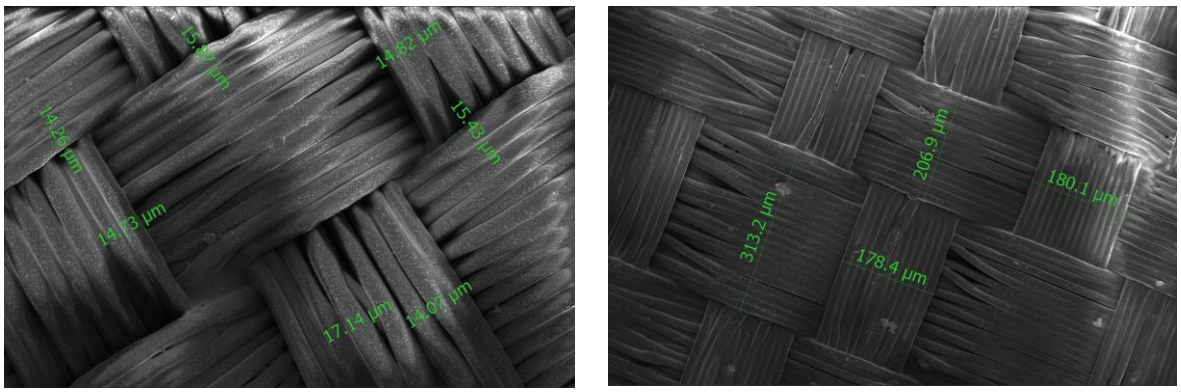

a b

Figure 17. Example of determination of diameters of:
a – filaments (sample 1); b – yarns (sample 3)

Based on the pictures achieved by the SEM device, also diameters of the single filaments, as well as threads were determined, Figure 17. There were taken 20 measurements per each parameter of each sample. The results were compiled in the Table 5.

Table 5. Structural characteristics of the considered fabric samples

Sample	Filament diameter [µm]	Thin yarn diameter [µm]		Thick yarn diameter [µm]		Thin yarns/ 1 edge		Thick yarns/ 1 edge	
		Warp	Weft	Warp	weft	warp	weft	warp	weft
1	15.15	128.8	152.3	187.9	225.9	22	18	2	2
2	24.77	160.2	198.8	202.4	255.8	20	15	2	2
3	19.39	179.8	206.9	238.5	313.1	15	12	2	2
4	20.48	155.8	200.2	219.7	321.7	42	32	2	2
5	20.60	141.3	225.1	218.3	318.0	20	15	2	2
6	20.23	159.4	224.9	220.0	322.4	20	15	2	2
7	18.43	148.7	187.5	309.0	347.9	42	32	2	2
8	18.63	156.6	200.7	211.7	320.2	18	15	2	2
9	15.11	161.0	214.8	280.1	356.8	20 *)	35 **)	2	2
10	20.74	158.9	225.0	220.0	325.3	20	15	2	2

*) Figure 18a

**) Figure 18b

a b

Figure 18. Weave type in sample 9, threads count: a – warp, b - weft

Based on the Table 5 and Table 3 (Section 7), it can be concluded that obtaining thinner fabric is highly correlated with adjusting thinner filaments. However, it doesn't have correlation with the diameter of yarn, as the yarns in this type of fabrics are significantly flattered in the final product.

When an increased magnitude of 500x was used, the impregnation was clearly visible, Figure 19. The polyurethane resins/silicone not only glued the spaces between interlacements,

but also those between filaments. Therefore, the coverage of the fabrics causes achieving air impermeability when testing even under relatively high pressure drops (2000 Pa). Depending on the model and type of the fabric, the amount of impregnation and its general picture differed from each other.

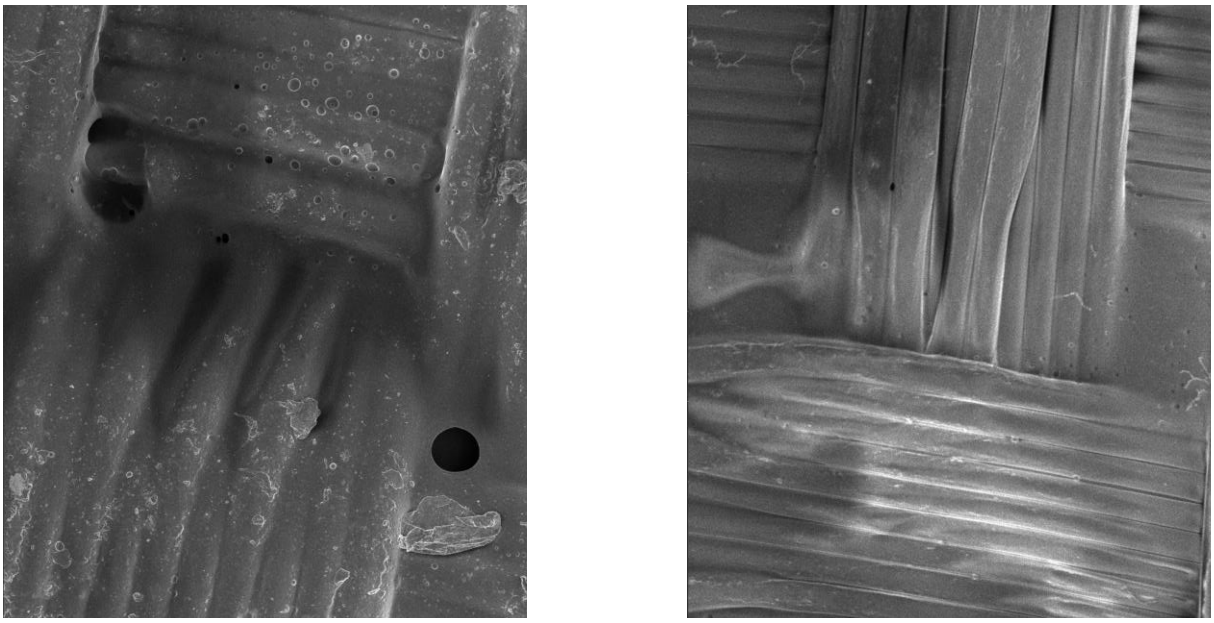

Figure 19. Impregnation on the analyzed samples: a – sample 1, b – sample 5

8. Ageing methods

Aging processes always have an impact on the appearance and performance properties of materials and products.

Fabrics no. 1, 2 and 6 were chosen to be applied to the degradation processes. The selection was caused by the fact, that samples no. 1 and 2 distinguished amongst the remaining samples. Whereas, sample no. 6 represented the group of samples (3 – 8).

Samples no. 9 and 10 were also characterized by different chemical groups and/or weave than the remaining samples. However, these were parachute fabrics and therefore were decided not to be chosen for the further analysis.

The following degradation methods that were applied to the fabrics no. 1, 2 and 6 were listed and described in sections 8.1 – 8.4.

8.1. Heating

High temperatures of 50°C, 60°C and 70°C were applied in the time cycles of 24h, 48h and 72h. The test was performed using the Steinberg SBS-ADO-2000 2170 W 136 l heating device. The method of degradation was chosen to simulate the conditions of improper storage of paragliding equipment, e.g. storing the equipment in a car trunk during hot and sunny summer.

8.2.Freezing

Stirling SU780XLE device was used in order to subject the considered samples to low temperature equal to -30°C in a time of 24 hours. Paraglider/parachute materials can be subjected to low temperatures for example, when an improper storage is done or when parachute high-altitude opening.

8.3.UV degradation

Paraglider wing is highly exposed to the UV radiation. Therefore, the samples were artificially aged in the QUV Accelerated Weathering Tester aging chamber by Q-Lab AATC TM186. The samples were irradiated in conditions similar to natural for a temperate climate according to the PN EN ISO4892-3 [46] standard, based on the Technical Report TR 010 ed. May 2004 "Exposure procedure for artificial weathering". The source of UV radiation were UVA-340 fluorescent lamps equivalent to midday sunlight (months: June, July). The applied conditions were following: intensity 0,76 W/m^2 (measured with lambda = 340 nm); temperature 60°C; time of performing the test 72 h; relative humidity 65%.

8.4.Flexing damage

Damage by flexing was applied according to EN ISO 7854 [47] Standard, Method C (i.e. Crumple/flex method). In this method a rectangular samples (of dimensions of 220 mm x 190 mm) were sewn into a cylindrical shape; whereas the diameter of shape was equal to 64 mm and its height 190 mm. The cylindrical coated sample was placed between 2 moving discs. One of the discs caused twisting of the fabric sample (by rotating on its axis; 200 twists/minute); whereas the other disc compressed the fabric by a pushing motion (152 strokes/minute). This simultaneous actions were repeated 9000 times. The test was performed using Crumple Flex Tester TF117C.

9. Ageing influence on the materials characteristics

9.1.Color stability

A Conica Minolta CM-3600d spectrophotometer (Sony, Tokyo, Japan), with a spectral measuring range of 360 nm –740 nm, was used to analyze the effect of degradation factors on the color stability of aged and unaged samples. In accordance with the PN-EN ISO 105-J01 [48] standard, the change in color and brightness was determined in accordance with the CIE-Lab color space of Equation [49]:

$$dE^*_{ab} = \sqrt{\Delta a^2 + \Delta b^2 + \Delta B^2}, \quad (11)$$

The visual, and sometimes invisible, alteration of the outward appearance can be determined directly by measuring the color change (dE*ab) of their surface. This is one of the most important measurements as the aging begins at the surface of materials. The results obtained during the color change test are presented in the Figure 20.

Ultraviolet aging caused the greatest color change for all 3 – 8 samples, reaching the value of 17.13-20.01. Both of materials no. 1 and 2 presented similar resistance to the aging process as the dE*ab parameter gained 18.21 for sample no. 1 and 16.42 for sample no. 2. On the other hand, the color change of the remaining samples subjected to the UV aging was 4.92 for the sample no. 9 and 3.97 for the sample no. 10. The decreased dE*ab values observed for the filled samples are related to the presence of an increased amount of Si-C, C-N-C, Si-O-Si and Si-CH_3 groups. Research showed that these compounds can absorb radiation on their surface and thus inhibit the ultraviolet aging of material [50]. According to the results, material modification accomplished by combined polyurethane and silicone resulted in a significant increase of resistance to the UV radiation.

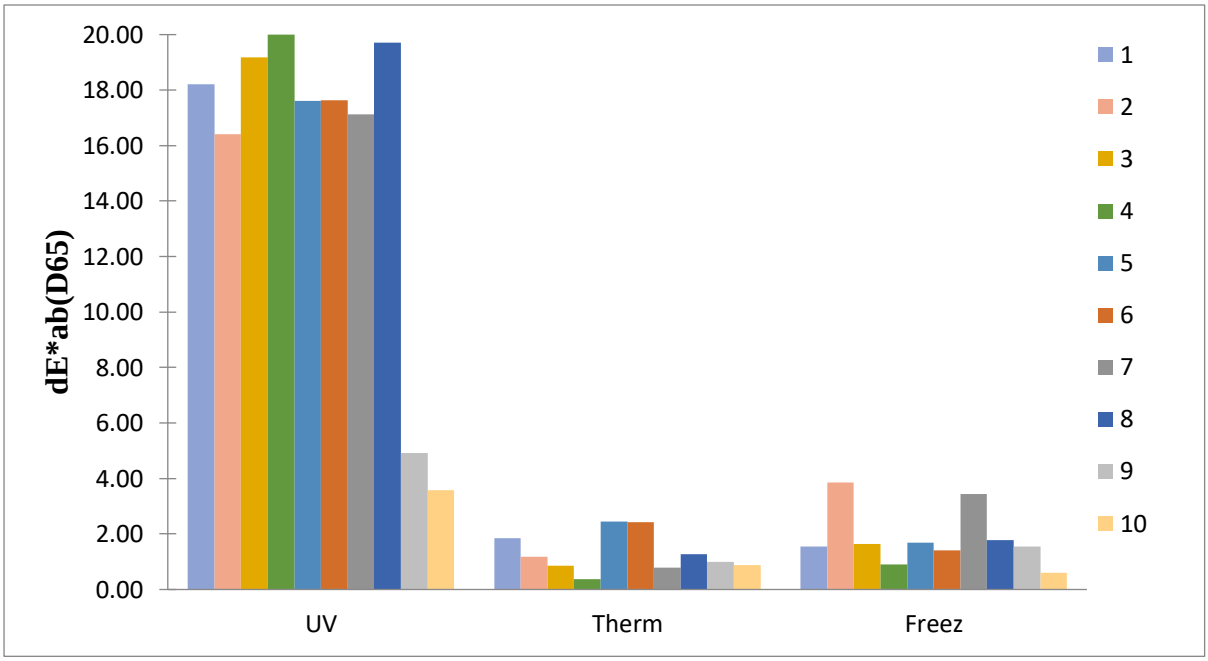

Figure 20. Color change of the analyzed samples
to the UV, Thermal (heating) and Freezing aging.

High temperature showed different relationship to color change; e.g. it had the lowest influence on the color change of the Sample no. 4, dE*ab = 0.38 (whereas, this sample was the most susceptible to the UV radiation). Whereas, samples 9 and 10 were changed at the medium level, when temperature of 70 °C was applied. The greatest color change was observed in case of samples no. 5 and 6 (respectively dE*ab = 2.44; dE*ab = 2.43).

According to the freezing results, the most susceptible were samples no. 2 and 7 (dE*ab around 3.50); whereas the dE*ab parameter was around (but lower than) 2 for the remaining samples. The lowest color change presented the sample no. 10 (dE*ab = 0.61).

However, it was observed that the both, high and low temperatures, did not have noticeable influence on the color of the tested samples, when organoleptic evaluation was performed. According to the literature, the tolerance of the dE*ab is usually 5 [51].

9.2.Air permeability change

The air permeability parameter values of degraded samples were measured using the same methods and device, as these described in Section 7.1.. However, pressure drops of 200 Pa, 1500 Pa, 2000 Pa and 2500 Pa were applied.

The obtained results were compiled in the Table 6. below.

Table 6. Air permeability values representing the considered fabrics subjected to ageing

	Ageing method	**200 Pa**	**1500 Pa**	**2000 Pa**	**2500 Pa**
Sample 1	heating 50°C 24h	0.000	0.000	0.000	0.053
	heating 50°C 48h	0.000	0.000	0.000	0.057
	heating 50°C 72h	0.000	0.000	0.000	0.053
	heating 60°C 24h	0.000	0.000	0.000	0.060
	heating 60°C 48h	0.000	0.000	0.000	0.053
	heating 60°C 72h	0.000	0.000	0.000	0.060
	heating 70°C 24h	0.000	0.000	0.000	0.058
	heating 70°C 48h	0.000	0.000	0.000	0.059
	heating 70°C 72h	0.000	0.030	0.043	0.070
	Freezing	0.000	0.030	0.040	0.059
	UV	0.000	0.040	0.059	0.077
	flexing damage	0.050	0.685	0.865	1.125
Sample 2	heating 50°C 24h	0.000	0.000	0.000	0.125
	heating 50°C 48h	0.000	0.000	0.000	0.103
	heating 50°C 72h	0.000	0.000	0.000	0.107
	heating 60°C 24h	0.000	0.000	0.000	0.103
	heating 60°C 48h	0.000	0.000	0.000	0.107
	heating 60°C 72h	0.000	0.000	0.000	0.100
	heating 70°C 24h	0.000	0.000	0.000	0.118
	heating 70°C 48h	0.000	0.000	0.000	0.108
	heating 70°C 72h	0.000	0.050	0.090	0.270
	Freezing	0.000	0.055	0.080	0.117
	UV	0.000	0.083	0.310	0.430
	flexing damage	1.120	2.655	3.125	3.692
Sample 6	heating 50°C 24h	0.000	0.000	0.000	0.083
	heating 50°C 48h	0.000	0.000	0.000	0.075
	heating 50°C 72h	0.000	0.000	0.000	0.085
	heating 60°C 24h	0.000	0.000	0.000	0.105
	heating 60°C 48h	0.000	0.000	0.000	0.125
	heating 60°C 72h	0.000	0.000	0.000	0.105
	heating 70°C 24h	0.000	0.000	0.000	0.095
	heating 70°C 48h	0.000	0.000	0.000	0.093
	heating 70°C 72h	0.000	0.057	0.088	0.120
	Freezing	0.000	0.045	0.298	0.090
	UV	0.000	0.042	0.060	0.277
	flexing damage	2.050	7.200	9.500	11.600

According to Table 6 and Figure 21, when pressure drop of 200 Pa was applied, only samples damaged by flexing were permeable. Thus, flexing damage has the greatest influence on the air permeability change among all considered aging factors.

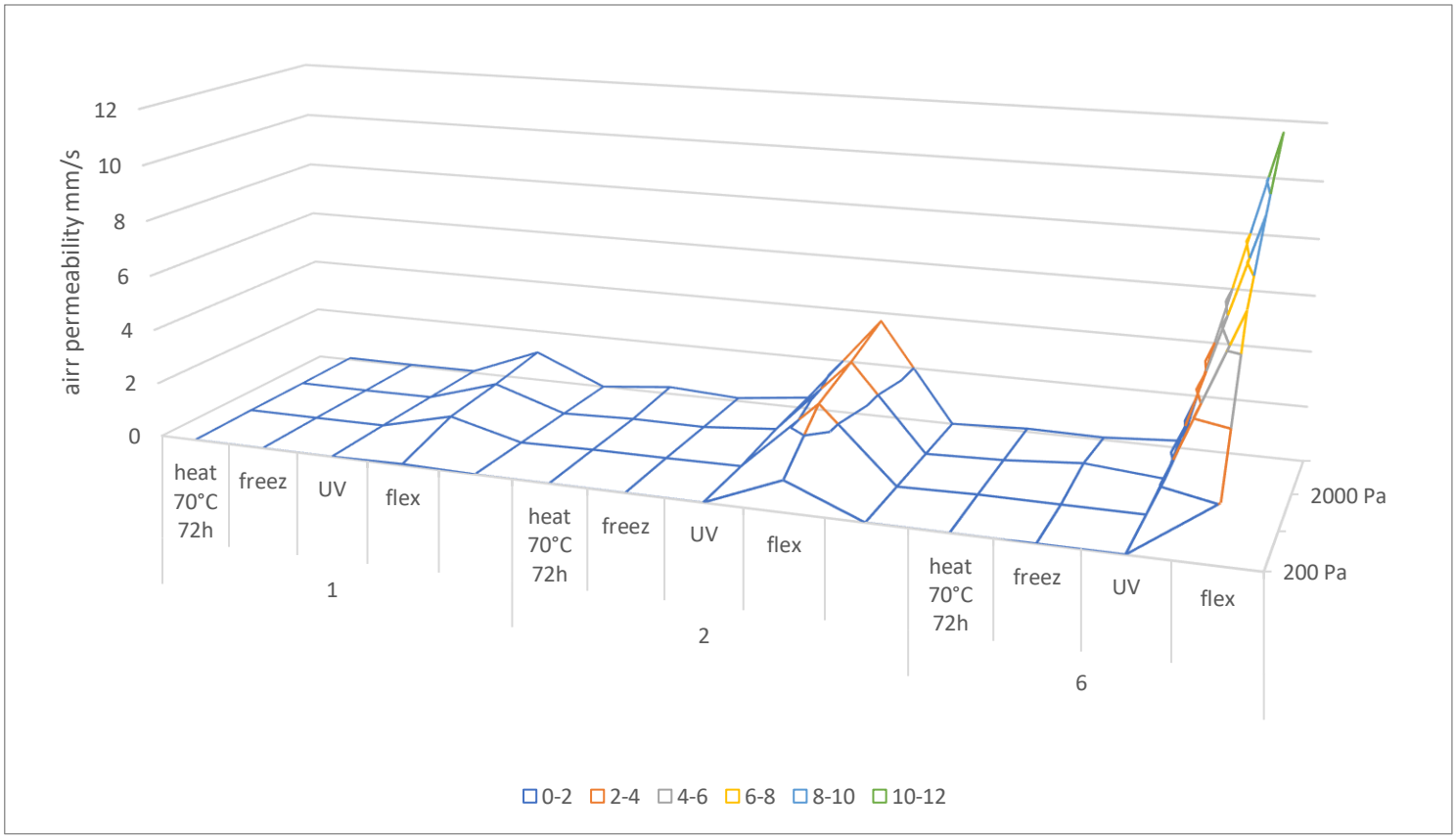

Figure 21. Air permeability parameter of Samples 1, 2, 6 subjected to: heating (70°, 72h), freezing, UV ageing, flexing damage

For fabrics no. 1 and 6, UV degradation had higher influence on the air permeability change compared to temperature factors. When a sample no. 6 was considered, freezing had, however, greater influence than the UV degradation.

When increased pressure drops were applied (1500 Pa – 2500 Pa), the air permeability values of samples subjected to all types of degradation were greater than zero. However, it did not apply to all temperatures and time cycles of heating.

Surface charts presenting the dependences of air permeability values from the applied times and temperatures of heating, as well as the pressure drops were compiled in the Figure 22 below.

Based on the charts it can be concluded, that the most susceptible to this type of ageing, was the material no. 2; whereas the least visible changes in the air permeability value were observed in the case of sample no. 1. Increasing of the time and temperature of heating, as well as the pressure drop, has a significant impact on the obtained permeability values.

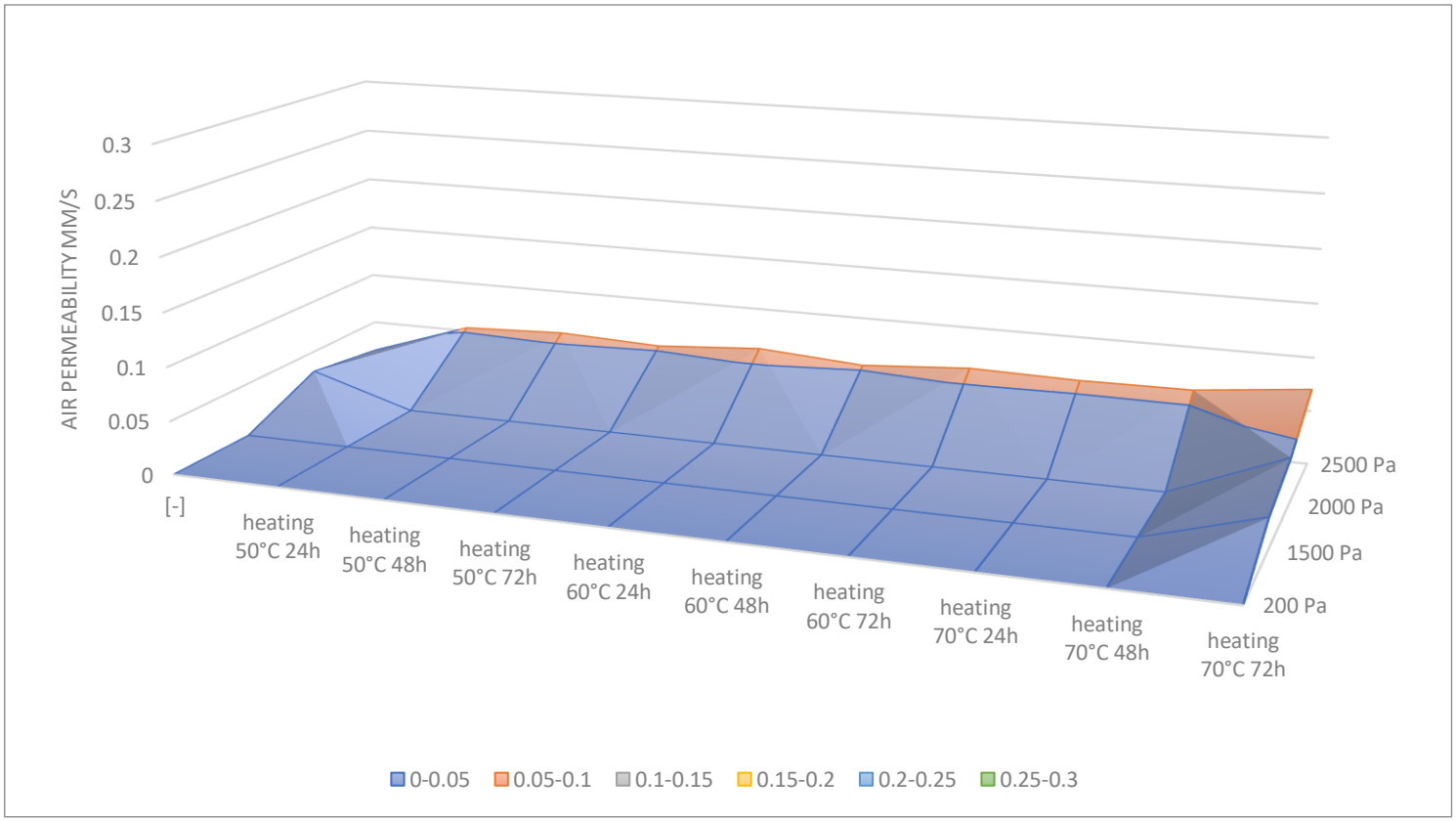
AIR PERMEABILITY MM/S
0.3
0.25
0.2
0.15
0.1
0.05
0
[-]
heating 50°C 24h
heating 50°C 48h
heating 50°C 72h
heating 60°C 24h
heating 60°C 48h
heating 60°C 72h
heating 70°C 24h
heating 70°C 48h
heating 70°C 72h
2500 Pa
2000 Pa
1500 Pa
200 Pa
0-0.05
0.05-0.1
0.1-0.15
0.15-0.2
0.2-0.25
0.25-0.3

a

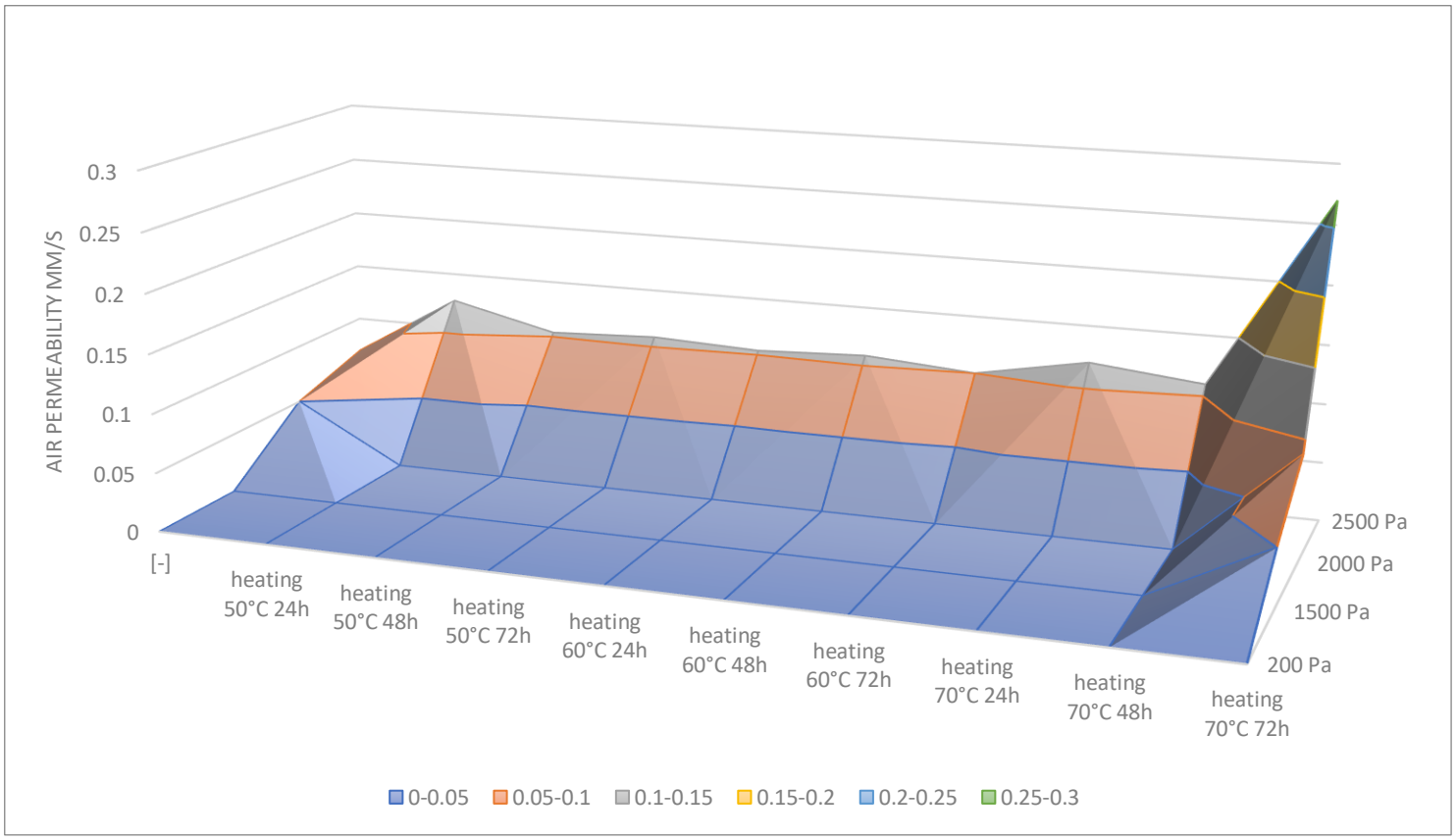
AIR PERMEABILITY MM/S
0.3
0.25
0.2
0.15
0.1
0.05
0
[-]
heating 50°C 24h
heating 50°C 48h
heating 50°C 72h
heating 60°C 24h
heating 60°C 48h
heating 60°C 72h
heating 70°C 24h
heating 70°C 48h
heating 70°C 72h
2500 Pa
2000 Pa
1500 Pa
200 Pa
0-0.05
0.05-0.1
0.1-0.15
0.15-0.2
0.2-0.25
0.25-0.3

b

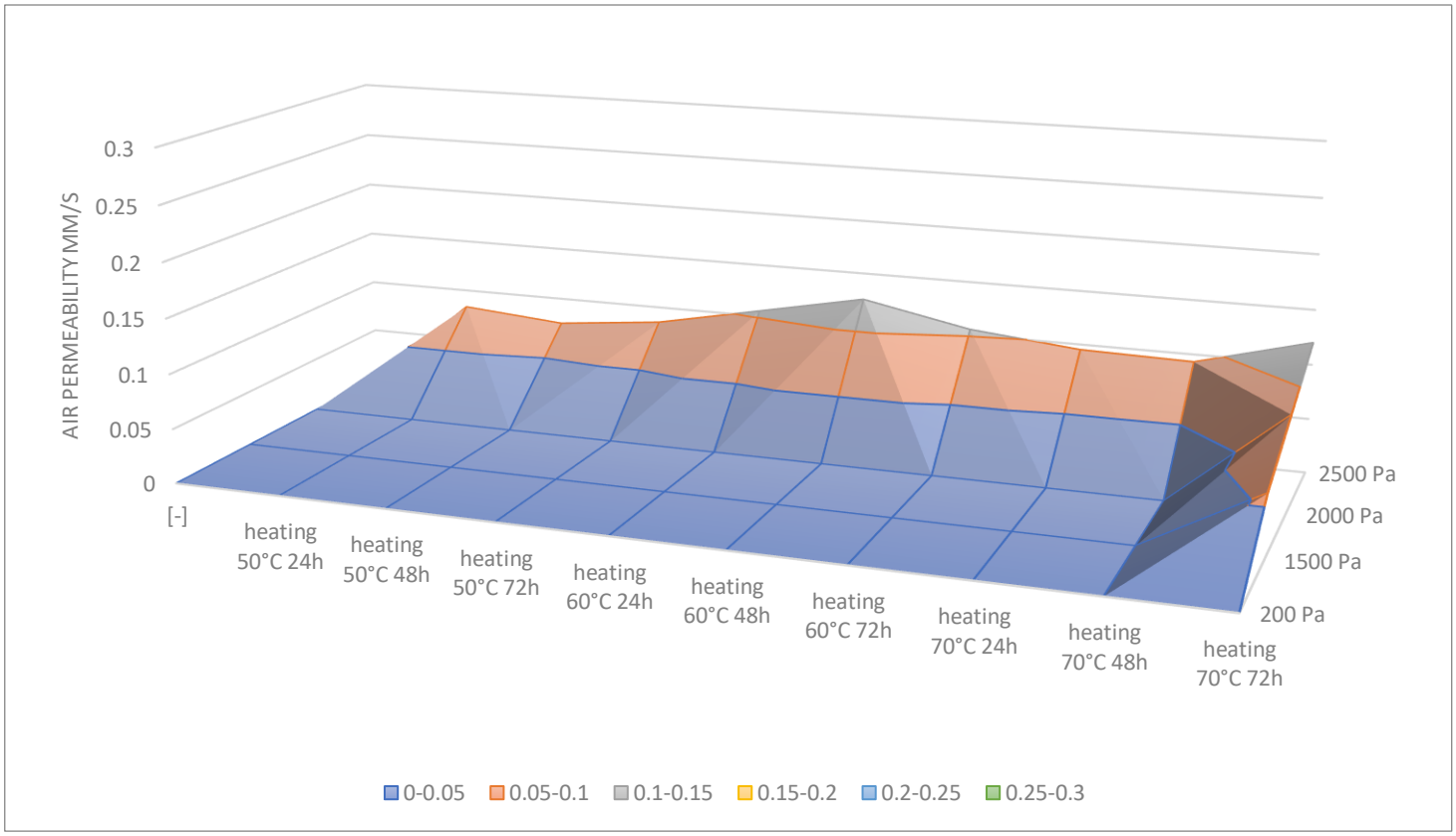

c

Figure 22. Surface charts of the air permeability change in the function of time + temperature and pressure drop acting on material: a – sample no. 1; b – sample no. 2; c – sample no. 6

9.3.Mechanical characteristics change

The tensile properties of fabrics not subjected and subjected to ageing were determined using an Instron device and according to the EN-ISO 13934 [52] standard. The width of the samples was equal to 50 mm, the distance between clamps was 200 mm and the speed of tensile 100 mm/min.

The test results were compiled in the Table 7 and in the Figure 23 below.

Table 7. Tensile test results of the samples subjected to ageing

Sample no.	Direction	[-]		Heating 70º, 72h		Freezing		UV		Flexing	
		F [N]	Ɛ [%]	F [N]	Ɛ [%]	F [N]	Ɛ [%]	F [N]	Ɛ [%]	F [N]	Ɛ [%]
1	Warp	340	21.2	318	23.2	400	30.6	121	10.3	339	21.0
	Weft	325	19.7	270	20.3	351	29.1	80	8.5	321	22.7
2	Warp	470	30.5	429	27.9	459	31.6	306	17.3	466	22.4
	Weft	465	29.9	425	27.4	451	30.4	224	16.3	402	22.4
6	Warp	269	20.6	258	19.3	251	18.6	263	21.1	260	20.1
	Weft	285	22.7	255	19.9	293	23.2	231	18.1	254	16.8

According to the results compiled in the Tables 7, 8 and Figure 21, the greatest influence on mechanical properties had ageing caused by the UV radiation. It was observed especially, when samples no. 1 and 2 were considered (decrease in warp respectively 64% and 35%; in weft respectively 75% and 52%). In the case of sample no. 6 the decrease of the tensile properties was observed, however it was insignificant; i.e. 2% (warp) and 19% (weft).

No significant influence of freezing on the mechanical properties of the considered samples was observed. Moreover, in the case of sample no. 1 subjected to freezing an increase of the obtained values was noticed. The coefficient of variation of tests regarding sample no. 1 not subjected to ageing and subjected to freezing was around 3 N, when tested into the warp direction and around 20 N, when tested into the weft direction. Thus, it can be concluded that the results reflected the actual state.

Flexing damage was expected to have a great influence on the decrease of mechanical characteristics of the considered samples, as it causes significant mechanical damage of threads and impregnation (the air permeability results confirm the above). However, the tensile results did not show this dependence. This is probably caused by the dimensions of the tensed sample, which significantly exceeded the area damaged by flexing. In order to find the actual dependence between flexing damage and breaking force, a single

yarn should be subjected to the test. However, limited access to the fabric samples prevented verification this thesis.

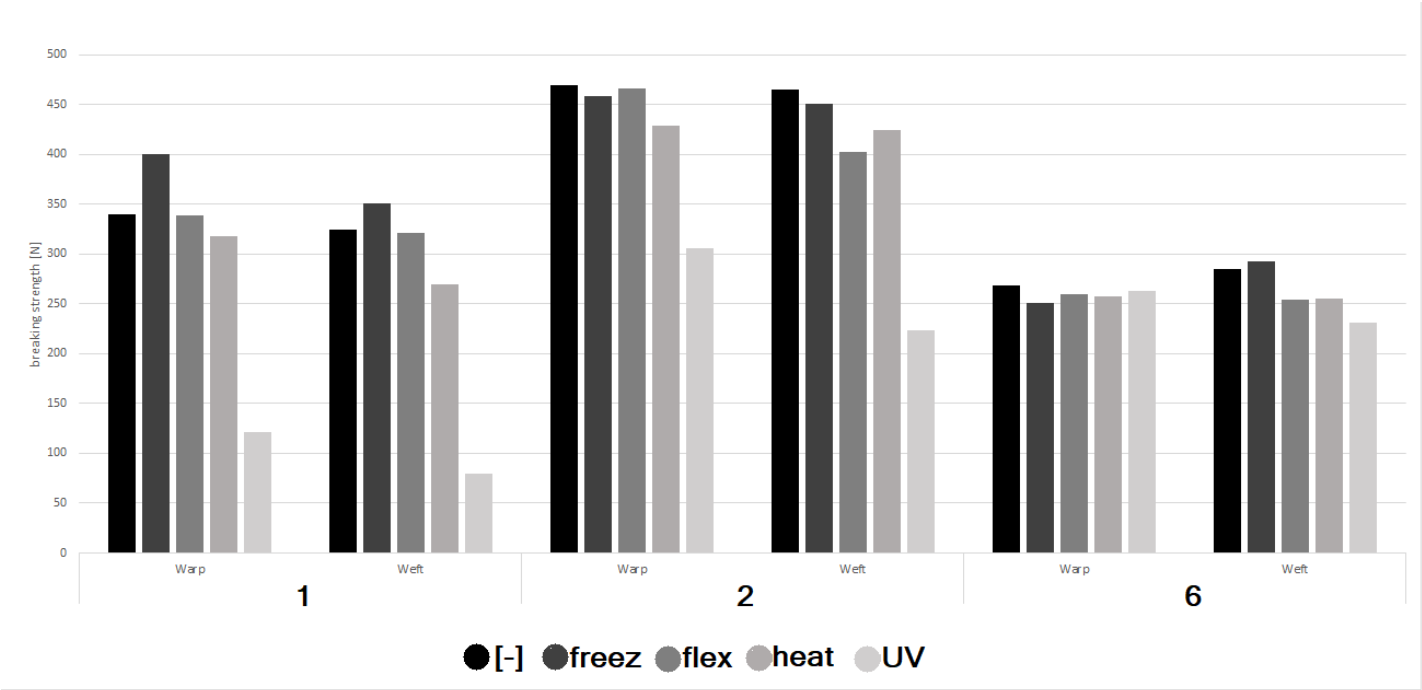

Figure 21. Graph describing the maximal forces during elongation of samples no. 1, 2, 6 not subjected ([-]) and subjected to ageing: Freezing (freez), Flexing (flex), Heating (heat) and UV radiation

Heating had noticeable, but not significant influence on the mechanical characteristics of the tested samples. The decrease of maximal force during elongation was between 6 % – 10 % comparing to the samples not subjected to ageing.

Young's modulus is a mechanical characteristic describing stiffness/elasticity of a considered material, when a force is applied lengthwise. Its formula is the following:

$$E = \frac{\sigma}{\varepsilon} \tag{12}$$

The stress (σ) is described by the force and the area of the sample; the area can determined by the width and the thickness of the sample under testing.

The below graph of load to extension recorded during tensile test is described by a curve, Figure 22. It presents a linear characteristic only in a fragment of it and the linear character does not begin on a starting point of the measurement. The first (nonlinear) part of the considered graph refers to straightening of threads in fabric due to their interlacement [53]. The second (linear) part refers to the actual tensile of the material.

At the same time, the values of Young's modulus which refer to forces above point B were not relevant to the considered case, which could be concluded based on further simulation results. The record applies to sample no 1. Depending on the tested direction, i.e. warp/weft, its stress at point B was in a range of 90 MPa – 100 MPa; whereas FEM analysis showed that maximum stress that was cumulated by the material when applied to paraglider wing during a flight with maximal overload was equal to 29.34 MPa, Table 13 in section 11.4.

Thus, the Young's Modulus was calculated for the A-B section, Figure 22.

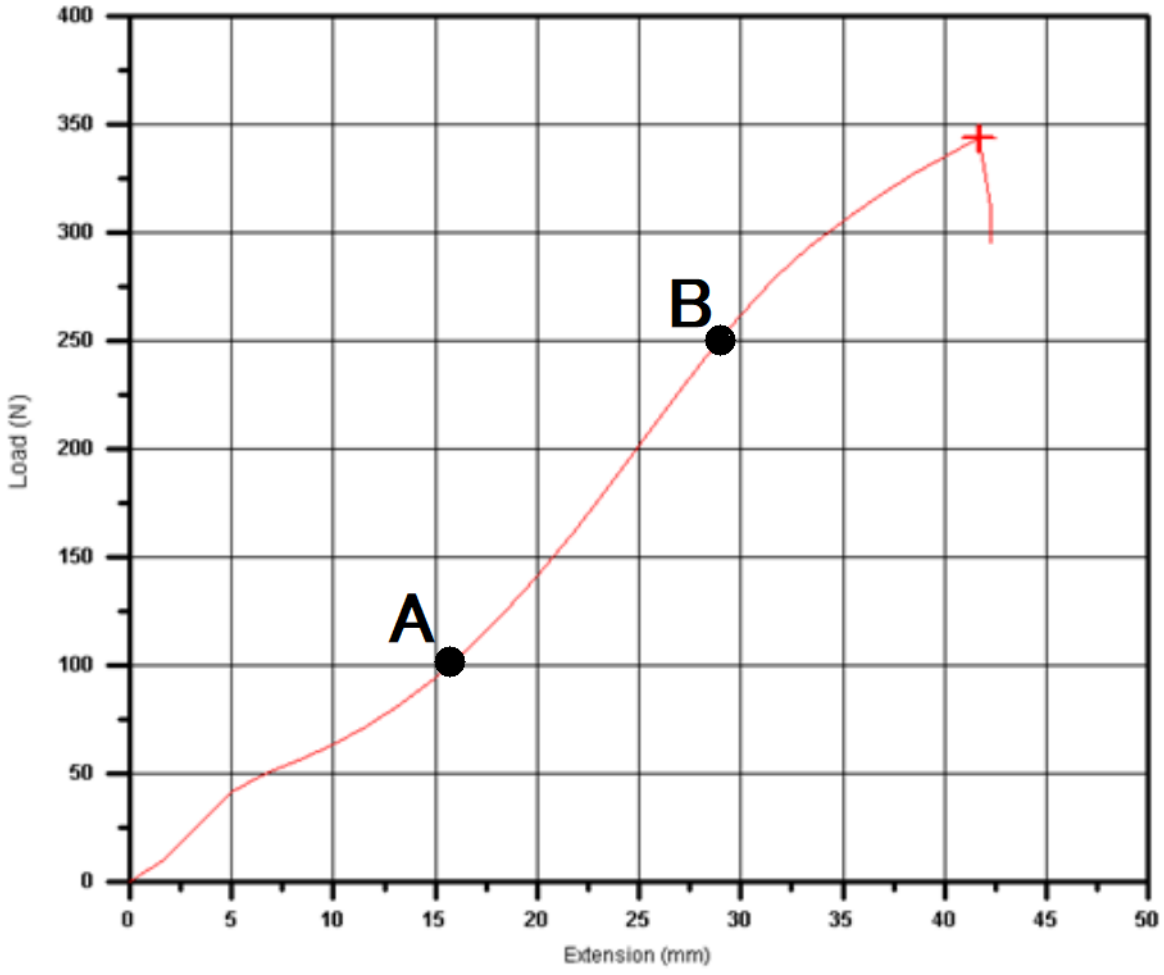

Figure 22. The exemplary graph for calculation of the Young's Modulus (sample 1, warp)

The Young's modulus values that were applying to the analyzed fabrics were determined according to the above presented scheme. They were listed in the Table 8 below.

Based on the values compiled below it can be noticed that they differ when both direction of one type of a fabric are considered. For the analyzed samples, the values of linear elasticity were usually slightly greater for the warp direction; whereas the biggest difference

was observed for the sample no. 2 subjected to the UV degradation (decrease of Young's modulus value into the weft direction was 43 %, when referring to warp). It is due to anisotropic character of woven fabrics. The change can be caused by number of yarns per length unit, use of different type of yarns in different direction of the material, etc.

Table 8. The obtained Young's modulus values

Sample	**E (MPa)**	
	Warp	**Weft**
1	800	644
2	799	653
6	378	355
1 (heating)	748	625
2 (heating)	736	611
6 (heating)	370	342
1 (freezing)	805	800
2 (freezing)	757	541
6 (freezing)	333	370
1 (UV degradation)	355	309
2 (UV degradation)	642	357
6 (UV degradation)	422	333
1 (flexing)	798	652
2 (flexing)	690	623
6 (flexing)	372	417

10. CFD numerical simulations

Based on the research described in the Section 6, a graph compiling pressure change depending on the distance from the leading edge in the symmetry plane was prepared and presented below, Figure 23.

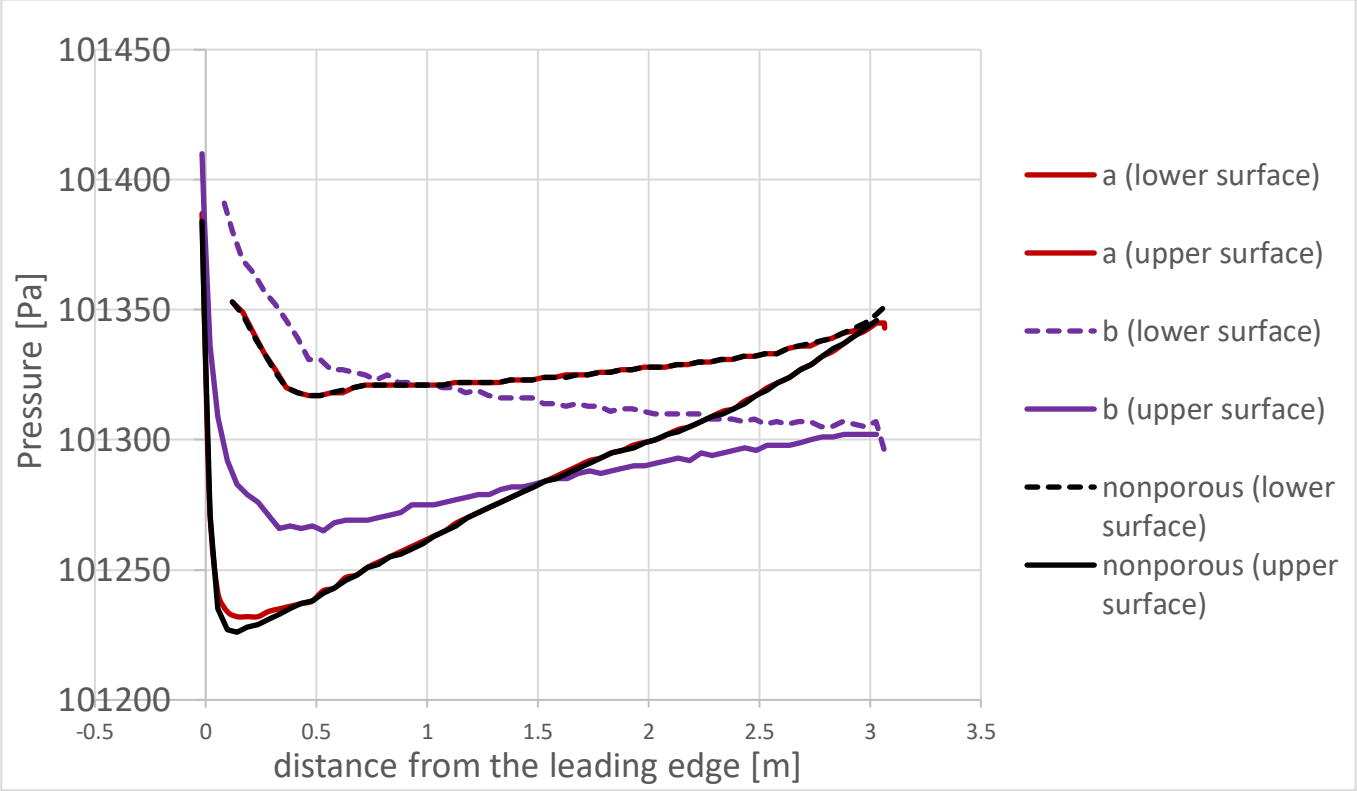

Figure 23. Graph compiling pressure change depending on the distance from the leading edge and the application of covering material (a, b, nonporous) in the symmetry plane

In the cases of materials *a* and *nonporous*, the pressure value (which was equal to 101325 Pa when undisturbed) increased rapidly at the leading edge; it was related to the collision of air with the wing body. Then a large and rapid pressure drop on the upper surface of the wing was observed; this was compliant with the principles of aerodynamics. On the upper surface, the pressure reached about 101230 Pa (for the nonporous cover) and , at distance of 0-0.5 m from the nose; then it increased steadily (exceeding 101325 Pa at distance of 2.5 m from the nose). On the lower surface of the wing, at distance of about 0.5 m from the leading edge, the pressure dropped by only about 15 Pa relative to the pre-set atmospheric pressure, then gradually increased until it reached about 101355 Pa at the trailing edge.

As for the above described cases, an increase of pressure reaching 101405 Pa on the leading edge of the sample b was observed; at the same time the average pressure inside the wing of 101398.35 Pa was recorded. Thus, the paraglider was assessed to be extremely unstable, i.e. the pressure at the leading edge would push the material and therefore disturb the aerodynamic shape.

According to the Figure 23 above and the results described in Section 6, the maximal pressure acting on a covering material of a paraglider wing was equal to 187 Pa (the biggest obtained difference between overpressure created inside the wing and the negative pressure outside of it); it was achieved when nonporous covering material was considered.

10.1. Material air permeability influence on the aerodynamic characteristics of a paraglider – method compiling the actual pressure drop acting on material and porous resistance

Based on the above described observations, it can be concluded that *porous media* (with the use of porous resistance value) is, in fact, a useful tool. However, when the porous resistance value was calculated based on air-permeability tested with the pressure drop of 2000 Pa, the simulation of flight results were suspected to be slightly inaccurate compared to the actual case.

Theoretically, porous resistance calculated based on a pressure drop value should not affect the actual results, when an obtained pressure acting on a material differ compared to the reference pressure based on which pressure resistance was calculated. See formula (9) again; pressure drop is divided by velocity of air penetrating a porous material (obtained in laboratory testing). However, some materials permeate air only when a sufficient pressure acts on them. Thus, it was decided to apply the method compiling the actual pressure drop acting on material and porous resistance for the considered samples in order to obtain more accurate results.

First, a reference case (paraglider covered with nonporous material) should be analyzed by the CFD tool in order to calculate pressure difference acting on a material; then, if needed, porous resistance parameter should be applied to these of analyzed materials, which were characterized by permeability values in accordance to the obtained pressure drop.

For example, in the normal and undisturbed flight conditions ($\alpha = 6°$, $p = 101325$ Pa, $T = 26.85$ °C, $v = 45$ km/h), all the samples no. 1 – 10 can be considered as impermeable (wall boundary condition, when a CFD simulations are performed). It is caused by calculated

maximal pressure difference between a covering material, which is equal to 185 Pa. All the analyzed samples, when tested with a pressure drop of 200 Pa were characterized by air-permeability equal to zero.

However, samples no. 1, 2 and 6 were chosen for the further analysis, including UV, thermal and mechanical degradation of them (see Sections 9 and 10). For some of the aged samples, air permeability parameter increased when tested with a pressure drop of 200 Pa. The calculated pressure resistance values were compiled in the Table 9 below.

Table 9. pressure resistance values according to the pressure drop of 200 Pa – samples no. 1, 2 and 6 after UV, thermal and mechanical degradation

Material	**Air permeability** $[\frac{l}{m^2 \cdot s}]$, pressure drop 200 Pa	**1/β [1/m^2]**
1 (flexing damage)	0.050	$1.12 \cdot 10^{14}$
2 (flexing damage)	0.095	$5.88 \cdot 10^{13}$
6 (flexing damage)	1.061	$5.27 \cdot 10^{12}$

The above obtained pressure resistance values were applied to the new CFD calculations. All: geometry, mesh, general assumptions and steps of the numerical simulations, were consistent with these described in the Section 6.

Additionally, for the cases with the assumption of non-porosity (*wall* boundary condition), i.e. nondegraded samples 1-10 and fabrics no. 1, 2 and 6 subjected to thermal and UV ageing, the following calculations were applied: 1) sensitivity of c_l/c_d ratio and maximal pressure difference value to angle of attack (2° - 12°) with constant velocity of *46 km/h*; 2) sensitivity of c_l/c_d ratio to velocity (30 km/h – 45 km/h) with constant angle of attack 6^o.

10.2. Calculation and results

The convergence was achieved after 1500 iterations. First, small value of Courant number was applied, and it was gradually increased in the course of numerical calculations. Moreover, spatial dicretization method was improved when the calculations were stabilizing. First upwing scheme was applied at the beginning of the numerical analysis; whereas, at the end of it, Third Order-MUSCL was used.

The Third-order discretization scheme is applicable for all types of equations (density/pressure based) and meshes created of all types of elements, what distinguishes this method from the QUICK discretization scheme (applicable only for structural meshes). It is based on the MUSCL (Monotone Upstream-Centered Schemes for Conservation Laws) and combines second-order upwind scheme and a a central differencing scheme [9]:

$$\Phi f = \theta \Phi f_1 CD + (1 - \theta)\Phi f_1 SOU \tag{13}$$

Spatial analysis are more accurate for this method when compared to first- or second-order upwing schemes. It is caused by descreasing numerical diffusion.

The results obtained in the course of numerical calculations were compiled in the Table 10 below. Based on the results it can be concluded that air permeability increase has an impact on the paraglider's aerodynamic characteristics decrease.

Table 10. Results obtained in the course of numerical calculations

Type	**Mass flow rate [kg/s]**	**Lift force [N]**	**Drag force [N]**	**c_l/c_d ratio [-]**
Wall	0	1519.29	115.36	13.17
Sample no. 1 flexing damage	0.003	1391.96	120.10	11.59
Sample no. 2 flexing damage	0.006	1338.12	121.98	10.97
Sample no. 6 flexing damage	0.071	1072.00	128.34	8.35

According to Table 10., the best characteristics presented paraglider covered with an air-impermeable material (when testing with a pressure drop of 200 Pa); i.e. paraglider covered with undegraded materials no. 1 – 10, and materials no. 1, 2 and 6 subjected to thermal and UV ageing. Its c_l/c_d ratio was equal to 13.17, with lift force equal to 1519.29 N and drag force of 115.36 N. The pressure distribution over the wing was presented in the Figure 24 below.

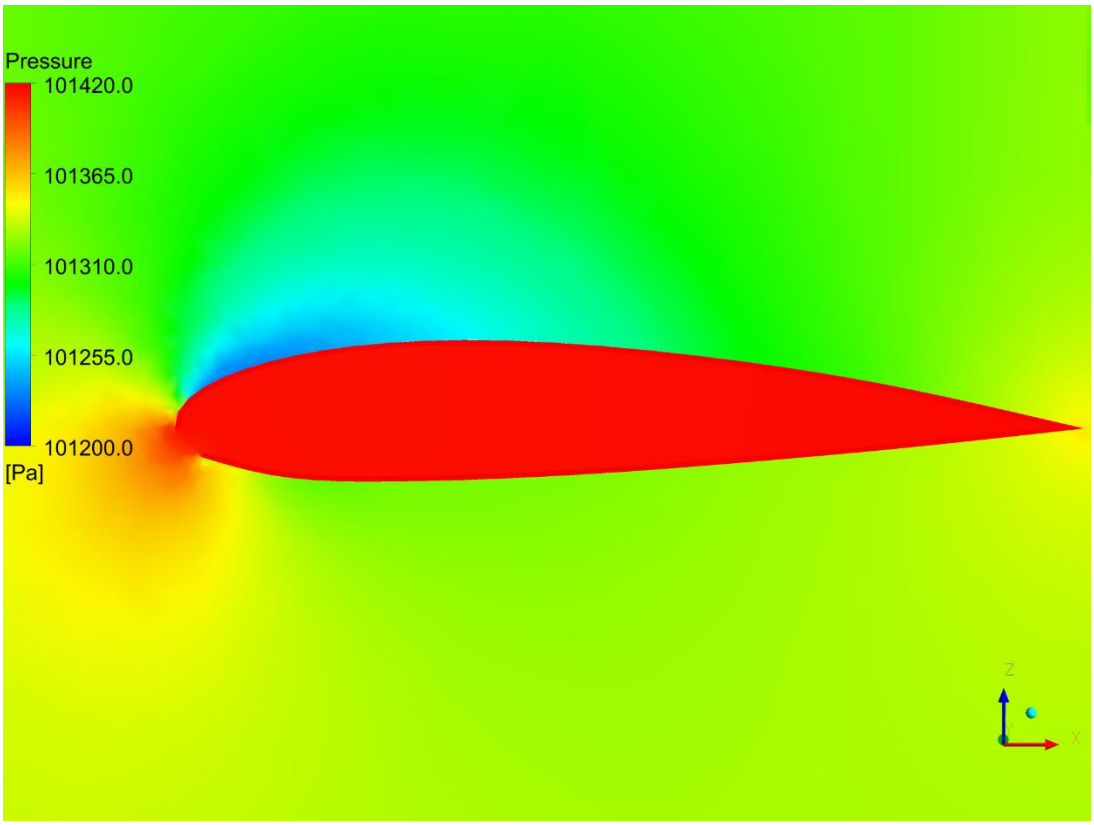

a

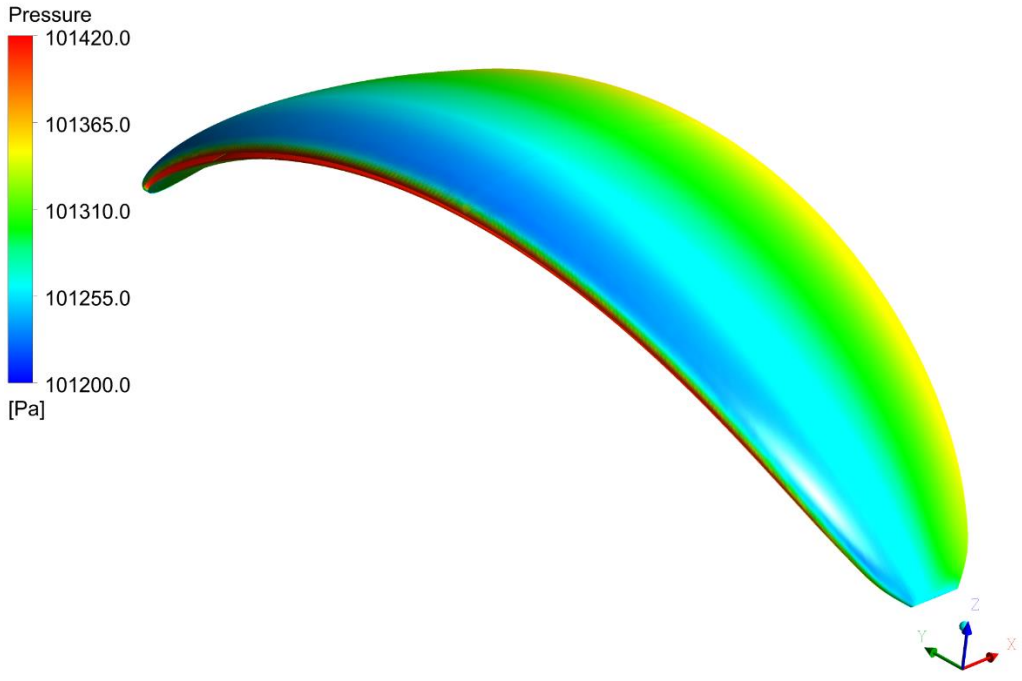

b

Figure 24. Pressure distribution over paraglider covered with an air-impermeable material (when tested with a pressure drop of 200 Pa); i.e. paraglider covered with undegraded materials no. 1 – 10, and materials no. 1, 2 and 6 subjected to thermal and UV ageing

Based on the pressure distribution in the Figure 24. on the previous page, it can be noticed that an overpressure at the leading edge of the paraglider was created. It was caused by the collision of the air streams with the flying object. The aerodynamic shape of the paraglider caused the pressure to have its drop at the upper surface of the wing. It secured creating of the lift force. The aerodynamic shape was possible to achieve by creating an overpressure inside the wing by air entering vents. Summarizing, the pressure distributions presented above are compatible with the numerical results compiled in the Table 10.

Paraglider covered with materials no. 1 and 2 subjected to the flexing damage presented slightly decreased characteristics. Compared to the above described case, lift force decreased (127.33 N when covered with material no. 2 subjected to flexing damage, 181.17 N when covered with material no. 6 subjected to flexing damage). Also, drag force increasement was observed (4.74 N and 6.62 N respectively). The forces values change influenced also values of the c_l/c_d ratio. They were respectively equal to 11.69 and 10.97. Pressure distribution over a paraglider covered with material no. 1 subjected to flexing was presented in the Figure 25 below. As the pressure distribution over paraglider covered with material no. 2 after flexing was not possible to be distinguished organoleptically compared to the other case, it was not compiled below.

According to Figure 25, the general conclusions can be compatible with these describing Figure 24 above. However, it can be noticed that in this case, the pressure drop was characterized by a pressure gradient (the border between the wing and surrounding it air was dissipated, not sharp as in the previous case). It is caused by the porosity of the covering material. Moreover, in the previously described case, the pressure on the upper surface had its sudden drop, then slightly increased (the color changed into blue, green and yellow). In the picture below, the increasement of pressure after its drop is slower (the color changed only into blue and green).

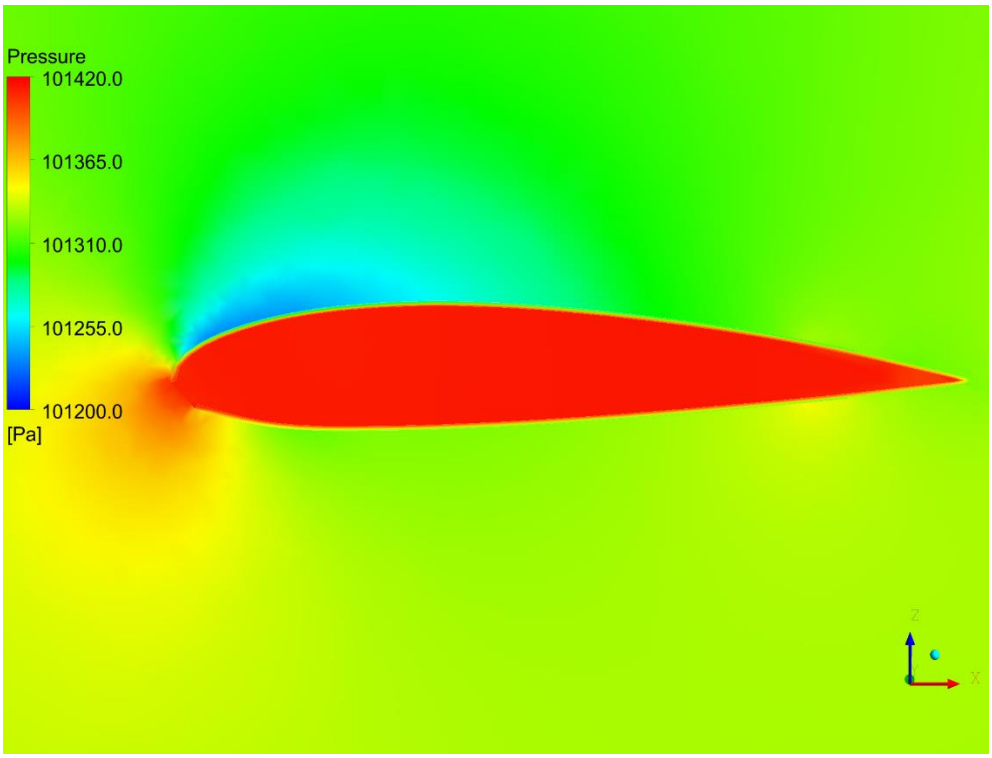

a

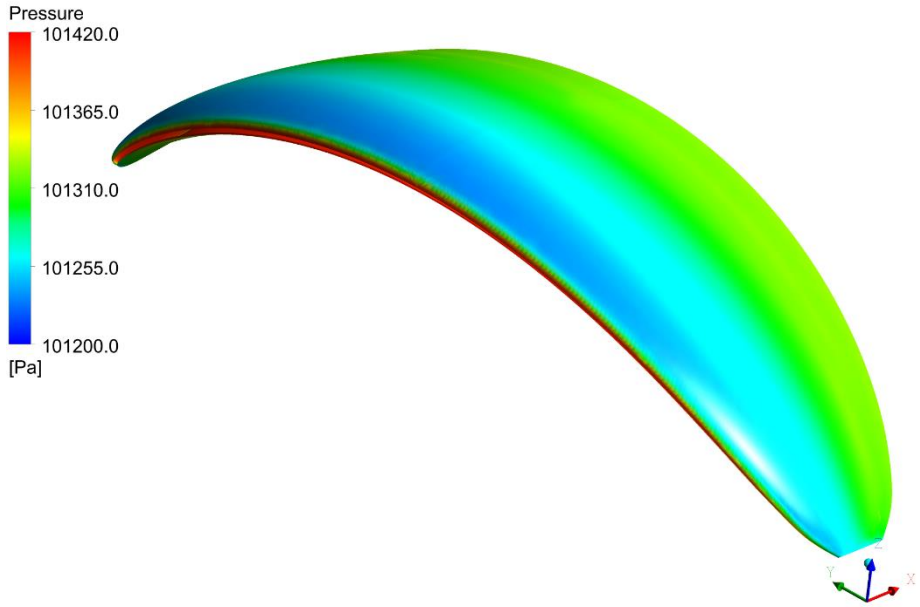

b

Figure 25. Pressure distribution over paraglider covered with material no. 1 subjected to flexing damage

Aerodynamic characteristics of a paraglider covered with material no. 6 subjected to flexing were significantly decreased compared to the above described cases. Its c_l/c_d ratio was equal to 8.35, which is 4.35 less than the value regarding paraglider covered with an impermeable

fabric. However, based on the pressure distribution over the paraglider (Figure 26 below), it was assessed to remain stable at flight. The pressure inside the wing was unevenly distributed, but still secured maintaining the aerodynamic shape of a paraglider; it was also higher than overpressure at the leading edge on the outer surface of the paraglider – thus, maintaining of an aerodynamic shape of a paraglider would be undisturbed by pushing the nose to the inside of an airfoil. Moreover, the negative pressure was created on the upper surface, which secured the creation of the lift force.

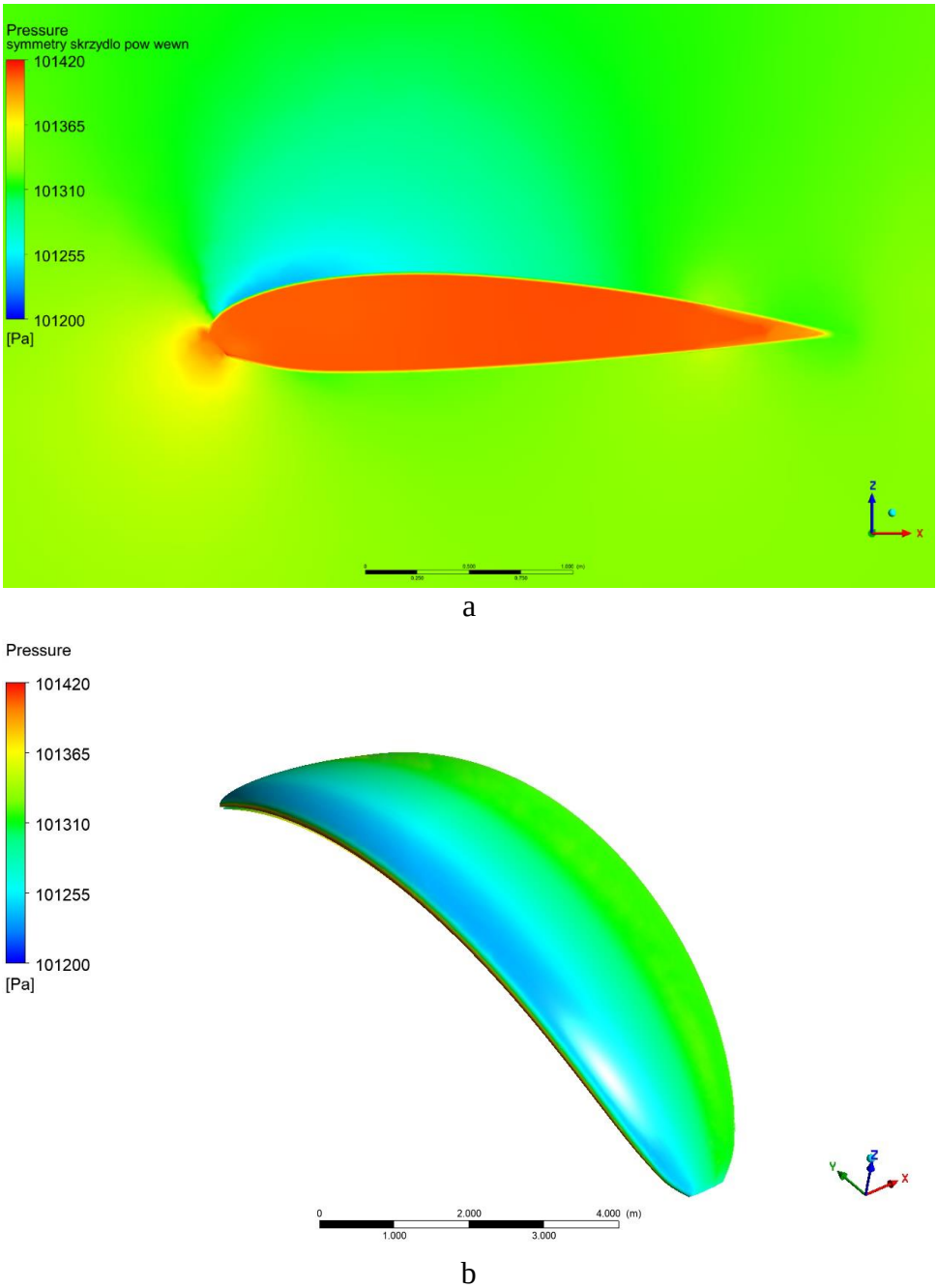

Figure 26. Pressure distribution over paraglider covered with material no. 6 subjected to flexing damage

Based on all the pressure distributions presented above (Figures 24 – 26), all the considered materials could be applicable to flight, when only the air permeability parameter is considered. However, a significant decreasement of aerodynamic characteristics is observed when damaged materials are considered. Thus, air permeability can not be the only parameter indicating the safety of a paraglider, as e.g. deformation, break of a material also can result in dangerous situations in flight.

In the picture below, streamlines of velocity as a variable were compared for two cases – paraglider covered with fabric no. 1 subjected to the flexing damage and paraglider covered with fabric no. 6 subjected to the flexing damage, Figure 27.

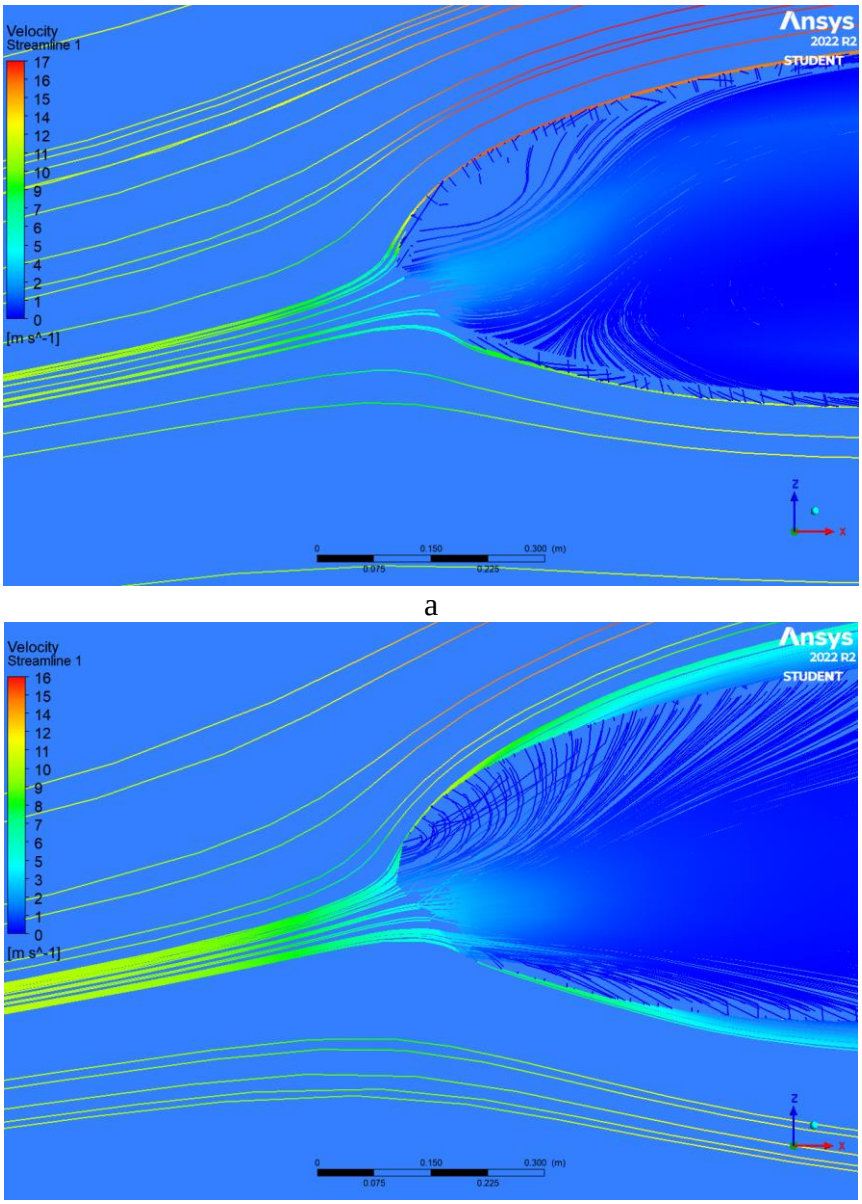

a

b

Figure 27. Streamlines in proximity of paraglider inlet:
a – fabric no. 1 subjected to flexing damage, b – fabric no. 6 subjected to flexing damage

Based on the picture, it can be observed that porosity of a material caused the particles to permeate through the paraglider coverage. However, in the first case, it was insignificant and almost did not influence the streamlines track around the paraglider on the lower and the upper surface. The stream of air of an increased velocity were observed on the upper surface boundary layer (in the immediate vicinity of the contact boundary between the material covering and the surrounding air, see Figure 27a). Whereas, the increased permeability of fabric no. 6 subjected to flexing damage disturbed the track of streamlines around the wing. An increased velocity streamlines appeared at a greater distance from the upper surface; moreover, the velocity was decreased compared to the previous case. Thus, it affected in decreasing of the lift force and increasing in the drag force values, Figure 27b.

As mentioned above, for the cases with the assumption of non-porosity, calculations of sensitivity of c_l/c_d ratio and maximal pressure difference value to angle of attack (2° - 12°) with constant velocity of 46 km/h, as well as sensitivity of c_l/c_d ratio to velocity (30 km/h – 46 km/h) with constant angle of attack 6° were performed.

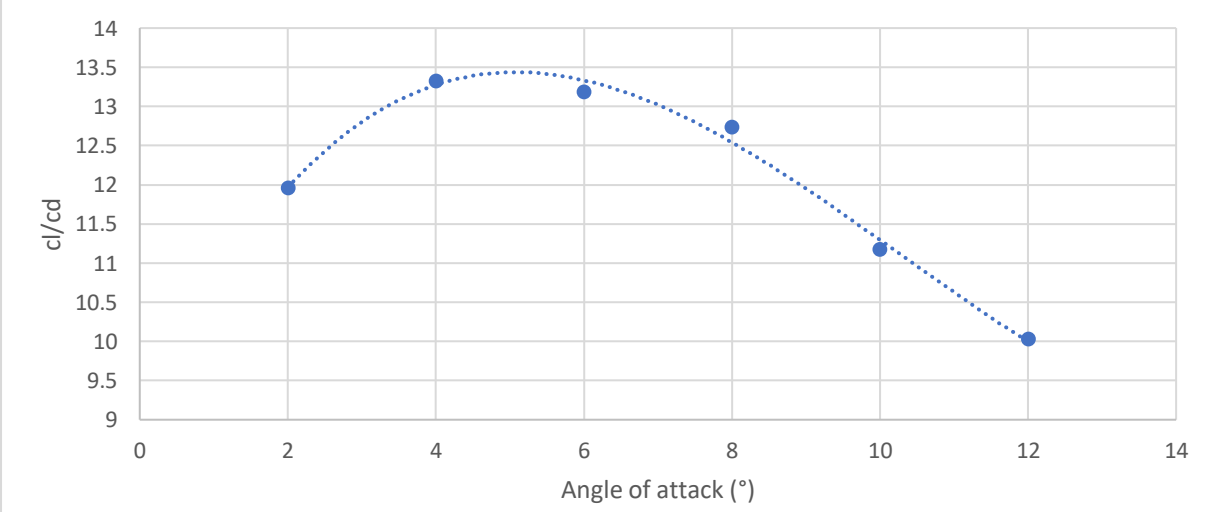

Figure 28. Sensitivity of c_l/c_d ratio to angle of attack

The c_l/c_d ratio, in addition to the geometry of the wing, also depends on the orientation of the wing relative to the direction of flight (angle of attack α), Figure 28.

The minimum drag force occurs in the case of an airfoil with an angle of attack equal to zero. The drag force is then theoretically equal to zero. Practically, it has a minimal value, which results from the movement of the wing and the friction of the air against the wing

surfaces. The more the angle of attack of the airfoil increases (regardless of the upward or downward direction, assuming a positive or negative value), the greater the drag force.

On the other hand, the more the wing is directed upwards relative to the incoming air streams, i.e. the greater the positive value of the angle of attack, the greater the lift. Its value increases until it reaches a maximum, which causes a rapid decrease of the lift and varies depending on the airfoil shape. In the case of the geometry under consideration, it was not achieved for α=12º (thus, the maximal value is not known).

Both of these factors affected the change in the pressure distribution around the paraglider, Figure 29 below. It can be mainly observed, when negative pressure above the wing is considered. The drop of the pressure was significantly greater, than in the previously considered cases.

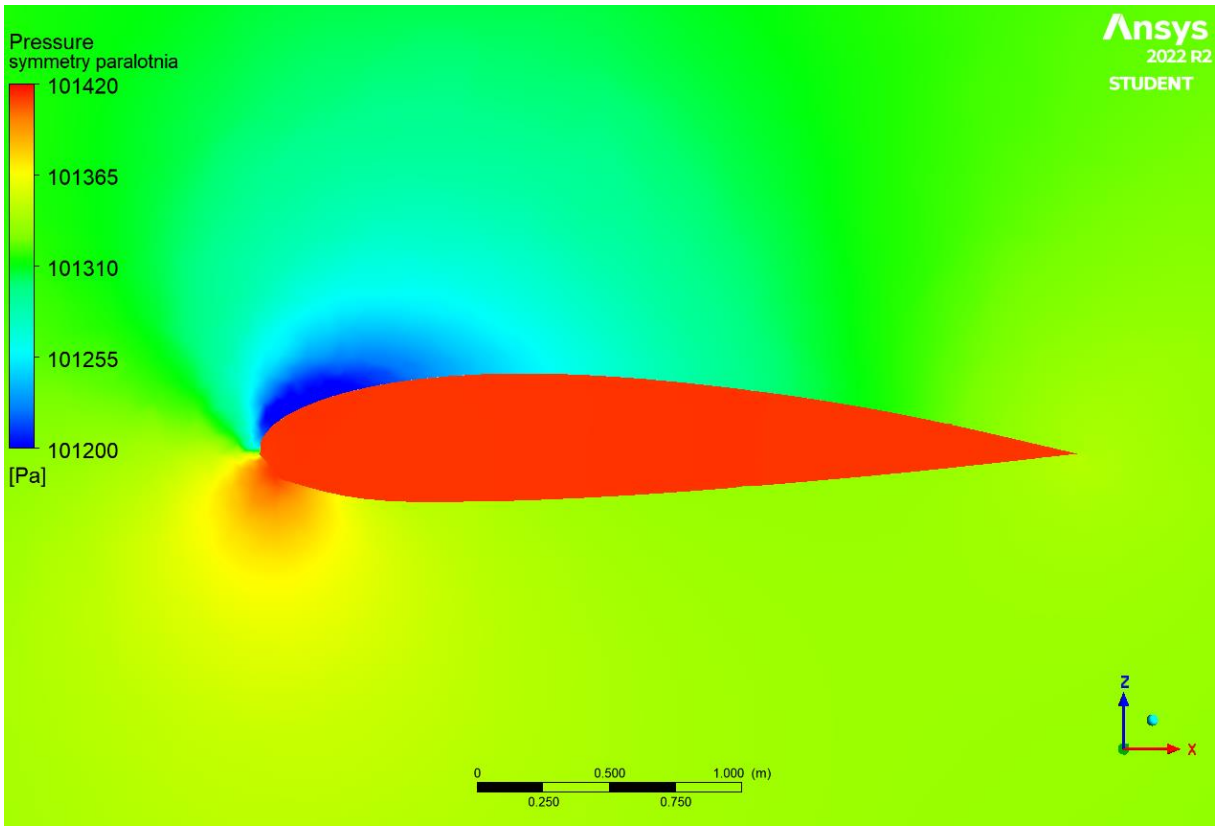

Figure 29. Pressure distribution over a paraglider wing in a symmetry plane;
α = 12°, v = 46 km/h

Calculations of sensitivity of c_l/c_d ratio to velocity with constant angle of attack 6º were performed for velocity range applicable to the considered type of flying object, i.e. 30 km/h to 46 km/h. It can be observed, that the greater the velocity, the greater the value of c_l/c_d of the considered wing; the characteristic is linear, Figure 30 below.

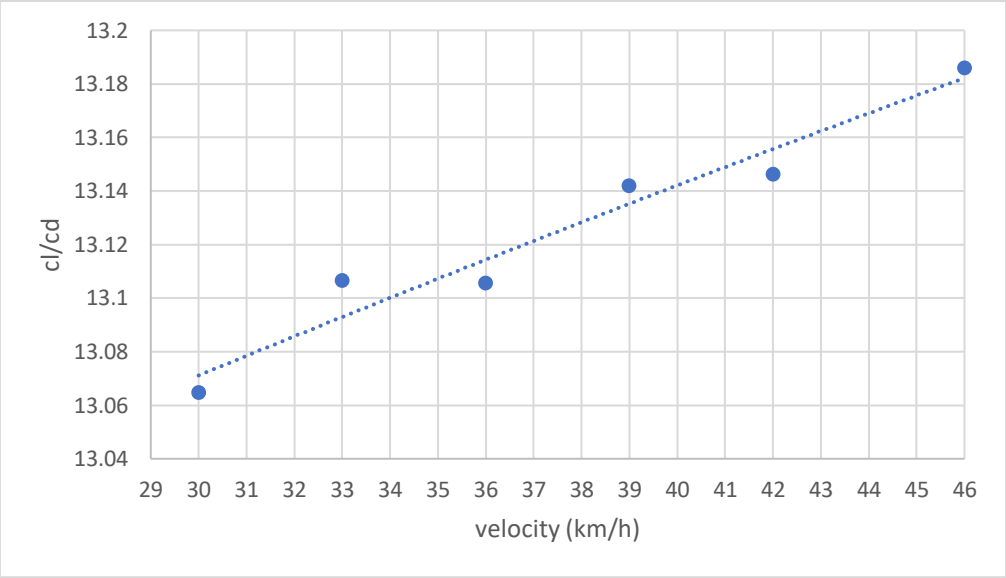

Figure 30. Sensitivity of c_l/c_d ratio to velocity (30 km/h – 46 km/h)

11. FEM numerical simulations

Stress, strain and deformation distributions over 3D model of a paraglider were determined using the ANSYS Structural program and the finite elements method (FEM).

11.1. Maximum overloads determining

The main sources of loads acting on a paraglider moving in the air are: 1) Aerodynamic pressure acting on the bearing surfaces; 2)Acceleration field: gravitational acceleration, accelerations due to pilot action (maneuvers), accelerations caused by gusts.

The distribution of aerodynamic pressures causes aerodynamic forces to act on the covering materials of a paraglider. The acceleration field is the source of body forces.

Please notice, that the lower air permeability of a considered material, the higher internal forces it is subjected to. It is caused by the more contrasting pressure distribution over the material. According to the results described in the previous section, it can be concluded, that the maximal pressure acting on a material differ depending on the flight conditions, see Figure 29. Pressure acting on a material is indicated by pressure difference between two sides of a material.

Thus, a graph compiling sensitivity of pressure acting on a material to angle of attack was presented below, Figure 31.

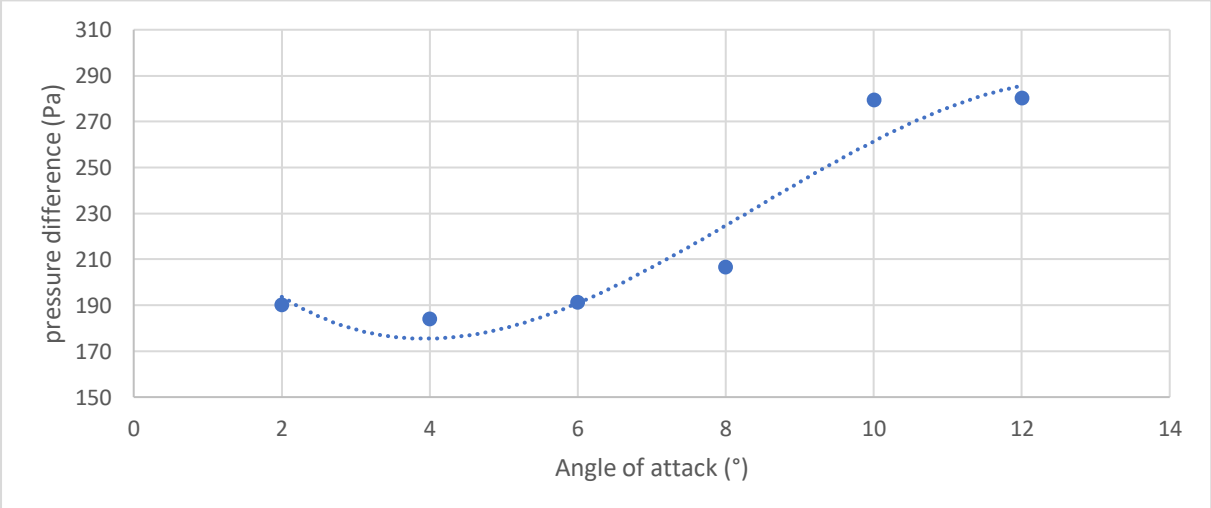

Figure 31. Sensitivity of pressure acting on a material to angle of attack

Based on the graph above, the maximal obtained pressure acting on a material was equal to 280.3 Pa, when the flight conditions were: v = 45 km/h and α = 12°. It is now assumed as pressure creating the highest tensions acting on a material during an undisturbed

flight. However, a flying object can be also subjected to increased overloads; they can be caused by e.g. maneuvers of a pilot, gusts, etc. All the mentioned can affect the pressure distribution and thus tensions inside the considered materials.

Thus, when the most extreme cases are analyzed, pressure acting on a material during the normal flight conditions (assumed to be v = 45 km/h and α = 6°) is multiplied by a maximal possible overload.

The distribution of aerodynamic pressure causes paraglider to be subjected to aerodynamic forces. When determining the loads acting on the object, lift and body forces acting in the same direction as the lift force are considered. The forces acting in remaining directions are much smaller and have a negligible effect on the structural calculations.

When determining the values of loads that can act on a flying object, a dimensionless load factor l_f [54] is used:

$$l_f = \frac{L}{L_0} = \frac{L}{Q} = \frac{L}{m \cdot g} \tag{14}$$

The maximal expected overload can be determined by e.g. flight envelope or results obtained by an electromechanical flight data recorder.

In the steady level flight of the paraglider, the load factor is equal to 1. In the first step of determining the load envelope, the minimum (paraglider filling with air) and maximum (possible to achieve by a paraglider) speed range should be marked on the graph. In the analyzed case, v_{min}=10 km/h and v_{max} = 47 km/h.

In the next step, a line corresponding to the maximum maneuvering loads is marked on the graph. They occur when the pilot, flying at a certain speed, causes the paraglider to reach the angle of attack corresponding to the maximum lift force. Then [54]:

$$l_{f\,MAN}(v) = \frac{L_{,MAN}(V)}{m \cdot g} = \frac{\rho S c_{l,MAX}}{2mg} \cdot v^2 \tag{15}$$

For the considered wing, the wing area in projection is S = 21 m^2, the maximum lift coefficient is $c_{l,MAX}$ = 1.54, and the maximum take-off weight is m = 95 kg. The calculations assume standard air density at sea level ρ = 1.226 kg/m^3.

The last factor affecting the acceleration field is the turbulence of the atmosphere. When the paraglider is subjected to a vertical (updraft) gust, the instantaneous angle of attack increases and consequently the lift and load factor increase.

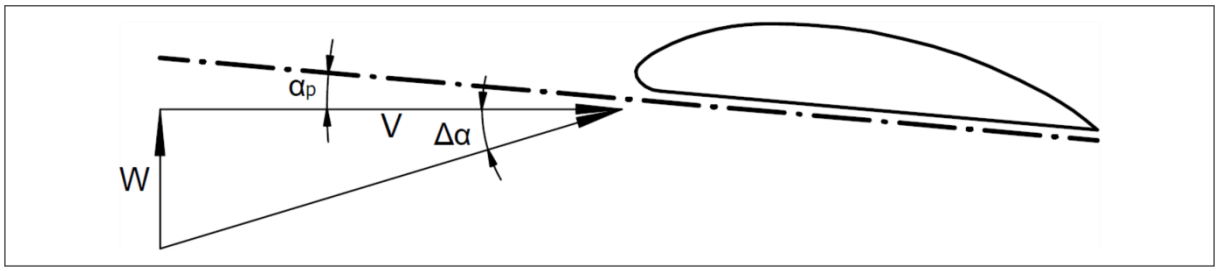

Figure 32. Change of flow parameters due to updraft, thermal column, etc.

The initial speed is v and the initial angle of attack is α_p. Under the influence of the updraft gust of a velocity W, the resultant flow around velocity changes and the angle of attack increases by the value Δα, Figure 32 above..

In the literature [54], the following relationship can be expressed by the load factor, the flight velocity and the velocity of updraft gust:

$$l_f = l_{f0} + \frac{\rho S}{2Q} \cdot \frac{dc_l}{d\alpha} \cdot \eta W \cdot v \tag{16}$$

The $\frac{dc_l}{d\alpha} = 0{,}1\frac{1}{deg} = 5{,}73\frac{1}{rad}$ derivative was used in the calculations (it is correlated with the characteristics $c_l=f(\alpha)$ of the applied wing). According to the formula proposed in [54], in the analyzed case the gust mitigation coefficient was equal to η = 0.1. According to [54], an updraft of a velocity of W = 7.5 m/s was considered. For the above data, the maximum value of the load factor equal to l_f = 3.8 was obtained (when a velocity of the paraglider of v = v_{max}=47 km/h was considered).

The Figure 33. below shows the load envelope (red line). The points within the envelope are the possible flight states (loads that can be obtained at a given velocity). Moreover, at a given flight speed, an updraft gust of a velocity of W = 7.5 m/s can cause overloads.

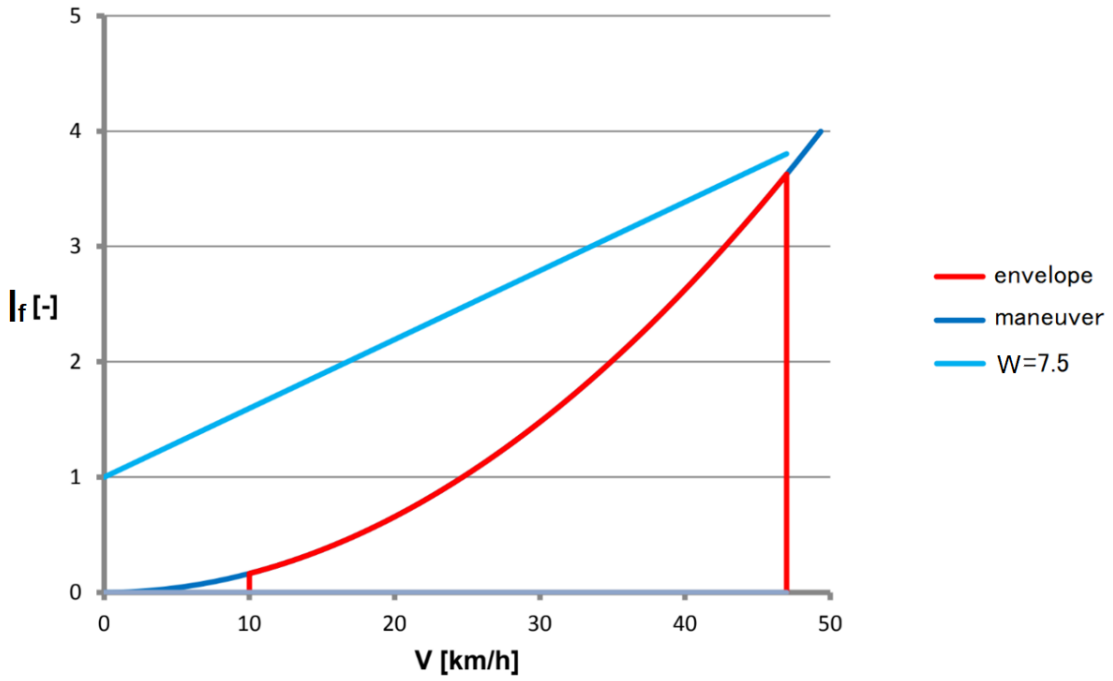

Figure. 33. Flight envelope

As can be seen in the Figure 33 above, in the analyzed case the maximum load factor resulting from the action of the gust was equal to $l_{f,max}$=3.8.

As mentioned above, information regarding overloads during a flight can be collected by electromechanical flight data recorders. According to a record of opening a wing-type parachute, achieved load factor was around 5.6 (the trade name of the parachute cannot be mentioned here due to trade secret). Paragliders are not expected to be subjected to as great overloads as parachutes. However, in fact, they are flying objects with no rigid structure (aerodynamic shape is achieved by overpressure of air filling the wing); thus, the maximum load factors can be increased compared to those estimated with the load envelope. Therefore, overload of 5.6 was assumed for the further structural calculations.

As mentioned above, during an undisturbed flight an impermeable covering material was subjected to a pressure acting on it, equal to 187 Pa. When multiplied by the assumed load factor, the maximal pressure drop of 1047 Pa was implemented for the structural analysis. Therefore, the air permeability parameter was reconsidered, in accordance to the pressure drop of 1500 Pa.

Pressure distributions over a paraglider covered with impermeable materials (undegraded samples no 1 – 8 and 10), as well as materials no. 1, 2 and 6 subjected to UV degradation

and freezing were chosen for the further analysis. The porous resistance values were calculated and compiled in the Table 11 below.

Table 11. The obtained porous resistance values

Material	**Air permeability** $[\frac{l}{m^2 \cdot s}]$, pressure drop 1500 Pa	**v [m/s]**	**1/β [1/m^2]**
1 (Heating 70°C 72h)	0.030	0.000030	$1.4 \cdot 10^{15}$
2 (Heating 70°C 72h)	0.050	0.000050	$8.38 \cdot 10^{14}$
6 (Heating 70°C 72h)	0.057	0.000057	$7.40 \cdot 10^{14}$
1 (Freezing)	0.030	0.000030	$1.4 \cdot 10^{15}$
2 (Freezing)	0.055	0.000055	$7.62 \cdot 10^{14}$
6 (Freezing)	0.045	0.000045	$9.32 \cdot 10^{14}$
1 (UV)	0.040	0.000040	$1.05 \cdot 10^{15}$
2 (UV)	0.083	0.000083	$5.03 \cdot 10^{14}$
6 (UV)	0.042	0.000042	$1.01 \cdot 10^{15}$
1 (Flexing)	0.685	0.000685	$6.12 \cdot 10^{13}$
2 (Flexing)	2.655	0.002655	$1.58 \cdot 10^{13}$
6 (Flexing)	7.200	0.007200	$5.82 \cdot 10^{12}$

When an initial CFD calculations were applied, it was noticed that some differences regarding the porous resistance parameter were too small to be considered, i.e. the results were alike. Therefore, for the permeable cases only three representative flows over paraglider covered with a permeable material were analyzed in order to export the pressure distribution for the FEM analysis. It corresponded to the following groups: (1) samples no. 1, 2, 6 subjected to heating, freezing and UV degradation; (2) samples no. 1, 2 subjected to flexing degradation; (3) sample no. 6 subjected to flexing degradation.

Maximal pressure acting the upper and lower surfaces of the fabrics under study referring to the symmetry plane were compiled in the Table 12 below.

Table 12. Pressure difference changes on the upper and lower surfaces of the considered materials in the symmetry plane (when maximal load factor is applied)

Samples: 1, 2, 6								
Distance from the leading edge	**0.125 m**	**0.500 m**	**1.000 m**	**1.500 m**	**2.000 m**	**2.500 m**	**2.750 m**	**3.000 m**
Upper surface	1047 Pa	991 Pa	879 Pa	772 Pa	672 Pa	560 Pa	476 Pa	392 Pa
Lower surface	420 Pa	560 Pa	532 Pa	504 Pa	487 Pa	465 Pa	420 Pa	392 Pa
heating, freezing, UV; samples no. 1, 2, 6								
Upper surface	1025 Pa	980 Pa	857 Pa	756 Pa	644 Pa	560 Pa	476 Pa	392 Pa
Lower surface	411 Pa	566 Pa	546 Pa	515 Pa	508 Pa	465 Pa	418 Pa	392 Pa
Flexing damage, samples no. 1, 2								
Upper surface	999 Pa	979 Pa	850 Pa	751 Pa	640 Pa	560 Pa	474 Pa	386 Pa
Lower surface	415 Pa	560 Pa	520 Pa	499 Pa	486 Pa	455 Pa	419 Pa	386 Pa
Flexing damage, sample no. 6								
Upper surface	700 Pa	677 Pa	581 Pa	438 Pa	287 Pa	157 Pa	72 Pa	28 Pa
Lower surface	336 Pa	464 Pa	433 Pa	350 Pa	260 Pa	156 Pa	71 Pa	28 Pa

As mentioned above, the pressure distributions compiled in the Table 12 referred to the symmetry plane. Therefore, it should be considered that a paraglider wing in a top view is of the shape of ellipse; thus, chord size decreases when approaching the side edge of the wing. Therefore, the values of pressure and corresponding to them distances were recalculated for each segment forming the paraglider.

11.2. Input data of the materials parameter

The laboratory tests results described in Section 9.3 were a basis for the input data of the FEM numerical calculation.

Apart from the Young's modulus and tensile strength values, the other indicators for this type of calculation were density (calculated based on the general properties of the analyzed materials, i.e. mass/area and thickness), thickness, shear modulus and Poisson's ratio. However, the accessible laboratory devices did not allow to obtain results regarding the shear modulus and Poisson's ratio. Thus, their values were implemented based on the literature describing Polyamide 6.6 fabrics of similar properties [53, 55].

11.3. Modeling geometry dedicated to the structural simulations

The analysis based on the same paraglider wing which was chosen for the CFD calculations. However, due to a different type of numerical method, the following steps of preparing the geometry differed comparing to the previous case. Again, a simplified geometry of a half of paraglider wing was modeled with the use of the *ANSYS Design Modeler* program.

The same file containing 3D coordinates that was used in Section 6.1 was imported into the program. However, for the FEM calculations no body was created based on the coordinates and no calculation area was modeled. The final geometry was created of walls covering the upper and lower surfaces of the paraglider, as well as ribs of an airfoil shape. Additionally, the walls forming the cover of a wing, were split in order to obtain smaller surfaces that were connecting to the closest airfoil faces. It allowed to obtain a better mesh quality, Figure 34.

The following methods of mesh creation were described below.

Edge Sizing - a specific number of divisions of an edge is given in order to dimension the mesh elements. In the discussed analysis, 24 nodes were forming each edge creating lower or upper shape of a rib, Figure 34a.

Face sizing – size of an edge is assumed at chosen surfaces. In the discussed analysis the ribs of airfoil shapes were dimensioned, Figure 34b.

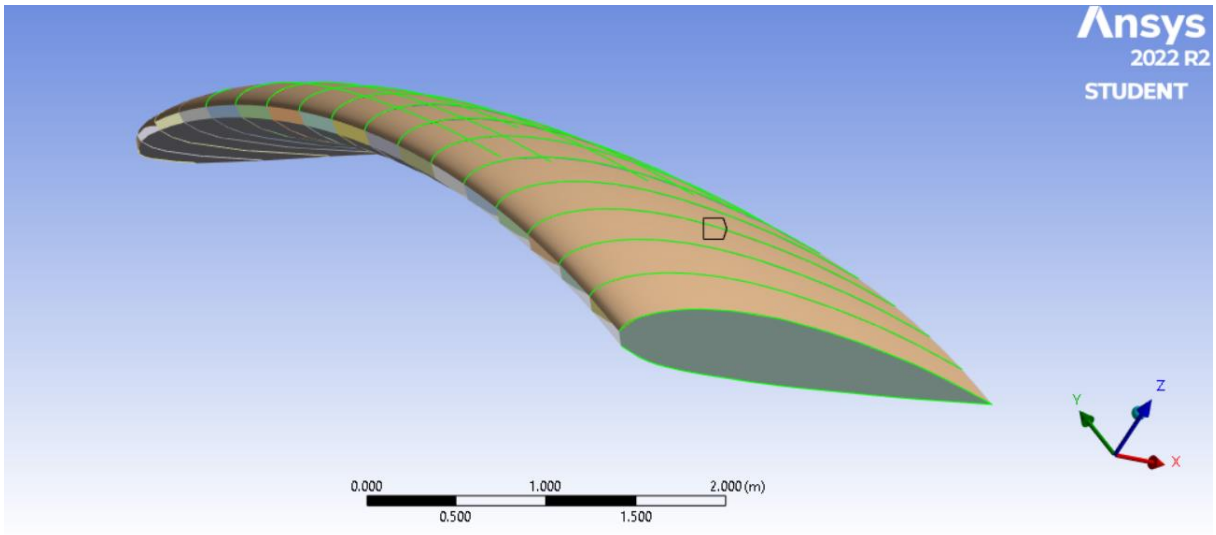

a

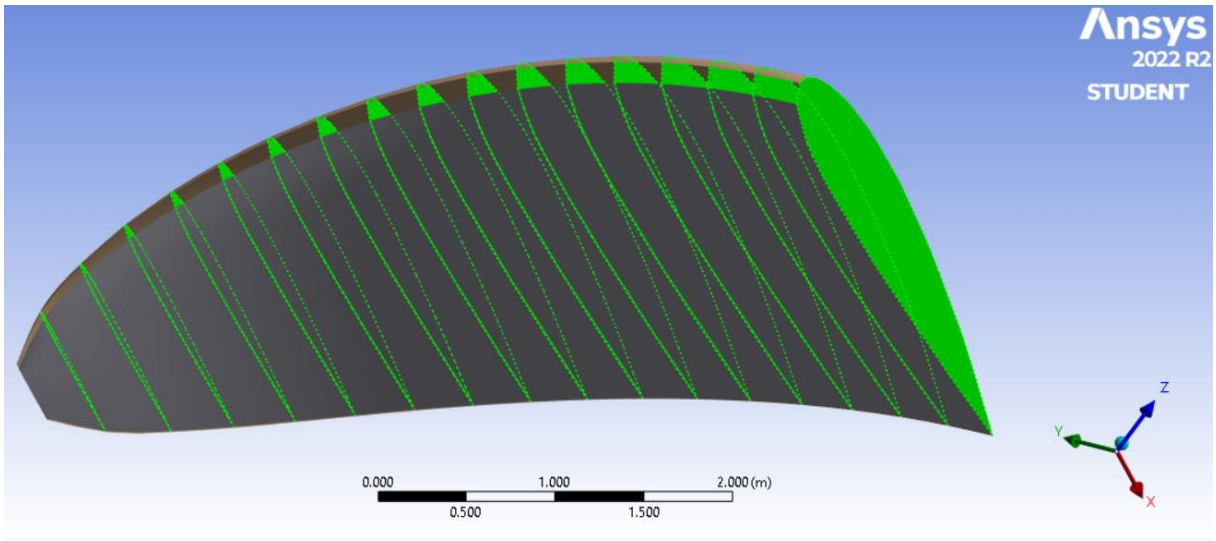

b

Figure 34. Methods of sizing applied to the case under consideration:
a – edge sizing, b – face sizing

The generated mesh (Figure 35) was a shell type, that contained 3933 elements, which resulted in a quite coarse mesh. However, it was characterized by mesh metrics, that provided authoritative results; they were the following: element quality = 0.89; skewness = 0.11; aspect ratio = 1.14. The generated elements were mainly structural and due to geometry nature only some of them remained unstructured. Moreover, an additional analysis of one case was done with a use of a dense mesh. The results were comparable to these described in Section 11.4 below.

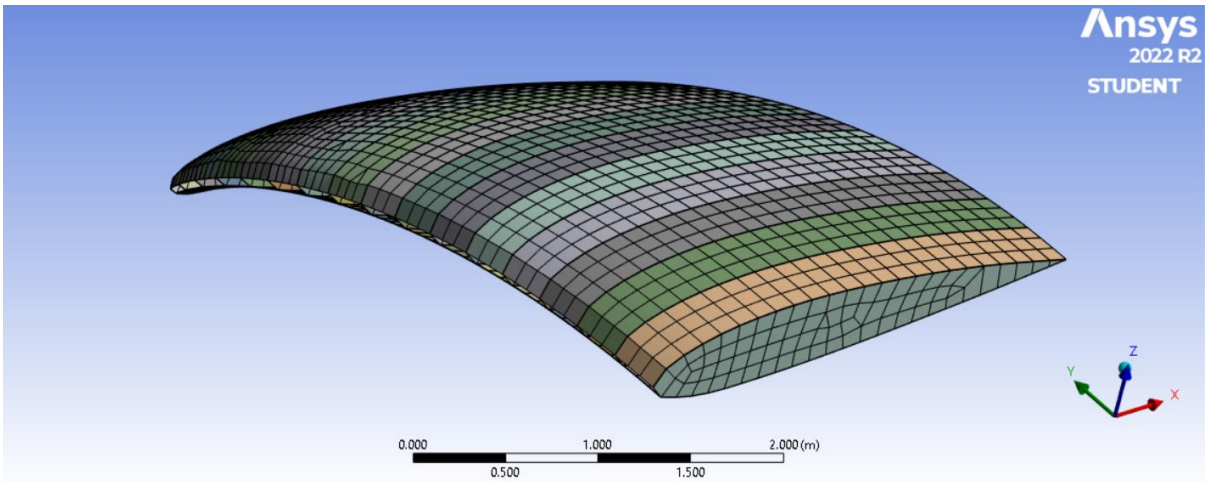

Figure 35. FEM mesh

In ANSYS Structural program contact regions were created in all the edges that were common for two or more surfaces. It was because in a real case each rib and brit are connected to each other by sewing.

In the Figure 36 below a fixed support application on ribs of an airfoil shape was shown. It was applied before the calculation in order to reduce degrees of freedom. This is a simplification of case under consideration; however, in normal flight conditions, the ribs practically do not move in respect to the full geometry of a paraglider wing.

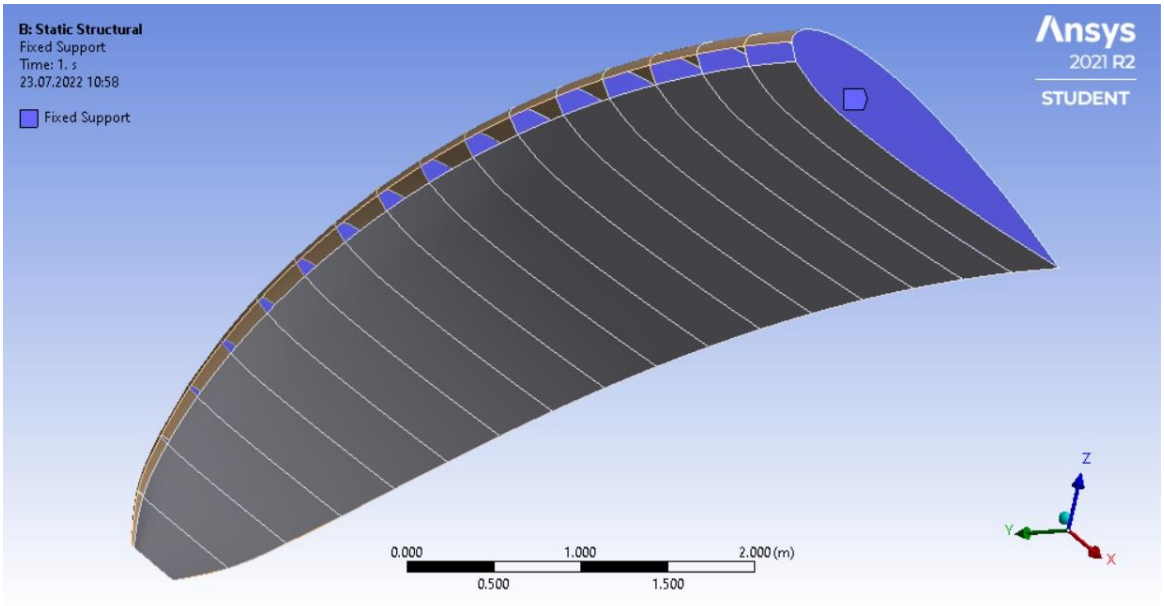

Figure 36. Attachment of the support for the numerical calculation

11.4. Results

The course of numerical calculation allowed to obtain numerical (Table 13) and visual (Figure 37) results regarding deformation, stress and strain of the considered woven fabrics.

Table 13. The minimum, average and maximum values of stress, strain and deformation of the considered cases

Sample	**Stress [Pa]**			**Strain [%]**			**Deformation [m]**		
	min.	**av.**	**max.**	**min.**	**av.**	**max.**	**min.**	**av.**	**max.**
1	0.000	4.501e6	2.934e7	0.0	1.0	7.2	0.000	0.009	0.038
2	0.000	3.598e6	2.220e7	0.0	0.9	6.4	0.000	0.008	0.033
6	0.000	2.400e6	1.555e7	0.0	1.0	7.2	0.000	0.009	0.037
1 (heating)	0.000	4.425e6	2.878e7	0.0	1.0	7.2	0.000	0.009	0.038

Sample	Stress [Pa]			Strain [%]			Deformation [m]		
	Min.	Av.	Max.	Min.	Av.	Max.	Min.	Av.	Max.
2 (heating)	0.000	3.502e6	2.185e7	0.0	0.9	6.6	0.000	0.008	0.034
6 (heating)	0.000	2.388e6	1.551e7	0.0	1.1	7.3	0.000	0.009	0.038
1 (UV degradation)	0.000	3.578e6	2.42e7	0.0	1.5	9.1	0.000	0.012	0.048
2 (UV degradation)	0.000	3.311e6	2.191e7	0.0	1.0	7.5	0.000	0.009	0.040
6 (UV degradation)	0.000	2.464e6	1.608e7	0.0	1.0	7.2	0.000	0.009	0.038
1 (freezing)	0.000	4.555e6	2.880e7	0.0	1.0	6.8	0.000	0.009	0.035
2 (freezing)	0.000	3.521e6	2.219e7	0.0	0.9	6.7	0.000	0.008	0.035
6 (freezing)	0.000	2.464e6	1.608e7	0.0	1.0	7.2	0.000	0.009	0.039
1 (flexing)	0.000	4.452e6	2.872e7	0.0	1.0	7.0	0.000	0.009	0.037
2 (flexing)	0.000	3.428e6	2.099e7	0.0	0.9	6.5	0.000	0.008	0.033
6 (flexing)	0.000	1.928e6	1.217e7	0.0	0.9	5.6	0.000	0.008	0.033

According to the Table 13, deformation and strain decreased with increasing of tensile strength of a material and/or decreasing of pressure acting on a material. The lowest deformation and strain values were achieved for the material number 2 not subjected to the ageing and materials no. 2 and 6 subjected to the flexing damage.

According to the results compiled and described in Section 9.3, the tensile properties of sample no. 2 were the greatest among all the considered fabrics. The deformation and strain values representant for this sample where achieved with the greatest pressure acting on the material, see Table 12.

Maximal pressure values acting on materials no. 2 and 6 subjected to the flexing damage were significantly decreased due to their increased air permeability parameters. Thus, it was possible to obtain insignificant values of stress and deformation.

The behavior of change of the stress value differed than the above. The thinner material and the stronger material, the bigger stresses were accumulated. Sample no. 1, which was characterized by the lowest thickness, obtained the highest stress values among all the materials.

When the tensile properties of this material were decreased (UV degradation), the maximal and average values of stress also decreased. This is consistent with the general principles

of mechanical strength of materials – with a rigid support, the stiffer materials transfer more stresses than the elastic ones.

Based on the above obtained maximal stress results and material characteristics, safety factors for all the considered cases were compiled in the Table 14 below.

Table 14. Safety factors

Sample	Safety factor
1	4.48
2	6.00
6	3.94
1 (heating)	3.75
2 (heating)	5.57
6 (heating)	3.65
1 (UV degradation)	1.33
2 (UV degradation)	2.91
6 (UV degradation)	3.19
1 (freezing)	4.83
2 (freezing)	5.86
6 (freezing)	4.06
1 (flexing)	4.43
2 (flexing)	5.47
6 (flexing)	4.70

Based on the above listed numerical values of the safety factor which were obtained by the stress parameter, it was initially concluded, that all the considered materials including these subjected to ageing, allowed a relatively safe use of a paraglider.

However, safety factor equal to 1.33 (sample no. 1 subjected to the UV degradation), is an insignificant number. Thus, the other obtained numbers were studied. The obtained maximal strain of the considered material was equal to 9.1 %, which is a greater value than elongation at break of this material (8.5%). Although the implemented overload was very high (5.6) and the maximal obtained values of strain rarely occurred when its distributions

were considered (Figure 37b), a paraglider covered with an UV degraded material no. 1 should not be allowed to use.

The obtained results differed mainly by the values; the behavior of the stress, strain and deformation distributions was alike. Therefore, the exemplary distributions were presented in the Figure 37.

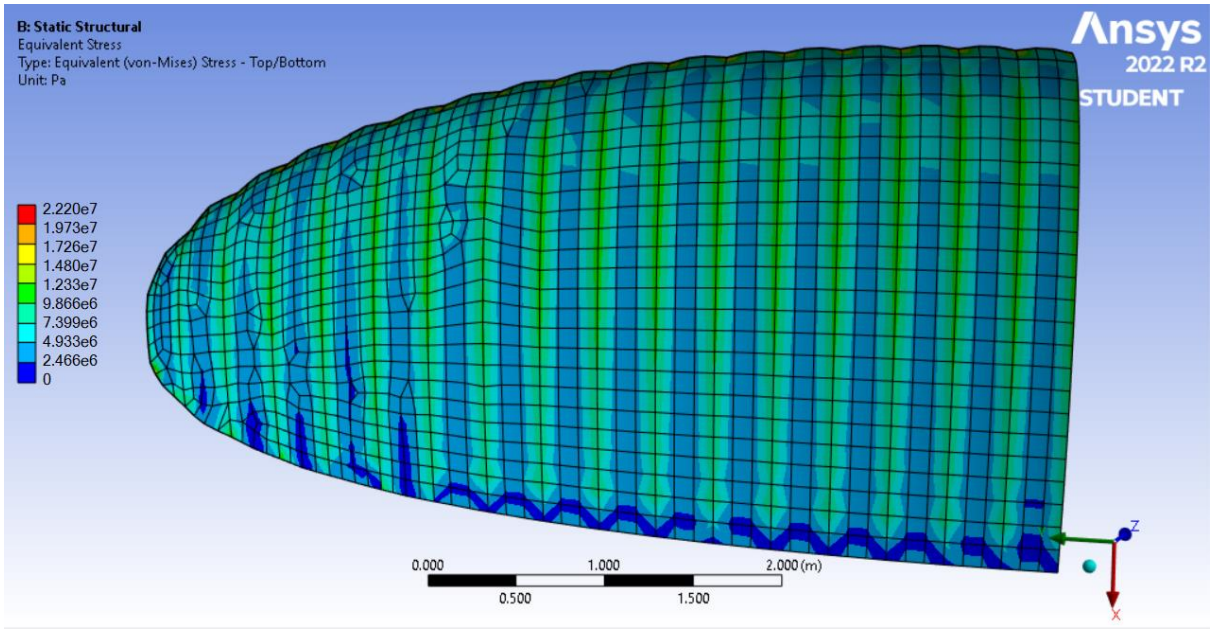

a

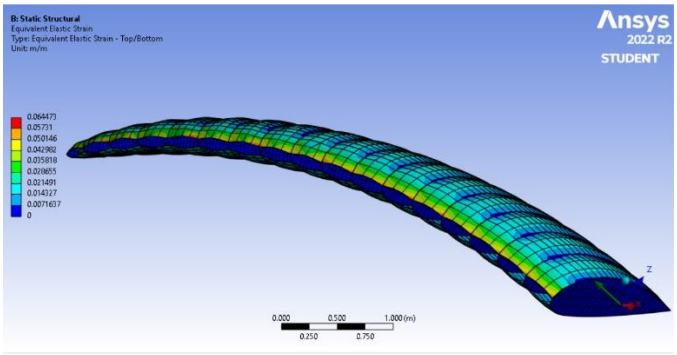

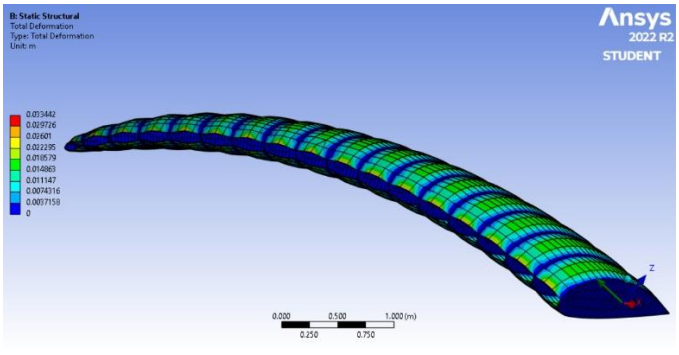

b c

Figure 37. Exemplary distributions of a) stress; b) strain; c) deformation over the considered wing based on covering with material no. 2

Based on the Figure 37, it can be concluded that distributions regarding stress (a) differed compared to the remaining (b, c). In the case of (a), the greatest stress was concentrated in a material in the immediate vicinity of the ribs (rigid support). When (b) and (c) where considered, their biggest values were noticed on the leading edge and in the regions between supporting ribs.

In the Figure 38 below, deformation distributions of two materials covering the considered paraglider were compiled: a – sample no. 2 not subjected to degradation (the lowest deformation among all the considered cases); b – sample no. 1 subjected to the UV degradation (the greatest deformation among all the considered cases). The difference is clear and visible organoleptically.

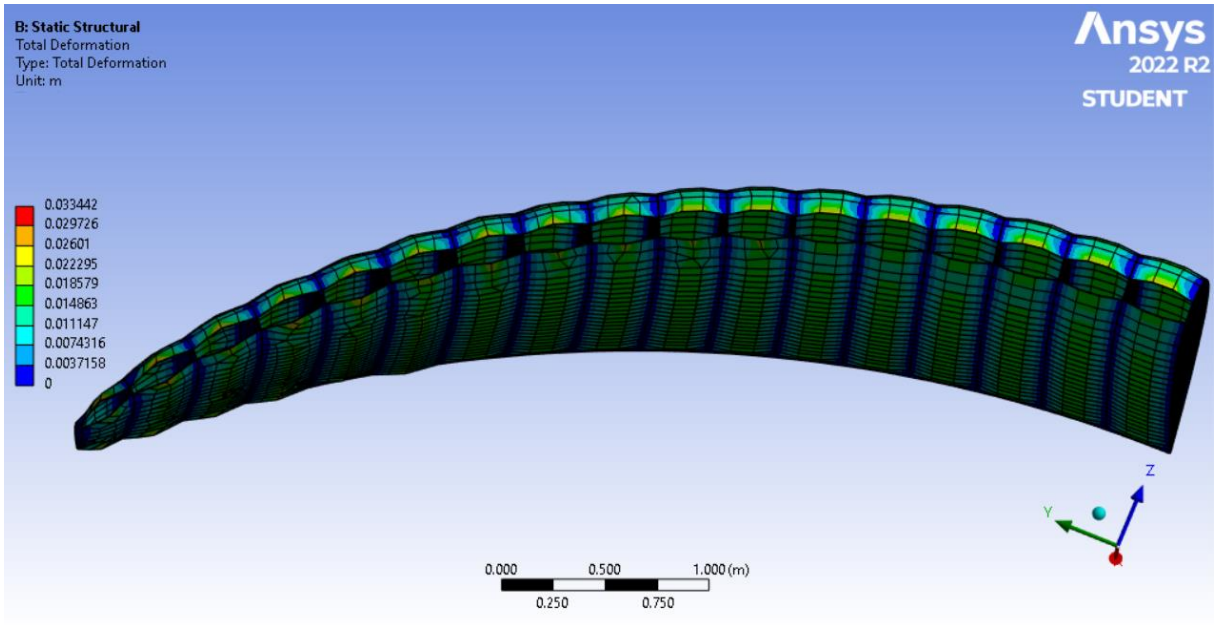

a

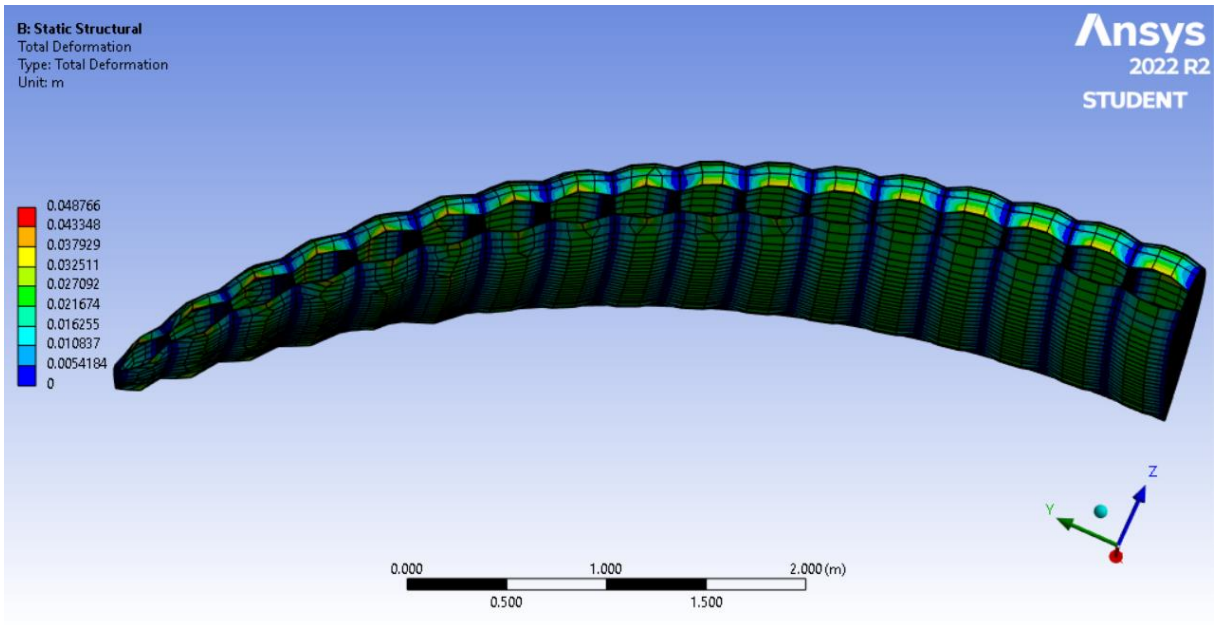

b

Figure 38. Deformation comparison of materials covering the considered paraglider: a – sample no. 2 not subjected to ageing; b – sample no. 1 subjected to the UV ageing

The maximum values of stress, strain and deformation over the paraglider were marked with the red color, which is almost not visible in the Figures 37 and 38. Therefore, the maximal values of stress were not the most representative ones; the greatest repetitive values (based on the visual observations) were compiled in the Table 15.

Table 15. The biggest repetitive values of stress, strain and deformation based on the visual results; averaged

Sample	**Stress [Pa]**	**Strain [%]**	**Deformation [m]**
1	2.282e7	4.7	0.025
2	1.479e7	4.3	0.022
6	1.037e7	4.8	0.024
1 (heating)	2.238e7	5.6	0.029
2 (heating)	1.699e7	5.1	0.027
6 (heating)	1.205e7	5.6	0.029
1 (UV)	1.615e7	6.1	0.032
2 (UV)	1.460e7	5.0	0.026
6 (UV)	1.071e7	4.8	0.025
1 (Freezing)	1.920e7	4.6	0.023
2 (Freezing)	1.306e7	4.8	0.024
6 (Freezing)	1.012e7	4.8	0.025
1 (flexing)	2.234e7	5.5	0.029
2 (flexing)	1.633e7	5.0	0.026
6 (flexing)	9.457e6	4.3	0.025

According to the Table 15, the averaged maximal representative values of stress, strain and deformation were decreased when compared to the absolute maximums. They decreased around 30 – 40 % comparing to the values listed in the Table 13.

12. Analysis of the effect of material deformation on the aerodynamic characteristics of the paraglider (influence of both: air permeability and mechanical characteristics of materials)

Based on the numerical calculations described in Section 11 above, a new geometries of a deformed paraglider wing were obtained. It considered deformation created due to a pressure acting on a material.

According to the above results, the less stiff material, the greater the deformation occurred. The deformation is expected to have a significant influence on the aerodynamic characteristics of a paraglider wing.

Therefore, the study below describes mechanical properties of fabric influence on aerodynamic characteristics of a paraglider wing. However, the analysis in fact concern air permeability influence too. The air permeability parameter affect the pressure distribution acting on a material and therefore the deformation. The below described study is the last step of a multistage optimization procedure developed in order to perform assessments of paraglider materials considered to cover a given geometry of a paraglider wing.

One case was considered and it concerned paraglider covered with fabric no. 6 not subjected to ageing.

12.1. Preprocessing

The exported **.STL* geometry file of wing after deformation was not possible to be normally processed in the *ANSYS DesignModeler* program. Number of serious faults in the geometry caused limited action in the preparation of the CFD geometry model.

Therefore, before building the model, the deformed geometry needed to be cleansed and all the faults had to be removed. In order to do that, the geometry file was read by the *SpaceClaim* program.

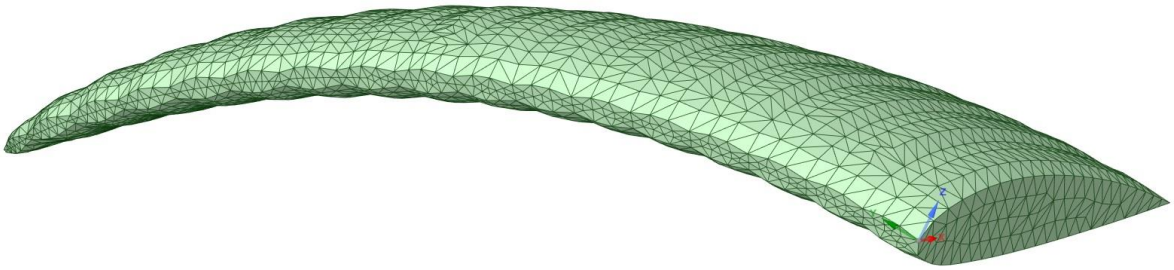

Figure 39. The deformed geometry after exporting to the *SpaceClaim* program

In the program the surfaces were created by small triangles (connected edges of the adjacent triangles were an approximation of the surface of the paraglider), Figure 39. However, some gaps were found between the triangles. The repair of the geometry faults was to remove the small gaps and fill them in order to create a whole surface.

The repaired geometry sections could be recreated in the *DesignModeler* program and a geometry of a paraglider body could be built from them.

The prepared geometry was presented in the Figure 40 below.

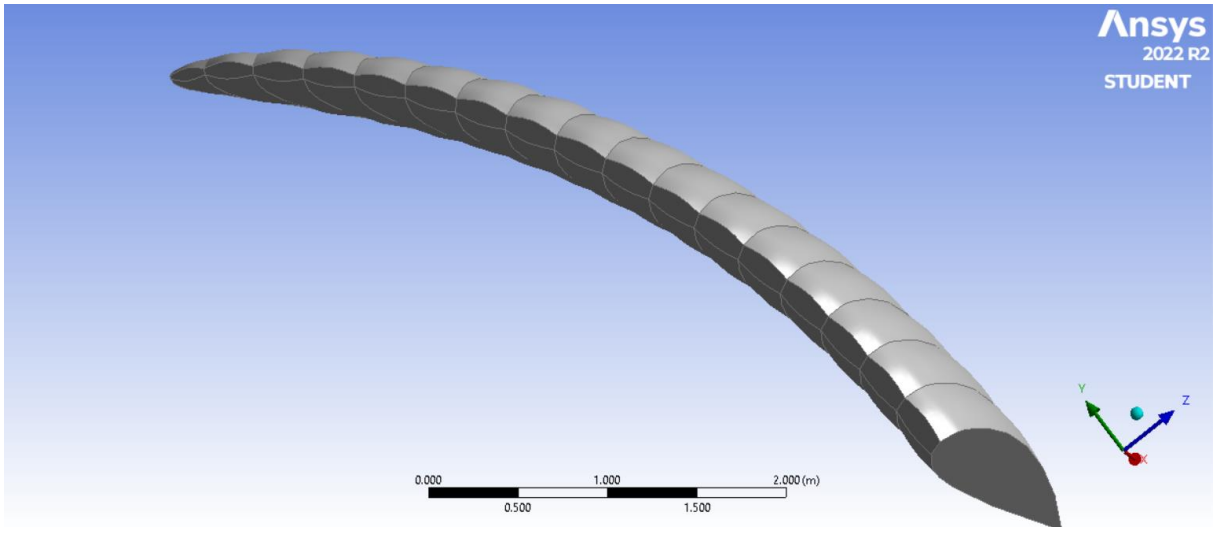

Figure 40. The imported and cleansed geometry of deformed wing

A cuboid calculation area was created around the modeled wing, as in the cases described in Section 6. To secure the results to be the most comparable to these from previous analysis, the measurements of the surrounding cuboids were exactly the same, i.e. 20 m in front of the wing and 40 m in other directions. The exception was wall forming a symmetry plane of the paraglider wing.

When the geometrical model was ready, it could be exported to the Meshing program. Creating structural mesh on the walls forming paraglider wing was found to be problematic due to more complex type of geometry, than it was in the previous steps of the research. For example, sweep method, which was found to be the most proper to form and guide cuboid elements through all the wing was only possible to be applied on the bigger segments forming the praglider geometry (these closer to the symmetry plane); for the segments approaching the side edge, sweep method failed to be applied.

Therefore, it was decided to generate unstructural (pyramid) elements over all the geometry.

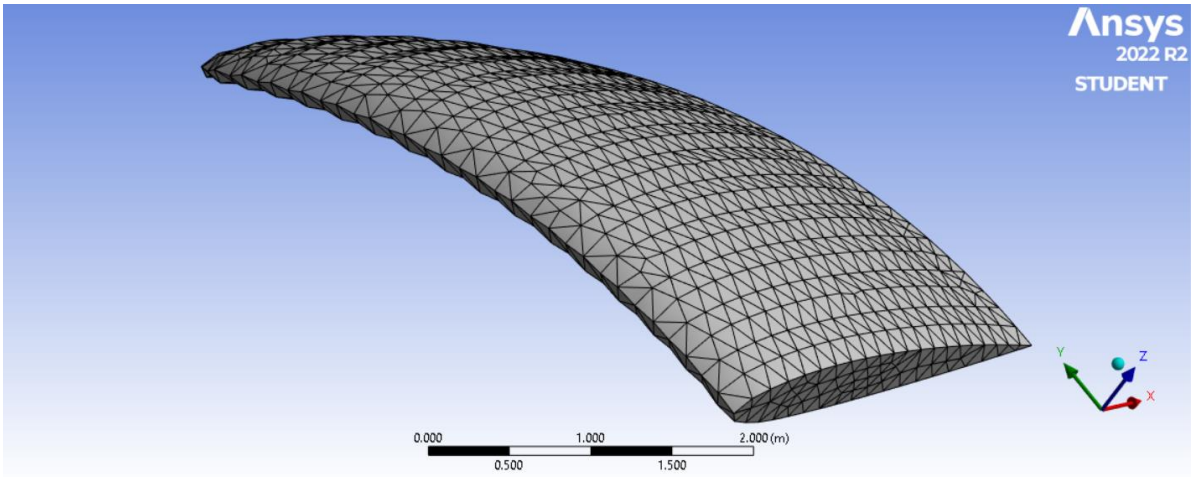

Figure 41.The generated unstructural mesh (wing)

However, according to the metrics, the generated mesh (Figure 41) still presented acceptable quality of elements. Its average skewness was equall to 0.22, with the highest value at 0.90. The orthogonal quality was at level of 0.77; the lowest value of it was equal to 0.10.

As mentioned above, the quality of mesh was at acceptable level. However, the accessible tools allowed to improve the quality after exporting the mesh to the *ANSYS Fuent* program.

Therefore, when the mesh was implemented to the program, *Make Polyhendra* tool was applied. It converts tetrahedral mesh elements to polyhedral elements. During the conversion, Fluent merges tetrahedral cells into polyhedral cells that have larger dimensions. Thus, using *Make Polyhendra* tool not only results in improving quality of a mesh; it also reduces number of elements and therefore – the time of calculation.

In the next step *Improve mesh quality* tool was used. It was applied to 0.1 % of elements that presented the worst quality over all the calculation area. The elements were improved in the course of 10 iterations.

The minimal orhogonal quality of the final mesh was equal to 0.20. It means, that quality of the element that presented the worst quality improved 100% when compared to the previous mesh. The final mesh was presented in the Figure 42 below.

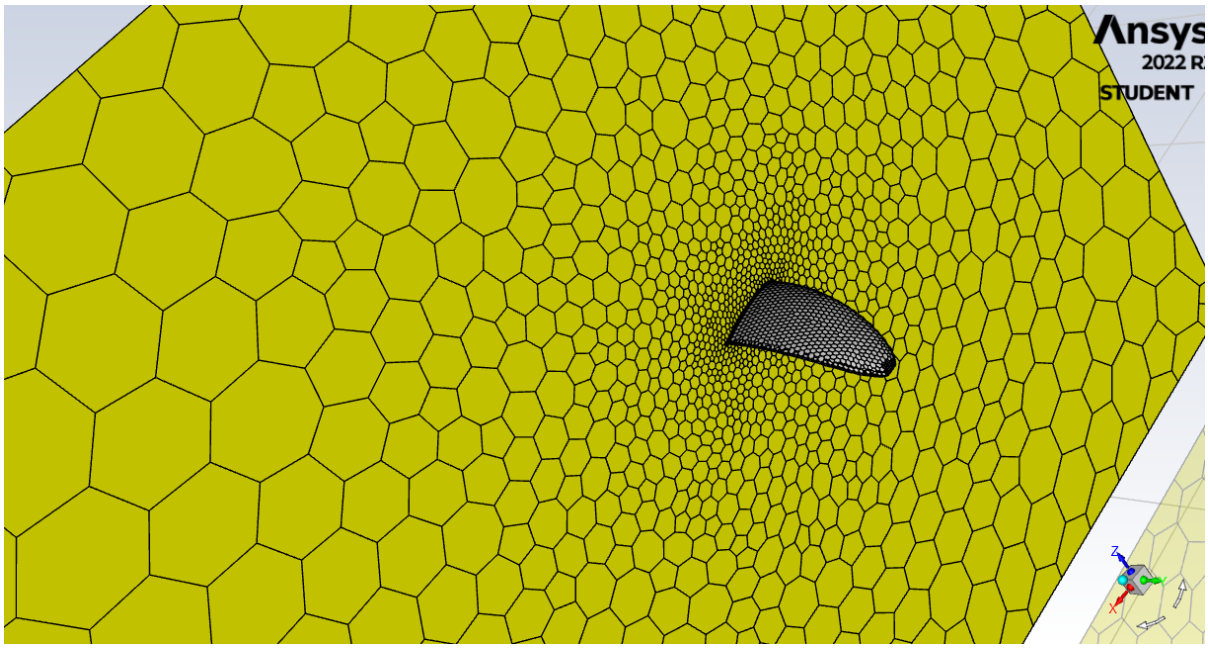

Figure 42. The final mesh after applying tools improving mesh quality

The undisturbed flight conditions were again as in the previously analyzed cases, i.e.: pressure 101325 Pa; temperature 26.85 °C; velocity 45 km/h; angle of attack 6°.

Spallart-Allmaras turbulence model was applied.

12.2. Calculation and results

The convergence was achieved after 1500 iterations. First, small value of Courant number was applied, and it was gradually increased in the course of numerical calculations. The Third Order-MUSCL discrestization scheme was applied again.

The results obtained in the course of numerical calculations were compiled in the Table 16 below.

Table 16. Result of CFD numerical calculations regarding

	Sample no. 6
Average pressure inside the wing	101420 Pa
Mass flow rate	0 kg/s
Lift force	1091.80 N
Drag force	115.56 N
c_l/c_d	9.45

Compared to the results regarding an undeformed wing, the c_l/c_d ratio decreased 25%. It proves that deformation caused by pressure acting on a material has a significant influence on the aerodynamic characteristics of a paraglider. However, the decrease was recorded for the deformation caused by pressure, when an overload of 5.6 occurred. Pressure acting on a material during the normal flight conditions would not cause such significant decrease of the aerodynamic characteristics.

Pressure distributions over the wing were compiled in the Figure 43 below.

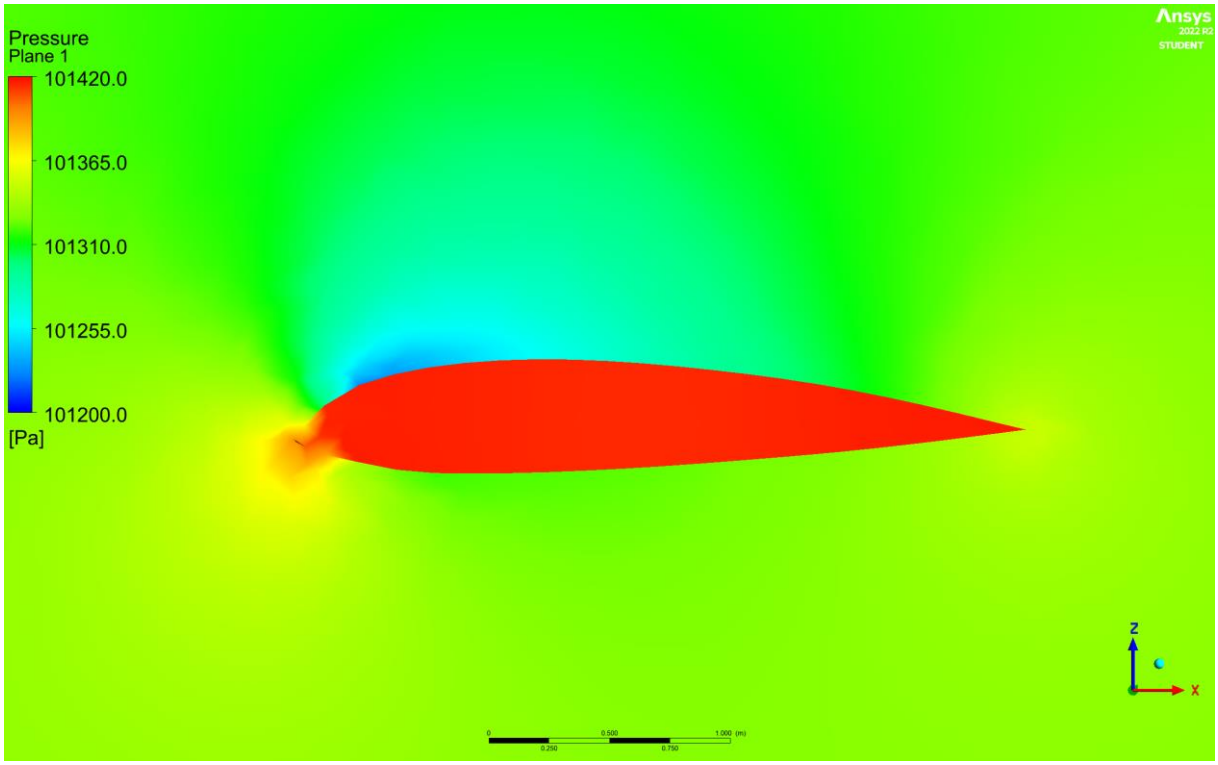

a

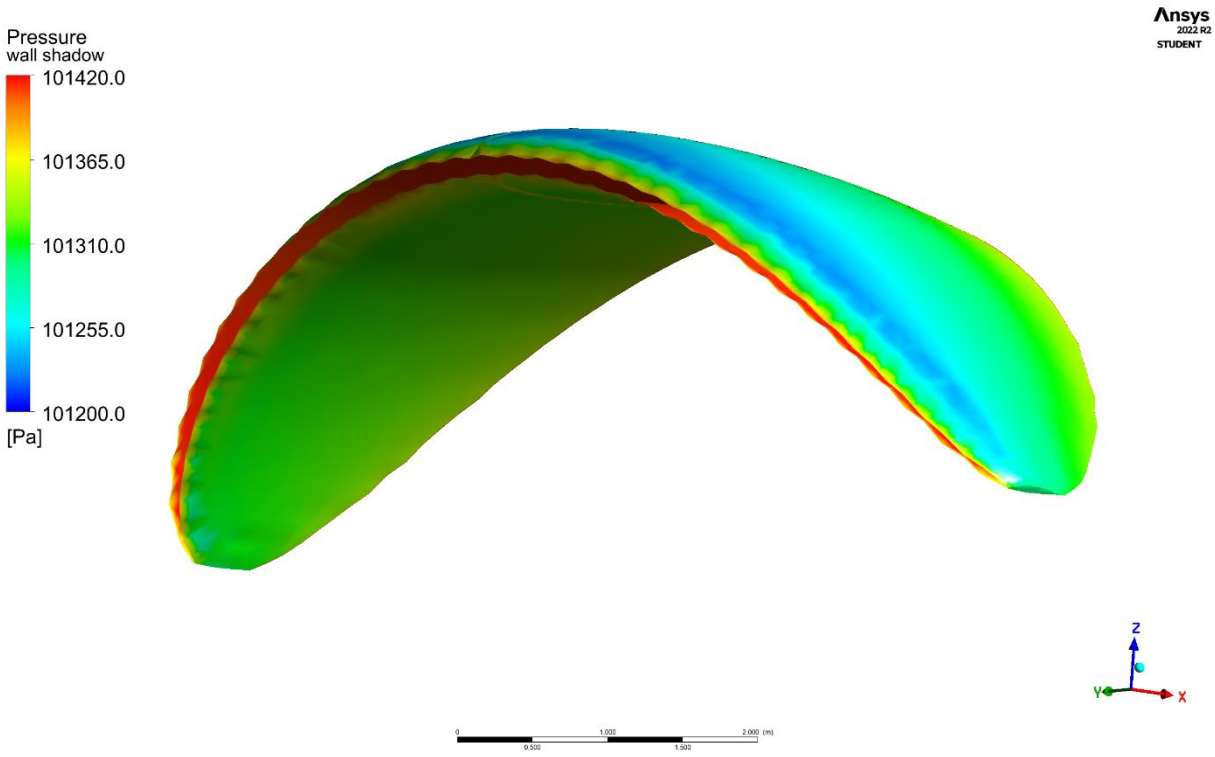

b

Figure 43. Pressure distributions over the deformed geometry, when flight conditions were v = 45 km/h, α = 6°: a – in the symmetry plane; b – on the walls of the paraglider

Based on the pressure distribution compiled in the Figure 43 above, it can be concluded that it was very advantageous. The overpressure inside the wing was evenly distributed; an insignificant decrease of it was observed only in a small distance behind the leading edge. The drop of a pressure on the upper surface of the paraglider indicated creation of a lift force which was consistent with the obtained results.

13. Single cover paraglider analysis

The below research is focused on paraglider covered only with the upper brits. The lower cover is applied only at the leading edge in order to initiate the path of the air streams, as well as the trailing edge, to maintain the shape of the airfoil, Figure 44.

Please notice that the applied airfoil is not a traditional type one. The under-cambered type Selig S1223 airfoil was used for preparing the geometry. The change of the airfoil was caused by different nature of the considered paraglider. Ribs of a shape of traditional airfoils (i.e. asymmetrical/flat bottom) would result in creating additional drag force, when no coverage at the lower part of the wing is applied.

The remaining characteristics and dimensions of the wing such us span, chord, radius etc. were assumed to be the same as for the previously analyzed case. Therefore, the following steps of preparing the geometry for both, CFD and FEM analysis also remained similar.

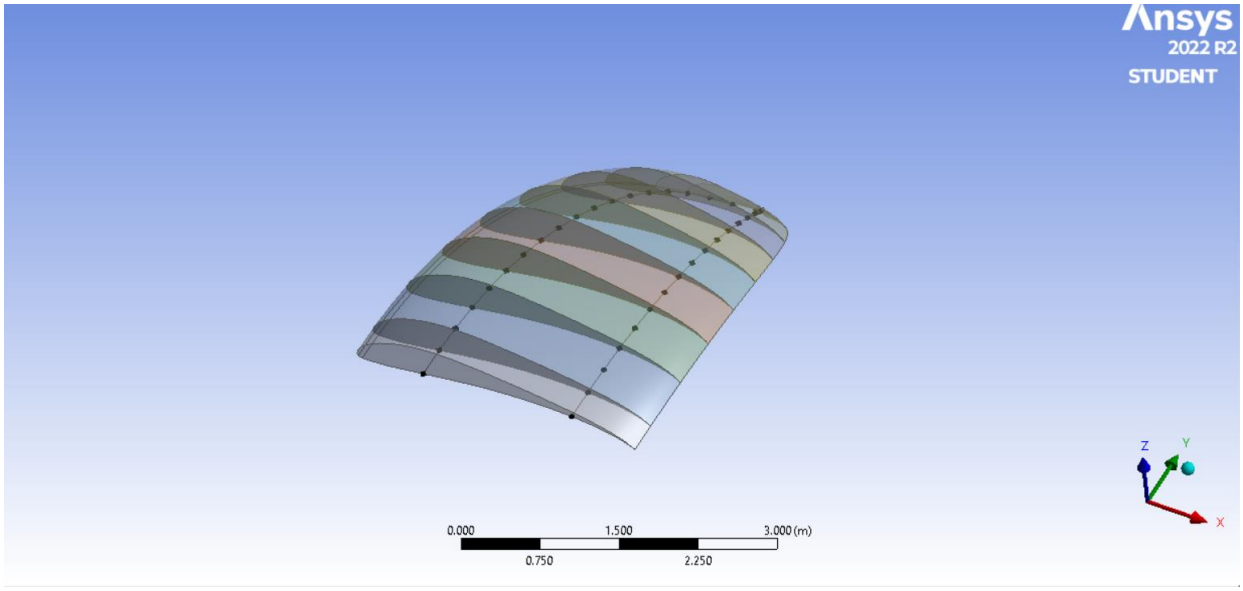

Figure 44. Geometry of the considered wing

The analysis of the above described wing has a significant importance from the view of packing volume and mass of the final product. Therefore, an expected surfaces of the covering fabrics of a traditional paraglider (studied above in Sections 6 and 9 – 12) and the new type of a paraglider were calculated; the ribs were included to the calculation. A normal type paraglider wing's surface was equal to 71.65 m^2; whereas the surface of materials that would be used in the production of a paraglider considered in this section was equal to 53.02 m^2. Based on the obtained results the expected mass and volume of a wing

in the respect of materials used was evaluated in the Table 17 below (based on parameters obtained in the laboratory testing, Table 2).

Table 17. Expected masses and volumes of a wing comparison in the respect of the applied geometry and covering materials

Sample no.	Mass (traditional type of paraglider) [kg]	Packing volume (traditional type of paraglider) [dm^3]	Mass (new type of paraglider) [kg]	Packing volume (new type of paraglider) [dm^3]
1	2.436	3.582	1.802	2.651
2	3.009	5.015	2.227	3.711
3	2.293	3.582	1.696	2.651
4	1.863	3.582	1.378	2.651
5	2.723	6.448	2.014	4.771
6	2.723	6.448	2.014	4.771
7	2.078	2.866	1.537	2.121
8	1.863	2.866	1.378	2.121
9	2.579	3.582	1.909	2.651
10	3.009	5.732	2.227	4.241

After applying the new geometry, in each case masses and packing volumes would decrease around 26 % comparing to the previously considered paraglider. The lowest expected masses were obtained for a paragliders covered with fabrics no. 4, 8 and were equal to 1.378 kg (single cover paraglider) and 1.863 kg (traditional paraglider); it means that the minimum mass decrease caused by the change of geometry was equal to 0.485 kg. Whereas the lowest volumes were obtained for samples no. 7 and 8; their values were equal to 2.121 dm^3 (when single cover paraglider was considered) and 2.866 dm^3 (for traditional paraglider). Thus, the minimum decrease of a volume caused by the geometry change was equal to 0.745 dm^3.

However, two factors were not included to the analysis. First, the packing volume was obtained based on the surfaces and thicknesses of the covering materials and ribs. Therefore, the calculated volume would be possible to obtain, if an under pressure packing was applied. For paragliders, a hand packing is used.

Moreover, the above calculations did not include additional elements, i.e. fabric allowances, sewing threads, plex stiffening elements, lines and risers. Therefore, the actual masses and volumes would be significantly increased comparing to the obtained results.

13.1. CFD Simulations

In the previous CFD analysis, the ribs were created only as a basis for the 3D geometry. They were not considered in the numerical calculations, as their appearance would have a negligible influence on the final results of the aerodynamic characteristics of a paraglider. The airfoil shape was maintained by the lower and upper surfaces of the wing.

In the case under study, the ribs could not be ignored, as the geometry was not closed at the bottom. Thus, an airfoil shape could affect the final results. When the geometry was generated, each segment of a paraglider created separate body, and to each rib, the *Wall* boundary condition was given.

The generated geometry of multibody part contained 10 bodies creating paraglider wing and 1 body creating the calculation volume. As in the cases described in Sections 6 and 12, the dimensions of the cuboid surrounding the paraglider remained the same in order to prepare the study to be possibly comparable to these described above.

After generating mesh in the *Meshing* program, the geometry contained mostly structural elements forming the wing (Figure 45a), and pyramid-type elements surrounding it (Figure 46b).

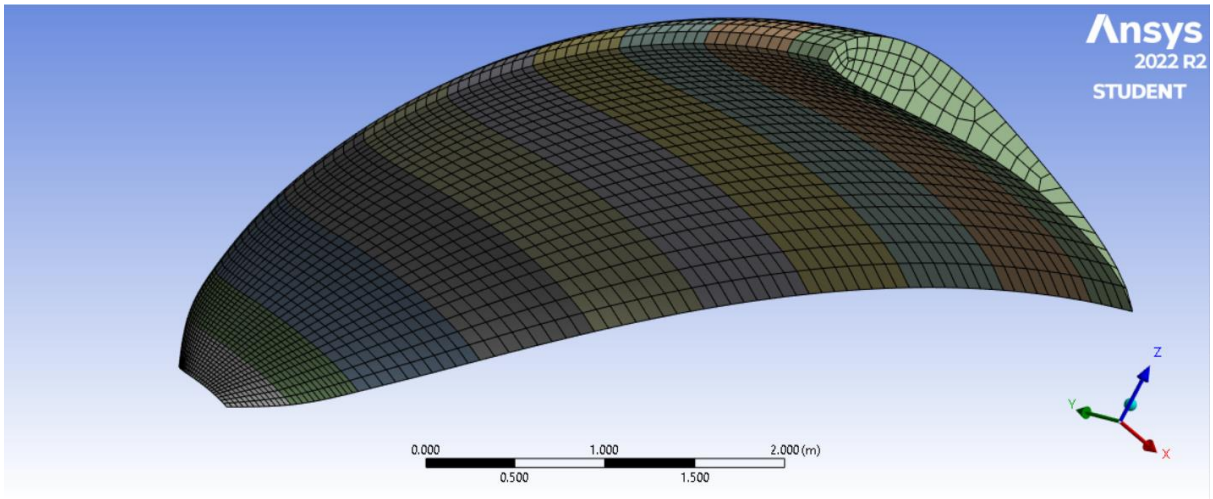

a

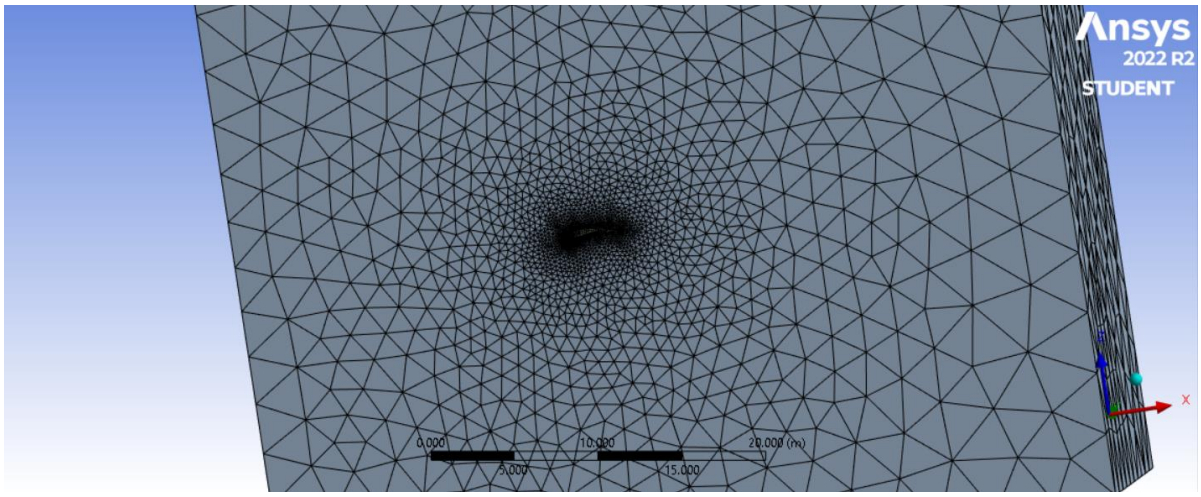

b

Figure 45. The generated mesh

The generated mesh contained 350556 elements, with the average orthogonal quality equal to 0.75 and its minimum value at the level of 0.11; The skewness metric was equal to 0.25 at its average, whereas its maximum value was equal to 0.90.

After exporting the mesh to the FLUENT program, the pre-processing was performed according to the steps described in the previous Sections regarding CFD calculations. Initially, also the angle of attack remained the same (α = 6°). However, it was noticed that the most advantageous in a respect to the aerodynamic characteristics, were the conditions with angle of attack equal to 12°. Thus, the further calculations were performed with the following conditions: pressure 101325 Pa; temperature: 26.85 °C; velocity: 45 km/h; angle of attack: 12°.

The convergence was achieved after 850 iterations. As for the previous cases, *Spallart-Allmaras* turbulence model and the *Third Order-MUSCL* discrestization scheme were applied. The obtained results were compiled in the Table 18 below.

Table 18. Obtained results regarding CFD calculations of a single-cover paraglider

	Fabrics no. 1 – 10
Mass flow rate	0 kg/s
Lift force	3472 N
Drag force	307 N
c_l/c_d	11.27

Based on the obtained results it can be observed that the lift and drag forces values were significantly increased compared to these previously obtained regarding a traditional type paraglider. It was caused by applying greater angle of attack, which was more advantageous for the case considered in this section. The nature of increasement of lift and drag force together with increasement of the angle of attack was described and explained in Section 10.2.

The distributions of pressure over the considered wing were compiled in the Figure 46 below.

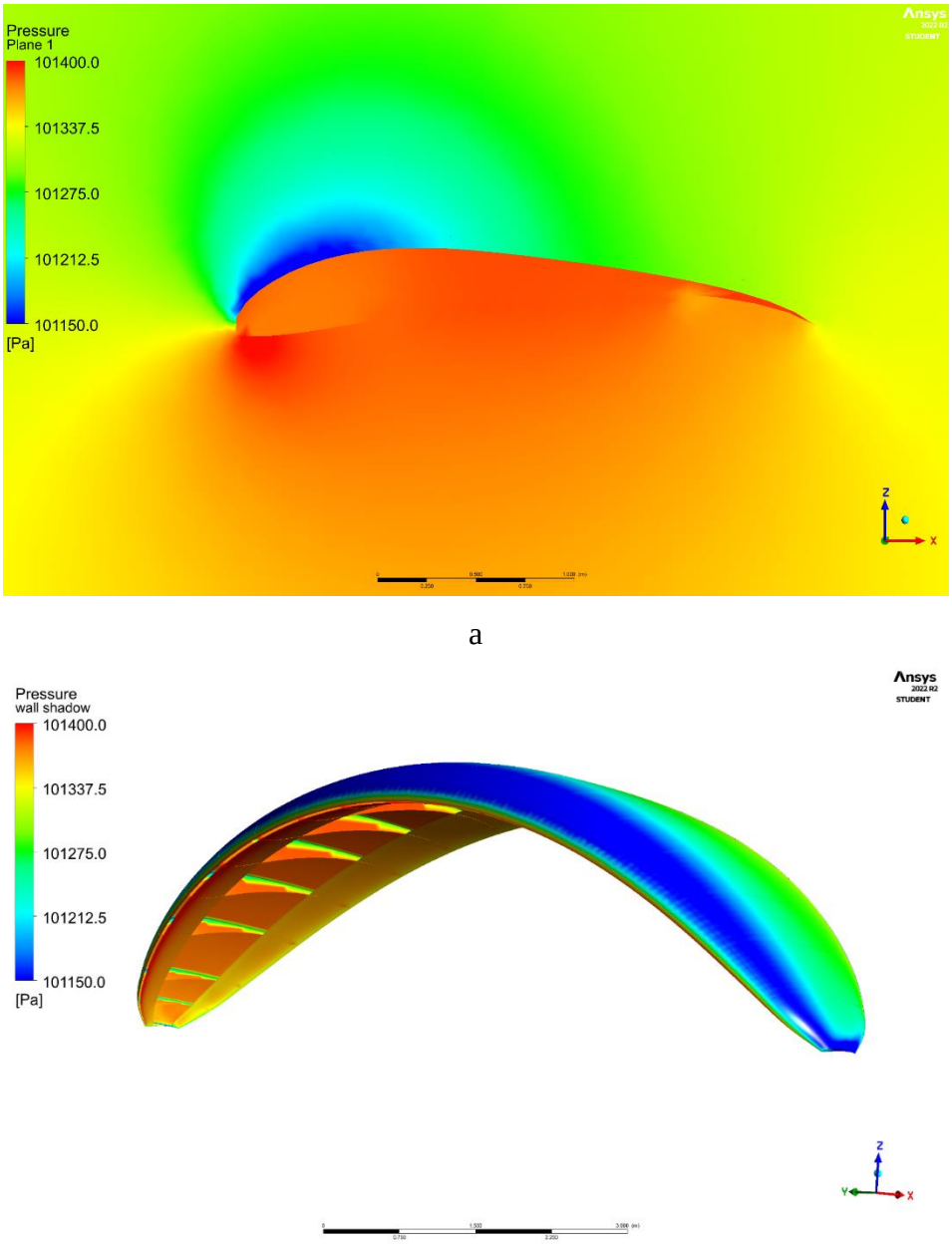

a

b

Figure 46. Pressure distributions over the considered geometry, when flight conditions were v = 45 km/h, α = 12°: a – in the symmetry plane; b – on the walls of the paraglider

According to the pressure distributions presented in the Figure 46, a significant pressure drop above the wing was observed. It was caused by applying an increased angle of attack. Unlike in the previously considered cases, the pressure inside the wing was unevenly distributed. However, due to a specific geometry, this was not possible to be achieved.

A huge overpressure was observed inside the wing at the trailing edge, which secured maintaining of the shape in this section. This was assessed as very important, as the distance between the upper and the lower cover there was insignificant. Thus, different character of distribution would cause e.g. mutual suction of both layers and distortion of the shape of the airfoil.

The overpressure that was created at the leading edge on the outer surface of the paraglider was higher than the one created inside the wing. However, it was not created entirely frontally. Thus, maintaining of an aerodynamic shape of a paraglider would be undisturbed by pushing the nose to the inside of an airfoil.

The overpressure acting on the lower surface of the paraglider could push the fabric to inside and therefore – disturb the original geometry of the paraglider. However, the value of pressure acting on the material was insignificant; moreover, ribs spaced every half meter would support and hold the front lower cover. A distance between the upper and lower cover in this section would secure maintaining of the aerodynamic shape.

The pressure distribution acting on ribs was uneven, Figure 46b. However, in a real case, holes are applied in the paraglider ribs in order to allow the air to distribute evenly. In the considered, simplified case, the holes were not applied. Thus, a significant intense of pressure was created by air at the lower sections of the ribs.

Figure 47 below presents streamlines of velocity as a variable.

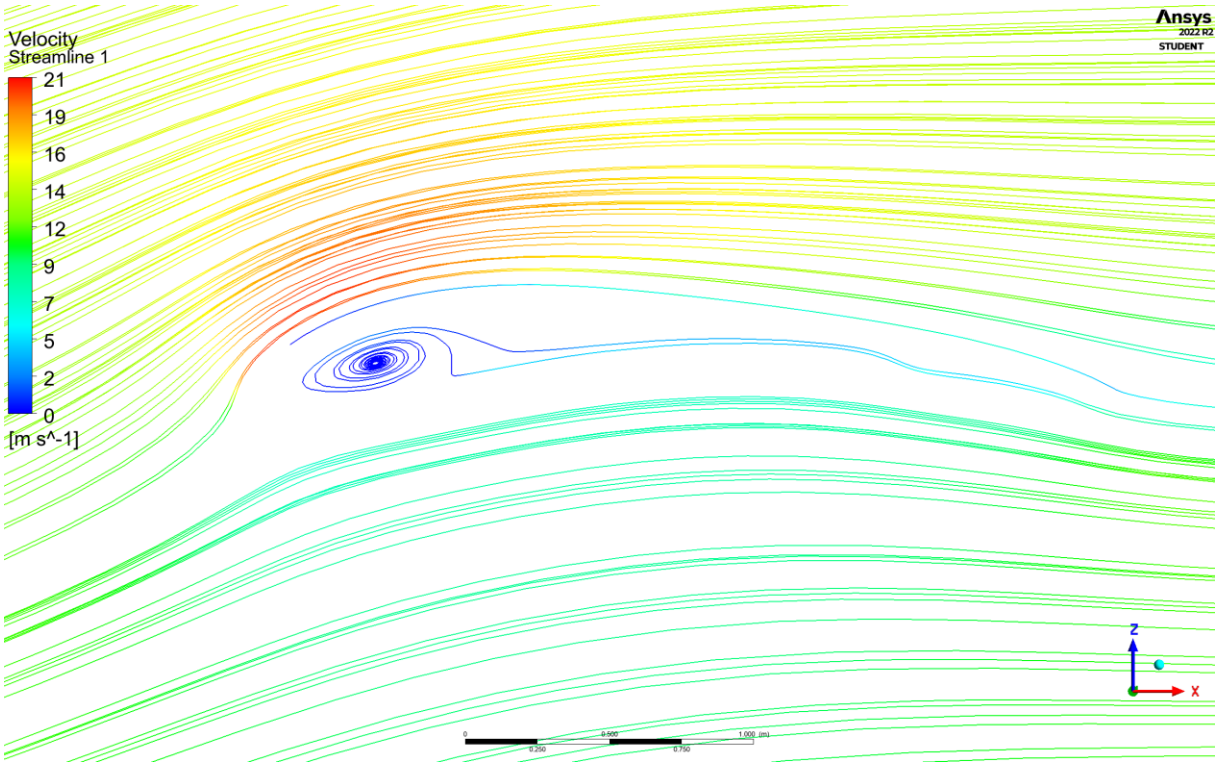

Figure 47. Streamlines of velocity as a variable

Based on the figure above streams of air of an increased velocity were observed on the upper surface boundary layer. Moreover, a vortex created inside of the wing was noticed, which was not observed in the previously considered cases. It may be a reason of the airfoil change, not implementing the lower covering material or increasing of the angle of attack. However, the geometry did not cause any other flow disturbances. The streamlines, especially on the lower cover, were smooth.

13.2. FEM Structural Analysis

The FEM structural analysis was based on the obtained pressure distribution over the paraglider wing and acting on covering materials. The following steps of preprocessing were the same as for the case considered in Section 11.3.

The pressure acting on a material in the function of distance from the leading edge in the symmetry plane was presented in the Figure 48 below. They were implemented into the structural calculations with the assumption of overload equal to 5.6, which was explained in Section 11.3.

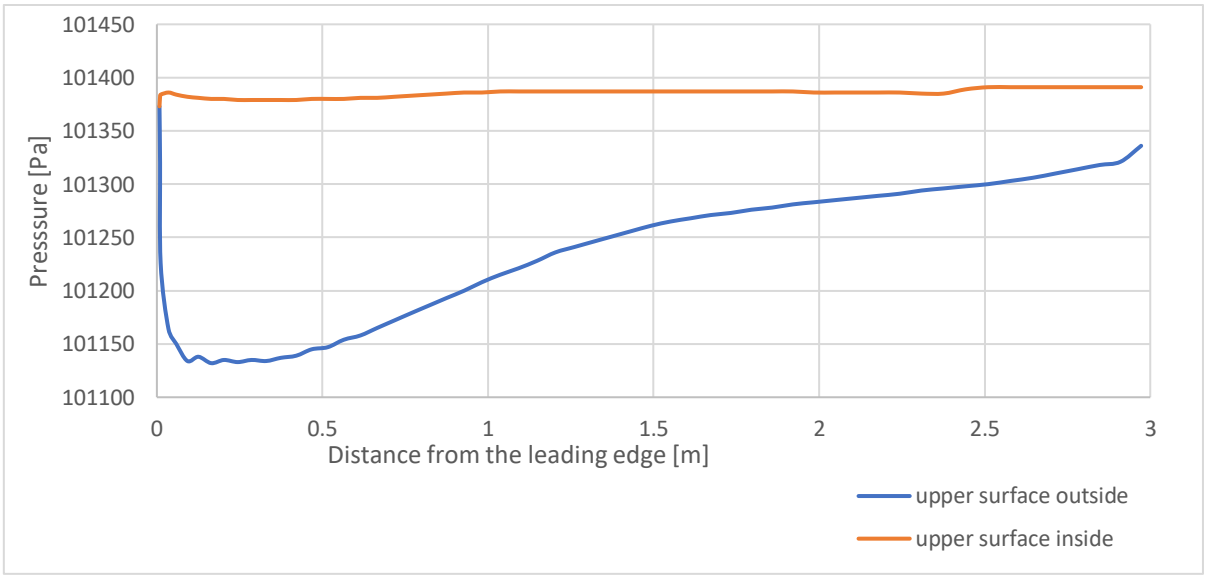

a

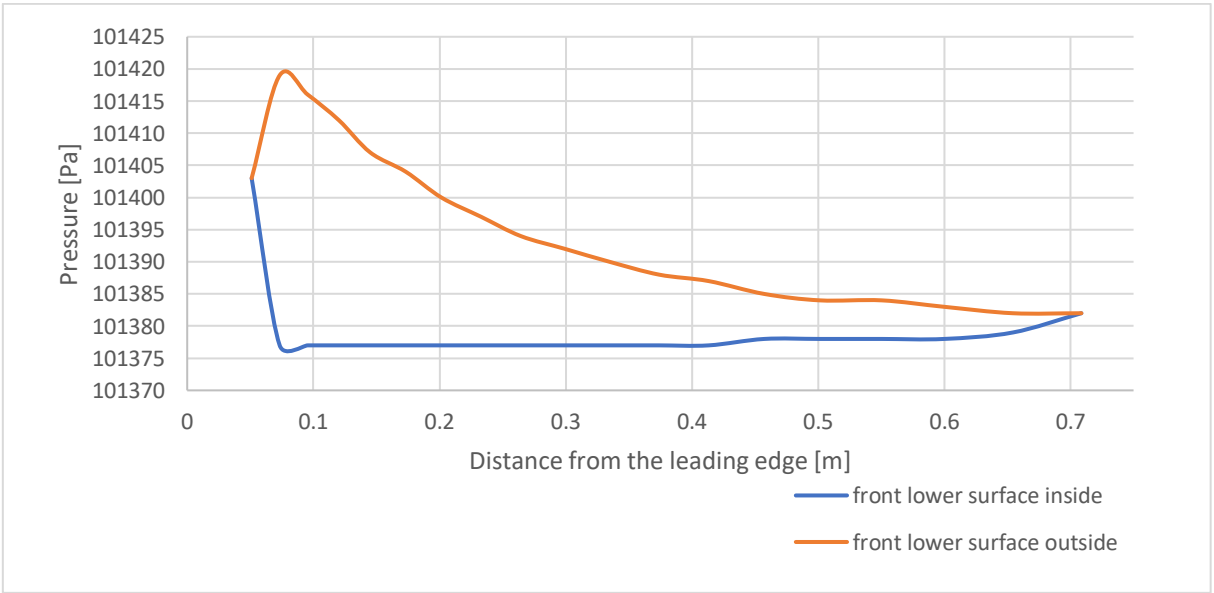

b

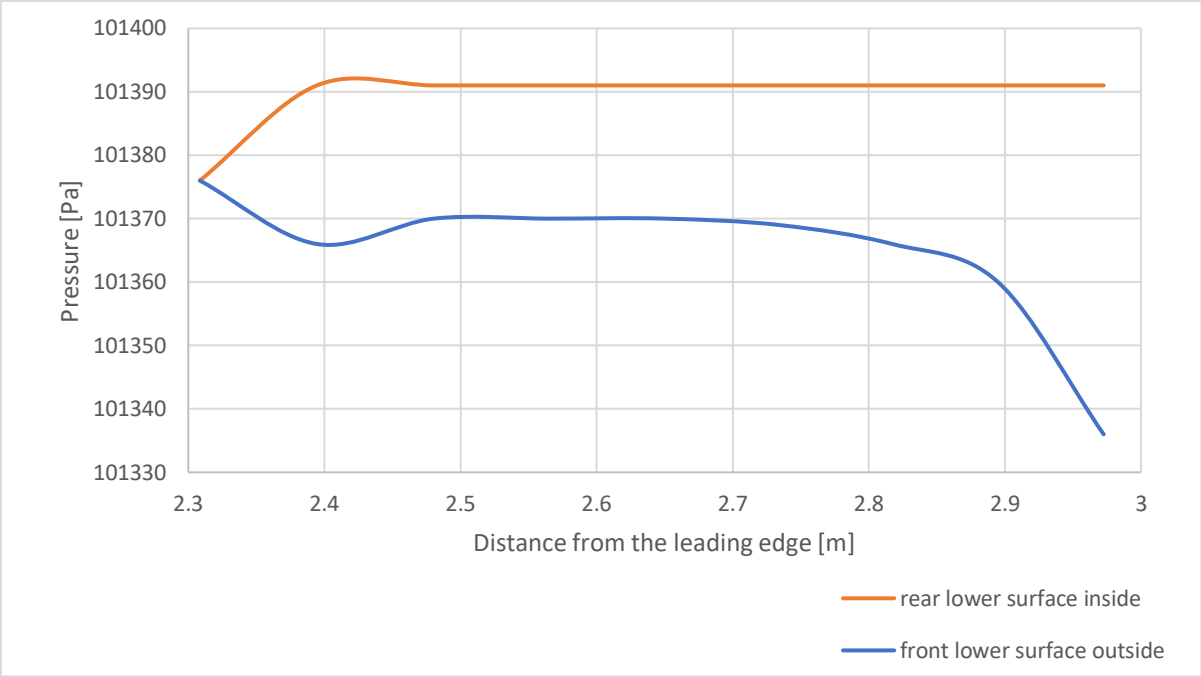

c

Figure 48. Pressure acting on a material in the function of distance from the leading edge in the symmetry plane: a – upper surface; b – front lower surface; c – rear lower surface

The mesh generated in order for the FEM calculations to be performed was a shell type, that contained 31514 elements. The mesh metrics were the following: element quality = 0.95; skewness = 0.06; aspect ratio = 1.08. Only some of the elements forming the mesh remained unstructured.

Only one covering material was considered in the FEM analysis, i.e. fabric no. 2 not subjected to ageing. The choice of this material was caused by the fact that this fabric was the strongest among all the previously considered. Whereas, the pressure acting on the paraglider material in the considered case is increased compared to the case described in the Section 11.3.

The course of numerical calculations allowed to obtain results regarding deformation, stress and strain of the considered woven fabrics in numerical values (Table 19), as well as their distributions over all the structure, Figure 49.

Table 19. Results obtained in the course of FEM numerical calculations

Sample	**Stress [Pa]**			**Strain [%]**			**Deformation [m]**		
	min.	**av.**	**max.**	**min.**	**av.**	**max.**	**min.**	**av.**	**max.**
2	0.000	3.272e6	2.645e7	0.0	0.6	6.8	0.000	0.006	0.043

Based on the results compiled in the Table 19 it can be concluded, that in the sense of proportion the results were comparable to these obtained during the analysis of a traditional paraglider (Section 11.3). However, the numerical values are slightly higher. It is caused by increased values of initial pressure acting on the materials.

The distributions of stress and deformation regarding the considered case were compiled in the Figure 49, below.

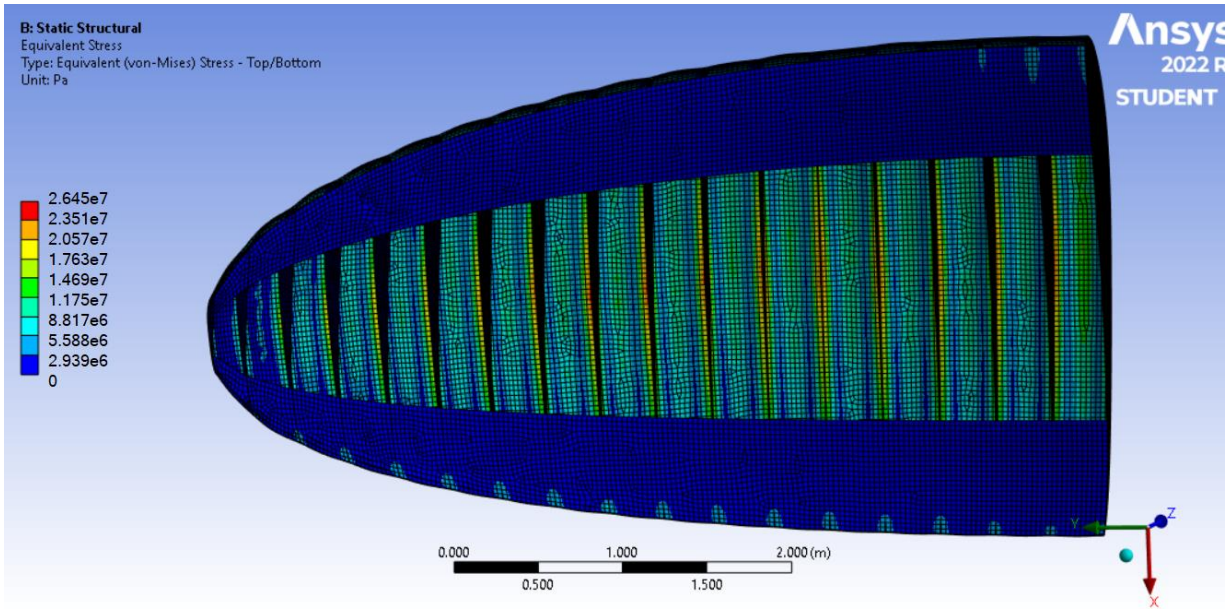

a

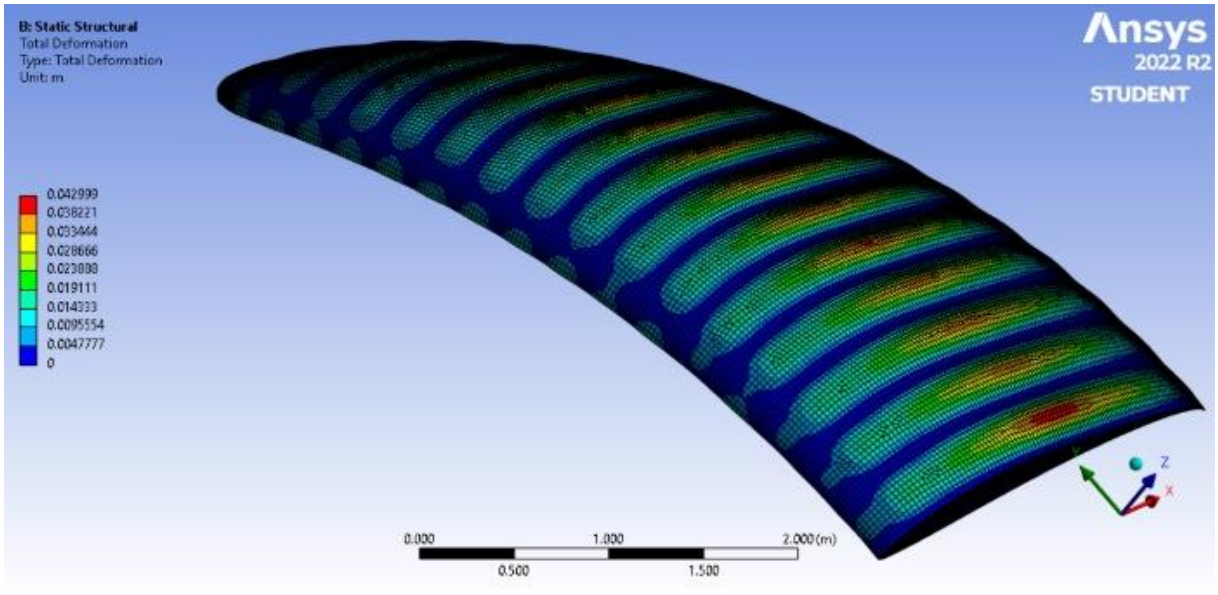

b

Figure 49. Distributions of stress and deformation over the considered type of paraglider

The distributions obtained during the analysis showed a similar dependences, as a traditional wing type. The greatest stress was concentrated in a material in the immediate vicinity of the ribs (rigid support); whereas, biggest values of deformation were noticed in the regions between supporting ribs. However, in the previous case that was described in Section 11.3, the most significant intensity of deformation was observed on its leading edge – in this case it was noticed in the section between the leading and trailing edges.

When a pressure distribution over the both geometries in the symmetry plane were analyzed, many differences were observed. Therefore, the nature of the deformation distribution over the considered geometry is explained.

The bottom surfaces were almost not deformed. Thus, as expected, the pressure distribution obtained in the course of the CFD calculations has no negative impact on maintenance of the aerodynamic shape of the paraglider.

14. Fields for the future development

The aim of this section was to indicate fields for the future development of research on a paraglider in the meaning of materials engineering.

As mentioned above, the paraglider contains the following basic components, i.e. wing, lines and harness. In the above analysis, only a wing and its covering materials were studied precisely.

It should be also noticed that material segments creating a paraglider wing are connected to each other by seams. Therefore, their permeability and strength properties can have a significant influence on the final product and its characteristics.

14.1. Estimation of seams in paraglider wing (according to [56])

The seam rupture is a complex issue to be considered. It has a perpendicular direction to an actual force acting on it caused by pressure distribution acting on a paraglider wing and its materials. Moreover, tensed sewing thread causes shearing and friction acting on the other components of the material; a variable friction force between a sewing thread and the weaving threads occurs.

For the further analysis of the seam load, the most important input data is the maximal pressure difference between two sides of a textile fabric forming paraglider brit. According to the previously obtained results, the maximal pressure difference was obtained,

with a velocity equal to v = 45 km/h and angle of attack α = 12º. Section 10.2. The maximal force acting on a paraglider wing was therefore equal to $\Delta p = p_{max} - p_{min} = 274Pa$.

The considered seams connecting the covering elements were according to the ISO 4916 [57] standard, the seam number is 1.01.03/301.301, Figure 50. The sewing conditions were the following: (1) *100%* PET sewing threads; (2) needle size&finish *Schmetz R 90 nickel plated*; (3) quilted seam 301; (4) density 3/cm; (5) sewing machine *Siruba company*.

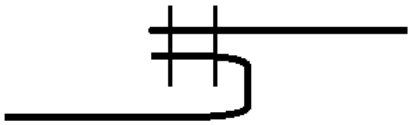

Figure 50. – Seam connecting the covering material [56]

In the below described physical analysis, a maximal force during elongation and relative elongation at break were obtained for sewn samples of fabrics no. 1 and 2. The tests were performed in the longitudinal direction and perpendicular direction to the seams, Figure 51. The distance between clamps was 20 cm, whereas the width of the samples was equal to 5 cm.

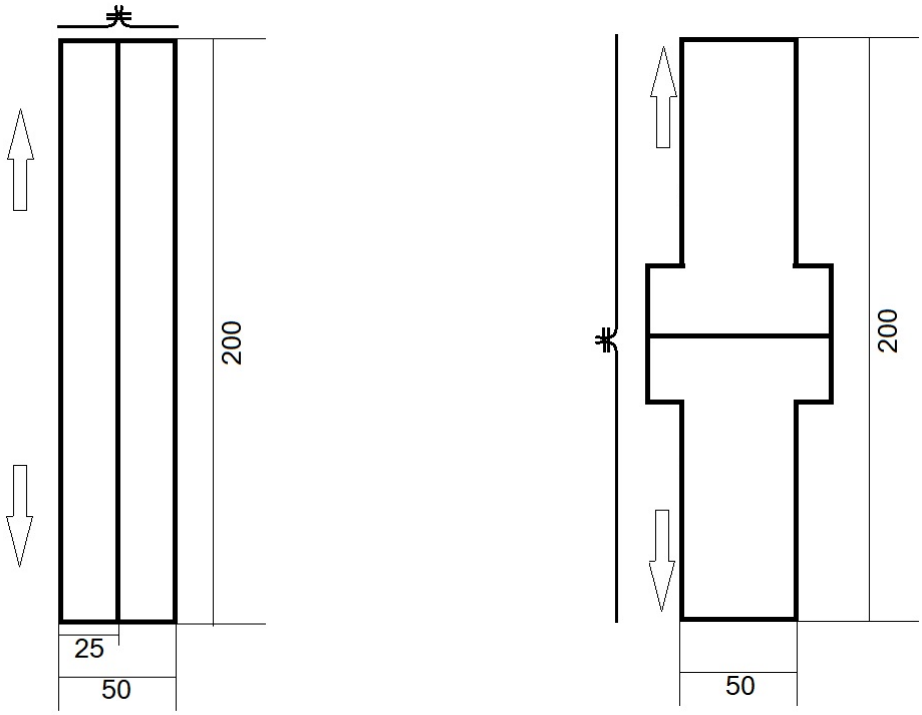

a b

Figure 51. – Technological project of seams. Determination of seam strength oriented parallel and perpendicular in relation to direction of acting force:
a) longitudinal seam; b) transverse seam

According to the Figure 52 below, the maximal force during elongation significantly differed depending on the direction of seam. When the seam was longitudinal to the direction of tensile, it acted as a reinforcement. Therefore, the obtained results were increased compared to the samples where no sewing was applied. When the seam was perpendicular to the tensile direction, shearing acting on the fabric threads caused breaking of the samples at smaller values of forces. When a warp direction was considered the obtained values of breaking force were the following: *490N* (longitudinal direction) and *194N* (perpendicular direction) for Sample no. 1; *577N* (longitudinal direction) and *331N* (perpendicular direction) for Sample no. 2. The corresponding values obtained for the weft direction were *600N*/*172N* (Sample no. 1); *581N/210N* (Sample no. 2). In case of all the performed measurements, the woven structures always broke, whereas the seams remained intact.

The differences of the obtained relative elongations at break of the considered samples were insignificant. The comparable values of elongation in all directions are advantageous, when flight of paraglider is considered.

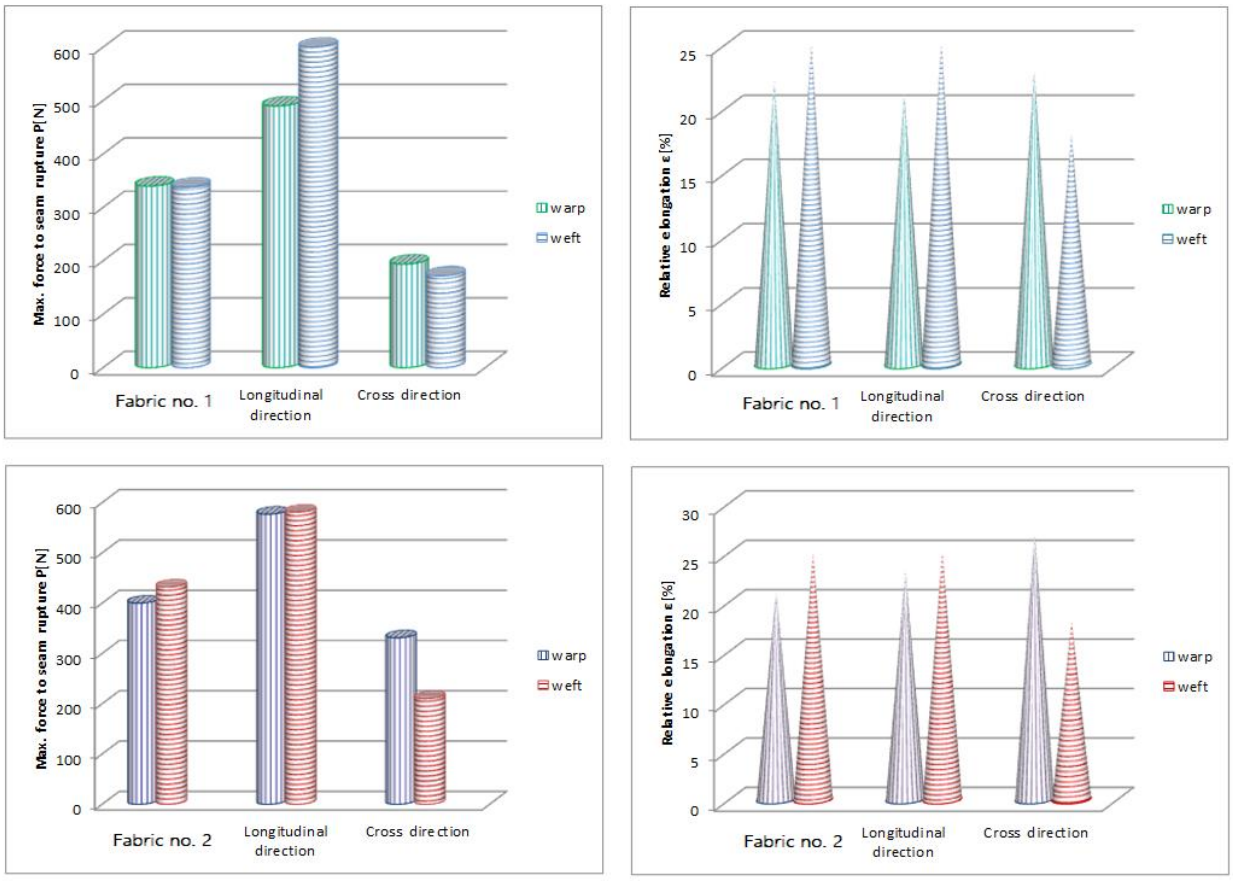

Figure 52. – Maximal force to seam rupture *F[N]* and relative elongation during rupture *ε[%]* vs. direction of acting force [56]

An accurate method was chosen in order to calculate the value of force transmitted through the seams connecting paraglider materials. To analyze the elementary forces acting on the considered system, a rectangular shape piece of material was studied (which expressed the shape of a single brit between two ribs in the symmetry plane), Figure 53. The dimensions were: y_1 – corresponding to the distance between airfoil-shape ribs, C_0 – corresponding to the chord of a paraglider. At the same time, along the C_0 sides, the seams were implemented as attaching joints.

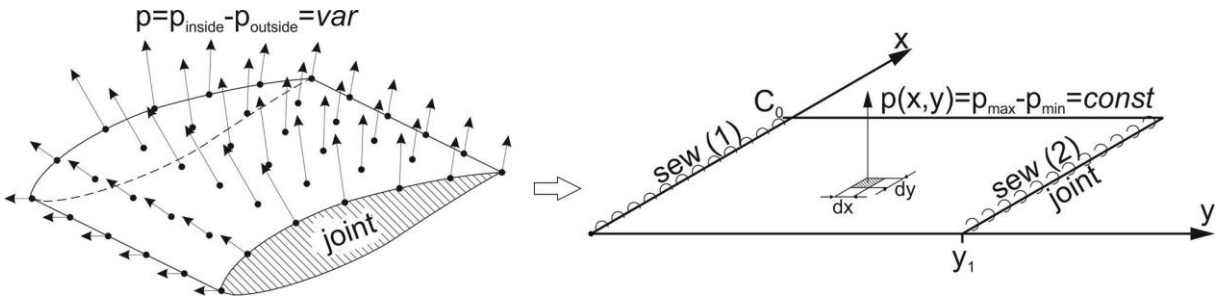

Figure 53. The real flight conditions (left side); the calculation model (right side) [56]

Thus, the force caused by the maximal pressure difference and acting on the considered system, was expressed as below:

$$F_{total} = \int_S \Delta p(x,y)\, dS = \iint_{xy} \Delta p(x,y) dx dy \tag{17}$$

The pressure difference was constant in the infinitesimal time-step. Thus, the integral was simplified to:

$$F_{total} = \Delta p(x,y) \int_S dS = (p_{max} - p_{min}) S = (p_{max} - p_{min}) C_0 Y_1 \tag{18}$$

The force caused by the pressure difference was balanced by internal force in seams denoted by the formula.

$$F_{total} = \int_{l_{sew1}} f_{sew1}(x) dx + \int_{l_{sew2}} f_{sew2}(x) dx \tag{19}$$

f_{sew1} and f_{sew2} were the forces per unit length on the joints; l_{sew1} and l_{sew2} were the lengths of the corresponding seams/joints. Assuming the constant forces $f_{sew1}=f_{sew2}=f_{sew}$ acting along the considered system, the below equation was obtained:

$$F_{total} = f_{sew1} \int_{l_{sew1}} dx + f_{sew2} \int_{l_{sew2}} dx = 2 f_{sew} l_{sew} = 2 f_{sew} C_0; \tag{20}$$

After transforming and comparing the above equations, the final form of the force acting on the seams per unit of length was:

$$F_{seam} = 0.5\ (p_{max} - p_{min})\ Y_1 \tag{21}$$

Introducing the current dimensions of the paraglider's wing, the obtained value of force was $F_{seam}=45.2N/m$. The samples subjected to tensile tests were of the width of 5 cm. Thus, the force acting on the system was equal to $F_{seam}= 9.04\ N/5\ cm$, when velocity was $v = 45\ km/h$ and angle of attack $\alpha = 6^{o}$. When the maximal overload of 5.6g was considered, the force acting on the seam system was $F_{seam}= 50.62\ N/5\ cm$.

Therefore, the quality index was relatively high and its value was between 3 and 5.5 depending on the direction of elongation and seams applied. Moreover, no information regarding breaking of paraglider during a flight in air was found in the literature.

Additionally, air permeability through the seams connecting paraglider fabrics was studied. In order to perform the testing, a single and a double seam type were considered. Different position of the seams and connected fabrics affect the final porosity of the system. Thus, three variants of position relative to the pressure drop were considered, Figure 54 below.

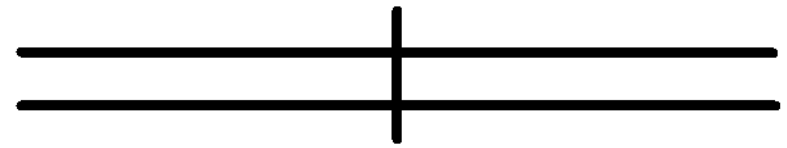

variant 1

variant 2

variant 3

Figure 54. Variants when testing the air permeability through the seams connecting paraglider fabrics

The remaining conditions of performing the tests were consistent with these described in Section 7.1. However, only pressure drops of 200 Pa and 1500 Pa, and samples no 1, 2 and 6 were considered. The obtained results were compiled in the Table 19 and the Figure 55 below.

Table 19. Results of air permeability through seams connecting paraglider fabrics

Sample	**Air permeability ($\frac{l}{m^2 \cdot s}$)**	
	200 Pa	**1500 Pa**
Sample no. 1 – single seam, variant 1	0.661	4.962
Sample no. 1 – single seam, variant 2	1.680	12.600
Sample no. 1 – single seam, variant 3	1.115	8.366
Sample no. 1 – double seam, variant 1	1.400	10.509
Sample no. 1 – double seam, variant 2	1.186	8.890
Sample no. 1 – double seam, variant 3	1.060	7.950
Sample no. 2 – single seam, variant 1	0.886	6.655
Sample no. 2 – single seam, variant 2	2.813	21.100
Sample no. 2 – single seam, variant 3	1.350	10.131
Sample no. 2 – double seam, variant 1	1.493	11.213
Sample no. 2 – double seam, variant 2	1.807	13.555
Sample no. 2 – double seam, variant 3	0.957	7.179
Sample no. 6 – single seam, variant 1	1.049	7.870
Sample no. 6 – single seam, variant 2	1.933	14.503
Sample no. 6 – single seam, variant 3	1.653	12.400
Sample no. 6 – double seam, variant 1	2.147	16.100
Sample no. 6 – double seam, variant 2	1.207	9.054
Sample no. 6 – double seam, variant 6	0.778	5.844

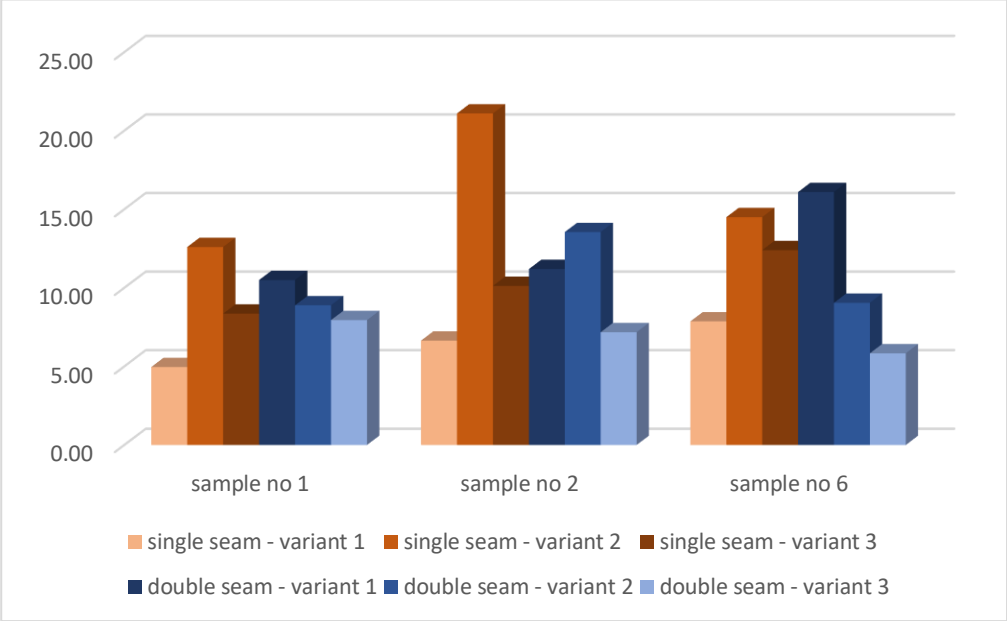

Figure 55. Graph compiling the results of air permeability through seams connecting paraglider fabrics

Based on the results compiled in the Table 19 and Figure 55, it can be concluded that application of seams affect a great increasement of permeability through the paraglider fabrics. All the considered woven fabrics no. 1, 2 and 6 not subjected to sewing or ageing were impermeable when tested with the pressure drops of 200 Pa and 1500 Pa were applied. Whereas, the sewn samples reached values between $0.661\ (\frac{l}{m^2 \cdot s})$ – $2.831\ (\frac{l}{m^2 \cdot s})$, when pressure drop of 200 Pa was applied and $4.612\ (\frac{l}{m^2 \cdot s})$ – $21.100\ (\frac{l}{m^2 \cdot s})$ when pressure drop of 1500 Pa was applied. Thus, it can be concluded, that some variants of sewing influences the air permeability even more significantly than the before analyzed ageing processes. However, ageing applies to all/ most of the surface; whereas sewing applies only to the material connections' locations. In all the considered cases the biggest values of air permeability were observed for the single seam, variant 2 (the maximum was reached for the sample no. 2).

14.2. Estimation of lines

Due to very high loads (stretching, bending) and exposure to external factors, paraglider lines should have specific properties (high tensile strength, resistance to mechanical damage and UV radiation). Because number and diameters of lines used in paragliding are minimized, the properties of lines are still being increased by the manufacturers (fewer lines accumulate loads from the larger surface of the wing). The quality and durability of the lines are improved and controlled in specialized laboratories.

Figure 56. Aramid braided core of paraglider lines (lines without outer sheath) and the same type of paraglider lines with the outer PET sheath (orange) [6]

The paraglider lines are made of high-performance twisted/braided core and the outer sheath, Figure 56. According to the literature [1, 6], the core (aramid or polyethylene) provides about 80% strength, while the PET outer sheath protects against damage caused by external factors and provides easier visual control. The exception are sport paragliders in which lines without outer sheath are used. However, lines in such paragliders must be replaced very frequently.

As mentioned, aramid fibers (mainly Technora) or high-performance polyethylene (Dyneema, Spectra) are used for core production. Both materials are very durable, but have slightly different properties, significant for the operation of the paraglider. Typically, lines from different materials are used for the production of one paraglider (for example, Technora, Dyneema and Dyneema cordless lines) [1, 6].

Aramid fibers are formed by a substance of long and regular chains of macromolecules with aromatic rings. They are arranged in a linear manner and adhere to each other along the fiber axis. This semi-crystalline structure of aramid fibers allows them to achieve very good physical and chemical properties [34]. They exhibit very high tensile strength, do not shrink under the influence of thermal factors and moisture. However, aramid fibers are characterized by their brittleness and low resistance to UV-radiation.

The polymer that builds high-strength polyethylene fibers is formed by a simple and linear macromolecule with repeating -CH2- monomers. High modulus polyethylene has a chemically identical structure to the standard polyethylene used. However, its molecular weight is higher (in the order of 10^6) [34]. Due to the high density of the fiber-forming substance, high-performance polyethylene is obtained as a result of gel-forming. It is resistant to bending and UV-radiation, but deforms under the influence of stretching, higher temperature and moisture. Due to the use of texturing process (stretching and stabilization at a given temperature), this problem has been minimized.

Polyester braid gives about 20% strength. It exhibits shrinkage under the influence of moisture, so it cooperates with stiff core fibers.

The previously mentioned optimization of the thickness of the lines is related to the loads transferred to them from the wing. Since there are more lines in the upper parts, their diameters are smaller. The diameters of the lines are successively increased in places where there are fewer of them (and thus they are exposed to higher loads).

Due to the fact that the lines help in maintaining the shape of the paraglider and stabilize the flight, the length of their individual elements and angles between them are not accidental. Their selection is closely related to the tensile forces that they transmit, Figure 57.

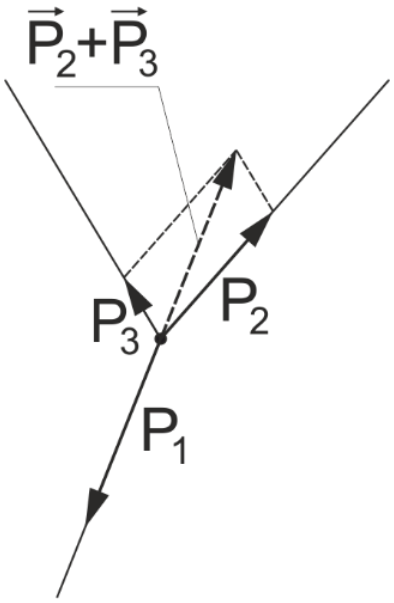

Figure 57. Distribution of forces in the branch node

The upper lines (which connect to the main lines) transfer the loads from the smaller area of the wing. The lengths and directions of main lines that are exposed to higher tensile forces are selected based on the resultant forces acting on the lines above them.

Based on data contained in Annex 1 [58] and studies on beginner's glider model, available for sale since 2014, arrangement and the number of lines were determined.

Based on the data provided in Annex 1 [58], the total length of the considered paraglider's lines was determined. It was from 421.11 m to 471.11 m (it is possible to symmetrically shorten / extend the brake lines). The lines were arranged in four rows (A, B, C, D) and row of brake lines.

Then, the diameters of the lines of the considered paraglider were determined with the use of the physical model of paraglider and a caliper, Figure 58. The laboratory tests according to existing standards were not conducted in order to not cause damage caused by sampling the lines.

Figure 58. measuring the diameters of the lines of the considered paraglider

The obtained results were summarized in the Figure 59 below.

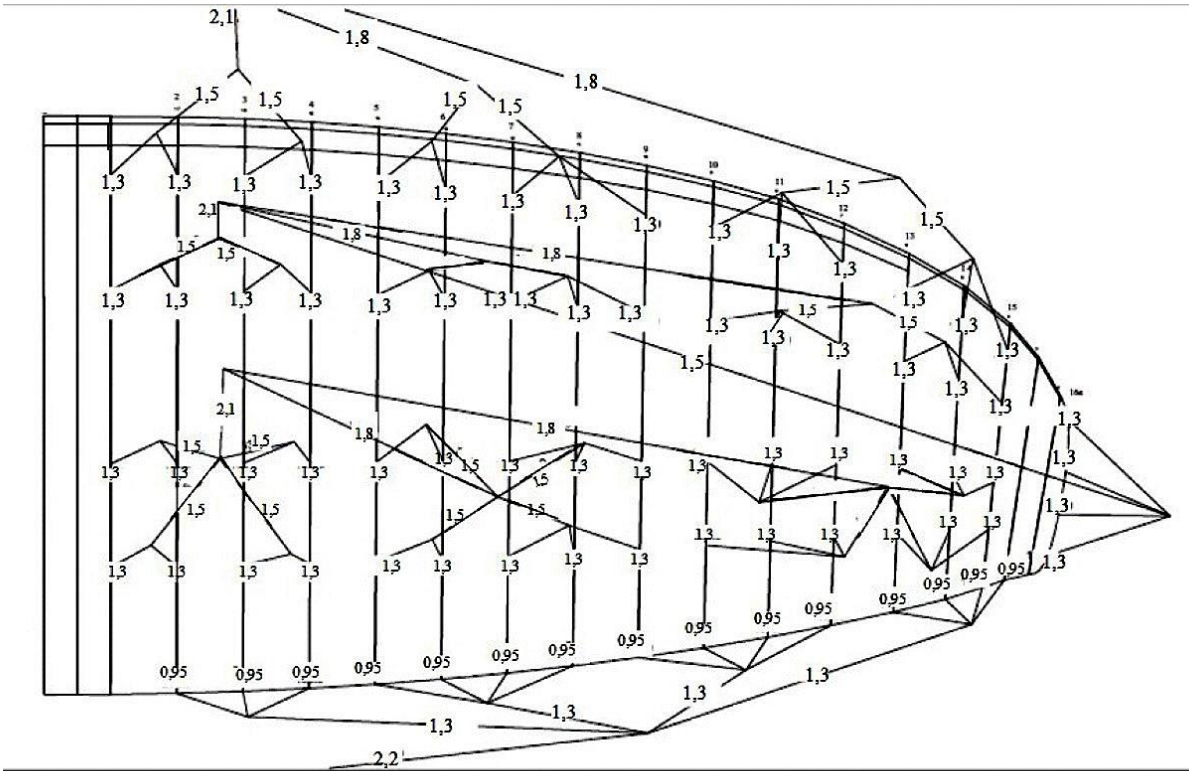

Figure 59. Obtained diameters (in mm) of the lines of the half of considered paraglider (based on [58])

According to the results compiled in Sections 10.2 and 11.3, when an overload of 5.6 is applied, the paraglider generates a lift force of:

$$L_{max} = L \cdot l_f \cong 8505\ N \tag{22}$$

128 Dyneema lines of a diameter equal to 1.3 mm were attached to the paraglider under consideration. In addition, 30 Dyneema lines of a diameter of 0.95 mm were attached to its trailing edge (these lines are attached to form brakes). Assuming that the brakes are completely unloaded, the average load acting on the single line of a diameter of 1.3 mm is:

$$N_{av,1} = \frac{L_{max}}{n_{\phi=1,3}} \cong 6.6\ daN \tag{23}$$

According to the data contained in Annex 2 [59], Dyneema line breaking strength of the considered diameter is equal to 146 daN. Therefore, it can be concluded that the lines are selected with a huge safety margin, even when the deterioration of the line parameters during use is considered.

It also proves that the sizing parameter of the lines is their minimum deformation during the flight. The elongation of the Dyneema line ϕ=1.3 at a load of N=5 daN is ε=0.05% (based on Annex 2 [59]). Minimal elongation/deformation of the lines ensures direct, immediate transfer of forces between the wing and the pilot. This allows to precisely control the wing and quickly react to the changing flight conditions.

Dyneema lines ϕ=1.3 connect to 50 Dyneema lines ϕ=1.5. Thus, the average line load is:

$$N_{av,2} = \frac{L_{max}}{n_{\phi=1,5}} \cong 17\ daN \tag{24}$$

The strength of the Dyneema line ϕ=1.5 is 216 daN, the elongation at a load of N=5 daN is ε=0.2% (based on Annex 2 [59]). These values are confirmed by the conclusions from the Dyneema line load analysis ϕ=1.3. The diameters of the paragliding lines are selected in such a way that the lines show minimal elongations under operational loads.

Summarizing, the purpose of improving the paraglider's performance is to minimize drag force. This is achieved by reducing the number and diameters of lines. The lines should also have dimensional stability, low mass and help in balancing the wing. Therefore, it is important to choose the right materials and the proper arrangement of the lines.

14.3. Harness – heat transfer

The aim of this section was to analyze heat transfer between a paraglider pilot wearing a PU- PET harness and the environment. The calculations have a general form and the applied model was simplified.

Temperature of the air was assumed to be changing constantly in time from 3°C to 15°C for 24 minutes. The change of the temperature was a result of gliding of the paraglider from the altitude of 2000 m above the sea level to 0 m, Figure 60.

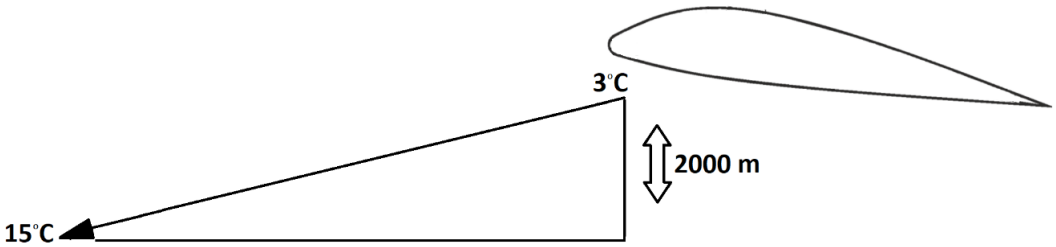

Figure 60. Change of the temperature of the air as a result of the height change

As mentioned above, the considered PU-PET harness, was a barrier between a pilot and the environment. The body temperature of the pilot was assumed to be equal to 36.6 °C. PU foam was a layer (thickness of 20 mm) of harness in contact with the body; another layer was a PET fabric of a thickness of 2 mm. The temperature of the air was variable and it was assumed to be changing constantly from 3 °C to 15 °C. This case is described by Figure 61.

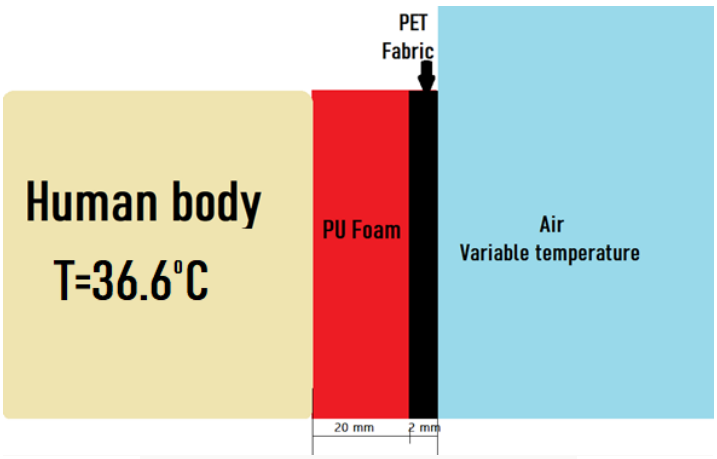

Figure 61. Case visual description

During the calculations, the influence of cooling / heating related to the air flow over the harness was neglected.

The first step of the program creation in the MATLAB environment was to define the physical constants and boundary conditions, Figure 62. Change of the constants related i.e. to the construction of materials was neglected (calculations are conducted for materials considered as nonporous layers).

```
lambdal=0.17; % heat transfer coefficient of PET
lambda2=0.022: % heat transfer coefficient of PU foam
cp1=1200; % specific heat of PET
cp2=1400; % specific heat of PU foam
ro1=1360; % density of PET
ro2=60; % density of PU foam
g1=0.002; % thickness of PET material
g2=0.02; % thickness of PU foam material
dt=l: % time step lenght
Tempz0=3; % oustide temp. for C=0, it is for h=2000
Tempzk=16; % outside temp for h=0
Tempw=36.6: % inside temp. of the case
alfa1=lambda1/cp1/ro1;
alfa2=lambda2/cp2/ro2:
TstO=(lambda1/g1*Tempz0+lambda2/g2*Tempw)/(lambda1/g1+lambda2/g2); % temperature on materials' contact for t=0
```

Figure 62. Definition of the physical constants and boundary conditions

Then, the matrices of time and coordinates were typed, Figure 63. The time matrix represented 1440 time steps, each of 1 s long. The coordinate matrix was focused on 2 layers of the PU-PET material, the total thickness of 2.2 cm – each element of matrix per 1 mm.

```
t=[0:dt:1440]; % matrix of time, 24 min. in step of 1 s
wsp1=[0:0.5*g1)g1]; % matrix of layer coefficients for PET
wsp2=[(g1+0.5*g1):0.5*g1):(g1+g2)] % matrix of later coefficients for PU foam
wsp=[0:(0.5*g1):(g1+g2)]; % matrix of coefficients
```

Figure 63. – Definition of the temperature and coordinates matrices

Then, the code for temperature distribution at the beginning of flight (t=0) was determined, Figure 64.

```
Temp0=zeros(length(wsp),1);
for i=1:length(wsp1)
    Temp0(i)=Tempz0+(Tst0-Tempz0)/(length(wsp1)-1)*(i-1);
end

for i=(length(wsp1)+1):length(wsp)
    Temp0(i)=Tst0+(Tempw-Tst0)/length(wsp2)*(i-length(wsp1));
end
```

Figure 64. Determination of the temperature at the beginning of flight

Another step was to type a code for determination of the external temperature in time, Figure 65.

```
Tempz=zeros(length(t),1);
for j=1:length(t)
    Tempz(j)=Tempz0+(Tempzk-Tempz0)/(length(t)-1)*(j-1);
end
```

Figure 65. Determination of the external temperature in time

The final step was to determine the temperature field over time, Figure 66.

```
Temp=zeros(length(wsp),length(t));
for i=1:length(wsp)
    Temp(i,1)=Temp0(i);
end

for j=1:length(t)
    Temp(1,j)=Tempz(j);
    Temp(length(wsp),j)=Tempw;
end

for j=2:length(t)
    for i=2:(length(wsp)-1)

        if i<=length(wsp1)
            Temp(i,j)=Temp(i,j-1)+alfa1*(t(j)-t(j-1))/(wsp(i)-wsp(i-1))^2*(Temp(i-1,j-1)-2*Temp(i,j-1)+Temp(i+1,j-1));
        else
            Temp(i,j)=Temp(i,j-1)+alfa2*(t(j)-t(j-1))/(wsp(i)-wsp(i-1))^2*(Temp(i-1,j-1)-2*Temp(i,j-1)+Temp(i+1,j-1));
        end
    end
end
```

Figure 66. Determination of the temperature field in time

Figure 67 presents graph of change of the temperature in a function of time and distance: interface Air-PET (s = 0 m), interface PU-Body (s = 0,022 m). Those 2 distances also described a boundary conditions given before starting the calculation. For the distance

s = 0 m temperature (T) changed linearly in time from 3°C to 15°C for 1440 seconds; for the distance s = 0.022 m temperature was always equal to T = 36.6°C

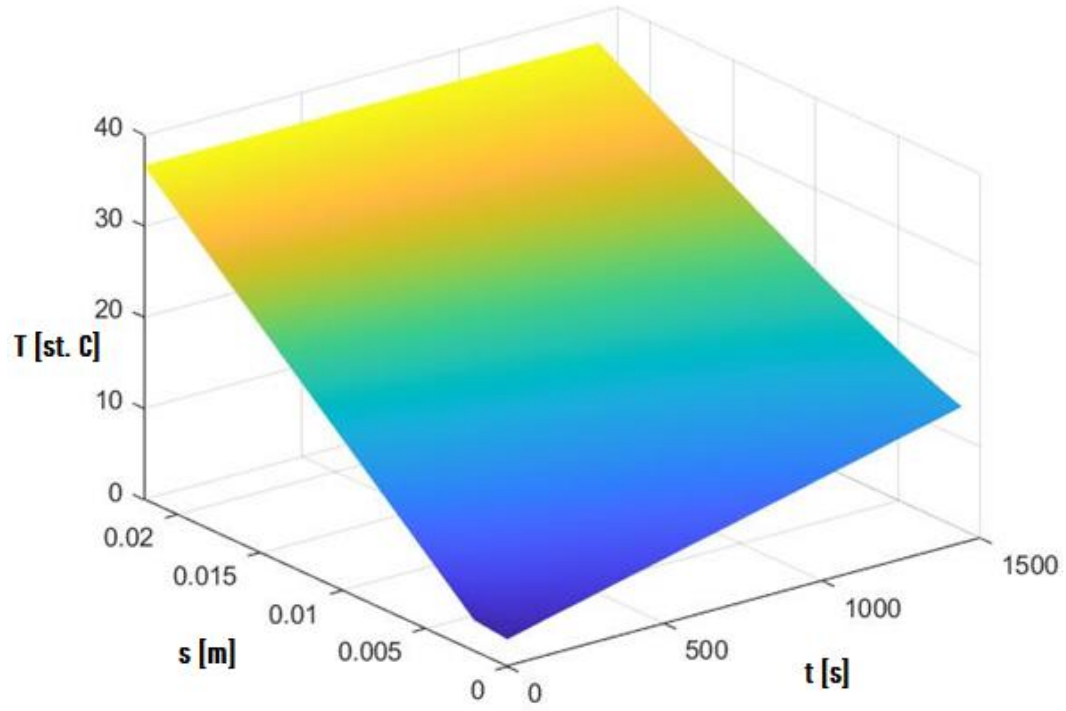

Figure 67. Changes of temperature field through the total thickness of a harness material (PU-PET) during flight

Based on the Figure 67 it can be concluded that solution was stable – there were no spots of unnatural picks of temperature etc.

The change of the temperature at the interface between materials was also calculated. Based on the Figure 68, temperature change at the interface was non-linear in the beginning of the flight. This proves that changes of temperature field (in the considered period of time) were dynamic, so the numerical methods were the appropriate tool to solve the problem. After approximately 2 minutes of the flight, the temperature changes became linear.

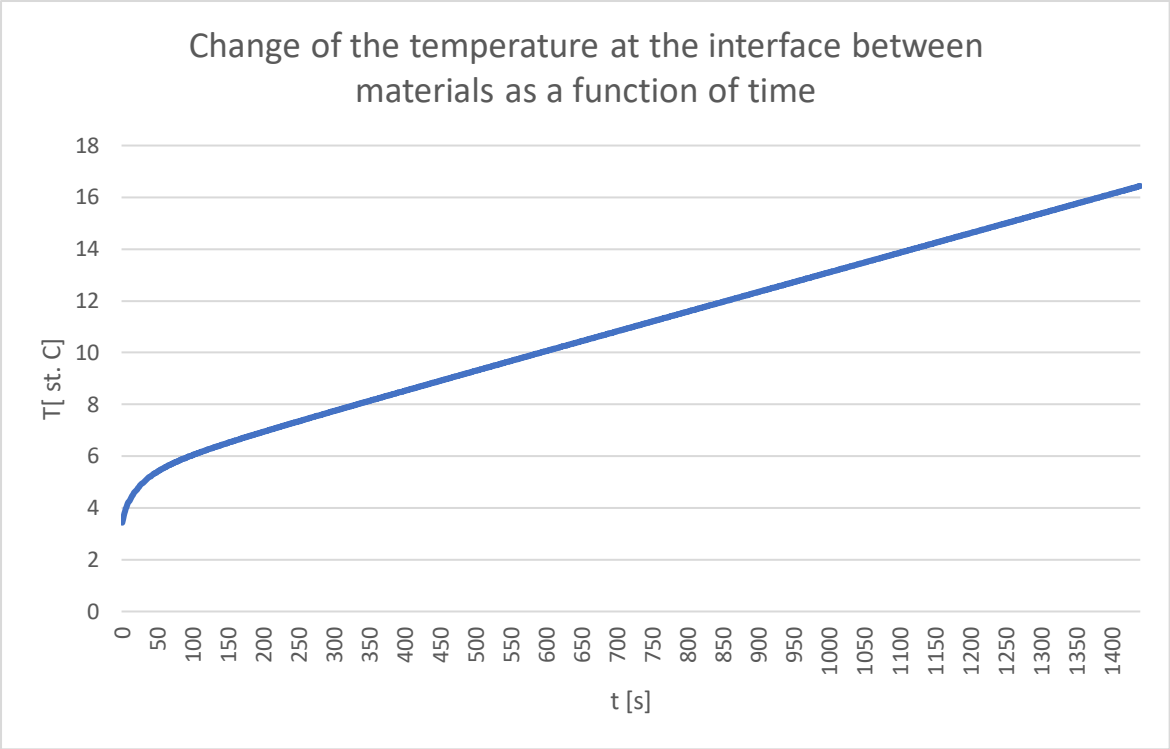

Graph 2. Change of the temperature at the interface between Polyurethane foam and polyester fabric in the function of time

15. Summary and conclusions

The dissertation was focused on numerical modeling and sensitivity of aerodynamic characteristics to shape and material properties of a paraglider.

Thus, in the first section of the dissertation a multistage optimization algorithm was introduced; it allows to: (1) determine the influence of material properties on the aerodynamic characteristics of paraglider; (2) select the covering materials advantageous to the considered constructions and assumptions of the final product.

In the first part, the laboratory tests were performed on ten different woven fabrics in the sense of material composition, as well as general, structural and mechanical characteristics; three of the fabrics were selected to be subjected to the UV, thermal and mechanical ageing and the determination of their influence on the material properties. The obtained laboratory results could be introduced to the further steps of the research.

The next steps concerned the numerical analysis in the terms of CFD and FEM Structural calculations performed on a model of a traditional recreational paraglider wing in the sequence: (1) study of the initial influence of air permeability on aerodynamic characteristics with applying of the *porous media* tool; (2) recalculating of the flow over paraglider after applying the more accurate permeability results, i.e. with the consideration of the actual pressure drop acting on the material during the flight; (3) study of the stress, strain and deformation in the materials covering paraglider; (4) determining the impact of deformation on the aerodynamic characteristics of paraglider.

The next section of the dissertation was focused on introducing a single cover paraglider model. A part of the above described algorithm was applied to the model, including calculation of the flow over paraglider after with the consideration of the actual pressure drop acting on the material during the flight and study of the stress, strain and deformation in the materials covering paraglider;

The last part described initial calculations estimating the safety factors of seams and lines, as well as the heat transfer through the harness. The topics were introduced as fields for the future development.

The obtained test results allowed the following conclusions to be formulated:

1. The analyze of paraglider/parachute fabrics shows that they are characterized by good relation of strength to the surface mass. The obtained air permeability values

of all the analyzed samples are equal to zero, when pressure drops of 100 Pa – 2000 Pa are applied, except material no. 9. All the considered samples are PA 6.6 fabrics coated with polyurethane resins or silicone/polyurethane. Based on the SEM records, the paraglider/ parachute fabrics are manufactured using multifilament yarns. A significant flatter of the yarns is probably a results of calendaring of the analyzed fabrics, as well as high values of weave factor and yarn extension, low crimp factor, as well as no/insignificant twist of the yarns. Tight weave and calendaring result in achieving required final parameters of the fabric, which is mainly air-permeability tending towards zero. Obtaining thinner fabric is highly correlated with adjusting thinner filaments. However, it does not have significant correlation with the diameter of yarn, as the yarns in this type of fabrics are flattered in the final product. Every analyzed sample is characterized by thicker and thinner yarns. The thicker yarns represent the reinforcement. All the considered fabrics present traditional ripstop of squares pattern; the exception is sample 9, where the reinforcement creates hexagonal pattern, which probably causes increased dimensional stability in all directions. In each considered case, reinforcement contains two thicker threads/1 edge (of the square or hexagon). Based on the SEM records of the magnitude of 500x the polyurethane resins/silicone not only glue the spaces between interlacements, but also those between filaments. Depending on the model and type of the fabric, the amount of impregnation and its general picture differs from each other.

2. The FTIR spectra enables to indicate samples of the expected highest mechanical properties; the samples expected to present the greatest strength properties, are fabrics no. 9 and 10; it is caused by the presence of the Si-C and -Si-CH3 functional groups. Moreover, sample no. 1 is characterized by the highest peak around the groups C=O and C-O.

3. Material modification accomplished by combined polyurethane and silicone results in a significant increase of resistance to the UV radiation, which causes a significant color change for all the analyzed samples, except from samples no. 9 – 10. The decreased dE*ab values observed for the samples are related to the presence of an increased amount of Si-C, C-N-C, Si-O-Si and Si-CH_3 groups. Both, high and low temperatures, does not have noticeable influence on the color of all the tested samples.

4. When pressure drop of 200 Pa is applied, all the analyzed samples are impermeable, except from these damaged by flexing. Thus, flexing damage has the greatest influence on the air permeability change among all considered aging factors.

5. Graph of load to extension recorded during tensile test shows that it presents a linear characteristic only in a fragment of it, and the linear character doesn’t begin on a starting

point of the measurement. The first (nonlinear) part refers to straightening of threads in fabric due to their interlacement. The obtained values of Young's modulus differ when both direction of one type of a fabric are considered; the change can be caused by number of yarns per length unit, use of different type of yarns in different direction of the material, etc. The greatest influence on mechanical properties has ageing caused by the UV radiation. The greatest decrease of the breaking strength is 75 %, when sample no. 1 is considered. The lowest decrease of the tensile properties is observed for sample no. 6, i.e. 2% (warp) and 19% (weft). No significant influence of freezing on the mechanical properties of the considered samples is observed.

6. According to the initial CFD calculations, the maximal pressure acting on a covering material of a paraglider wing is equal to 187 Pa, when normal flight conditions are applied and nonporous material is considered. Therefore, when using *porous media* tool (applied when numerical calculations of influence of air permeability on aerodynamic characteristics of a paraglider are performed), porous resistance value should be calculated based on the air-permeability values obtained when tested with a pressure drop consistent with the real conditions.

7. All the analyzed woven fabrics not subjected to degradation and subjected to UV and thermal ageing can be considered as impermeable, when normal flight conditions are applied. However, it does not refer to the mechanical degradation, i.e. flexing damage.

8. Based on the obtained CFD results it can be concluded that air permeability increase has an impact on the paraglider's aerodynamic characteristics decrease. The best characteristics presented paraglider covered with an air-impermeable material, as its c_l/c_d ratio was equal to 13.17. Paraglider covered with materials no. 1 and 2 subjected to the flexing damage presented slightly decreased characteristics. Aerodynamic characteristics of a paraglider covered with material no. 6 subjected to flexing were significantly decreased compared to the remaining cases; its c_l/c_d ratio was equal to 8.35, which is 4.35 less than the value regarding paraglider covered with an impermeable fabric. Moreover, the c_l/c_d ratio, in addition to the geometry of the wing and material characteristics, also depends on the orientation of the wing relative to the direction of flight and/or velocity.

9. When streamlines of velocity as a variable are compared for cases of paraglider covered with the permeable materials, it can be concluded that porosity of a material causes the particles to permeate through the paraglider coverage. In the case of the lowest air permeability value (fabric no. 1 subjected to flexing damage), the air streams permeating is insignificant and almost does not influence the streamlines track around the paraglider

on the lower and the upper surface. In the case of paraglider covered with fabric no. 6 subjected to flexing damage, the increased air permeability value disturbs the track of streamlines around the wing. An increased velocity streamlines appears at a greater distance from the upper surface; moreover, the velocity is decreased compared to the previous case. Thus, it affects in decreasing of the lift force and increasing in the drag force values.

10. The greatest pressure acts on paraglider materials when the greatest overloads during the flight are applied. They can be determined by CFD calculations (when an increased angle of attack and velocity are considered), flight envelopes or electromechanical flight data recorders. According to a record of opening a wing-type parachute, the load factor can achieve a value of 5.6. Paragliders are not expected to be subjected to as great overloads as parachutes. However, in fact, they are flying objects with no rigid structure; thus, the maximum overloads can be increased compared to those estimated with the load envelope. Thus, a maximal pressure drop that can act on a paraglider covering material is 1047 Pa. This value was implemented for the structural analysis.

11. Deformation and strain decreases with increasing of tensile strength of a material and/or decreasing of pressure acting on a material. The lowest deformation and strain values were achieved for the material number 2 not subjected to the ageing and materials no. 2 and 6 subjected to the flexing damage. The opposite is noticed for the fabric no. 1 subjected to UV degradation.

12. The behavior of change of the stress value differs than the above. The thinner material and the stronger material, the greater the stresses. Sample no. 1, which was characterized by the lowest thickness, obtained the highest stress values among all the materials. When the tensile properties of this material is decreased (i.e. UV degradation), the maximal and average values of stress also decreases. This is consistent with the general principles of mechanical strength of materials.

13. Distributions regarding stress differ compared to the strain an deformation distributions. the greatest stress is concentrated in a material in the immediate vicinity of the ribs (rigid support); whereas the biggest values of strain and deformation are noticed on the leading edge and in the regions between supporting ribs.

14. Safety factors of the considered materials not subjected to degradation range between 3.94 – 6.00. Safety factor of fabric no. 1 subjected to the UV degradation is equal to 1.33. Moreover, the obtained maximal strain is greater than elongation at break of this material (8.5%). Although the implemented overload is very high and the maximal

obtained values of strain rarely occur when distributions are considered, a paraglider covered with an UV degraded material no. 1 should not be allowed to use.

15. CFD analysis regarding deformed wing covered with fabric no. 6 shows that the c_l/c_d ratio decreased 25% compared to the undeformed wing. Deformation caused by pressure acting on a material has a significant influence on the aerodynamic characteristics of a paraglider. However, the decrease was recorded for the deformation caused by pressure, when an overload of 5.6 occurs. Pressure acting on a material during the normal flight conditions would not cause such significant decrease of the aerodynamic characteristics. However, the pressure distribution over the deformed wing is still assessed as very advantageous.

16. The introduced multistage optimization can support the paragliders manufacturers in the selection of materials that would be the most advantageous for the new models of wings referring to the studied geometry and requirements of the final product. However, the proposed algorithm can be transformed into an automatized and simple optimization tool.

17. Model of the paraglider wing covered only with the upper brits has a significant importance from the view of packing volume and mass of the final product. A normal type paraglider wing's surface is equal to 71.65 m^2; whereas for the single cover type it is equal to 53.02 m^2. The lowest expected masses are obtained for a paragliders covered with fabrics no. 4, 8 and are equal to 1.378 kg (single cover paraglider) and 1.863 kg (traditional paraglider); thus, the minimum mass decrease caused by the change of geometry is equal to 0.485 kg. The lowest volumes are obtained for samples no. 7 and 8; their values are equal to 2.121 dm^3 (when single cover paraglider is considered) and 2.866 dm^3 (for traditional paraglider); thus, the minimum decrease of a volume caused by the geometry change is equal to 0.745 dm^3.

18. According to the results of CFD calculations regarding the geometry of single cover paraglider, the c_l/c_d ratio is equal to 11.27, when angle of attack of 12^o is applied. Unlike in the previously considered cases, the pressure inside the wing was unevenly distributed; it is due to a specific geometry. An overpressure is observed inside the wing at the trailing edge, which secures maintaining of the shape in this section; different character of distribution would cause e.g. mutual suction of both layers and distortion of the shape of the airfoil. An overpressure that was created at the leading edge on the outer surface of the paraglider is higher than the one created inside the wing. However, the value of pressure acting on the material is insignificant; moreover, ribs spaced every half meter would support

and hold the front lower cover. A distance between the upper and lower cover in this section would secure maintaining of the aerodynamic shape.

19. When streamlines over the single cover paraglider are analyzed, a vortex is created inside of the wing, which was not observed in the previously considered cases. It may be a reason of the airfoil change or not implementing the lower covering material. However, the geometry does not cause any other flow disturbances. The streamlines, especially on the lower cover, are smooth.

20. In the sense of proportion the FEM structural results regarding the single cover paraglider are comparable to these obtained during the analysis of a traditional paraglider. However, the values of calculated parameters are slightly higher; it is caused by increased values of initial pressure acting on the materials.

21. The distributions of stress, strain and deformation obtained during the analysis showed a similar dependences, as a traditional wing type; however, in this case the most significant intensity of deformation is noticed in the section between the leading and trailing edges. Bottom surfaces are almost not deformed; pressure distribution has no negative impact on maintenance of the aerodynamic shape of the paraglider.

22. The quality index of seams in paraglider wing is relatively high and its value is between around 3 and 5.5 depending on the direction of elongation and seams applied.

23. Air permeability through the seams connecting paraglider fabrics differs depending on the applied type of seam, as well as material's position over the pressure drop.

24. Paraglider lines are selected with a huge safety margin. It confirms that the diameters of the lines are selected in such a way that the lines show minimal deformations under operational loads.

25. When heat transfer through the harness between surrounding air and the pilot are considered, changes of temperature field (in the considered period of time) are dynamic; thus, the numerical methods are the appropriate tool to solve the problem theoretically.

26. Each element of the paragliding system (i.e. wing, lines, risers, harness, pilot) is characterized by different behaviors, which require separate physical and mathematical descriptions. Assembling all the parts creates a global / complex model, which has completely different characteristics than those resulting from partial models. The construction, description and solution of this model is a very complex problem, far beyond the scope of doctoral dissertation.

REFERENCES

[1] Dudek, P. & Włodarczak, Z. (2006). *Paralotniarstwo* [Paragliding]. ARETE Bydgoszcz

[2] pxhere.com/en/photo/920251

[3] ukairsports.com/uploads/Skywalk-BREEZE.jpg

[4] dudek.eu/en/technologie

[5] Abłamowicz, A. & Nowakowski, W. (1980). *Podstawy aerodynamiki i mechaniki lotu* [Fundamentals of aerodynamics and flight mechanics]. Wydawnictwo Komunikacji i Łączności

[6] Uzochukwu, S. (2014). *Paraglider lines.* Skywings

[7] Kulhánek, R. (2019). *Aerodynamické Charakteristiky flexibilních křídel* [Aerodynamic characteristics of flexible wings] (dissertation). Faculty of Mechanical Engineering CTU in Prague

[8] Chapra, S. C. & Canale, R. P. (2021). *Numerical Methods for Engineers* (8th ed.). McGraw-Hill.

[9] ANSYS, Inc. (2010). *Introduction to ANSYS FLUENT*

[10] ANSYS, Inc. (2010). *Introduction to ANSYS Mechanical APDL*

[11] ANSYS, Inc. (2010). *Introduction to ANSYS Design Modeler*

[12] ANSYS, Inc. (2010). *Introduction to ANSYS Meshing*

[13] Babinsky, H. (1999). The aerodynamic performance of Paragliders. *The Aeronautical Journal*, 103(1027), 421–428. https://doi.org/10.1017/s0001924000027974

[14] Esperança, N. F. (2004). *Estudo da eficiencia aerodinamica de equipamento de Voo Livre* [Study of the aerodynamic efficiency of free flight equipment] (seminary). Faculty of Science and Technology University of Coimbra

[15] Zhu, X. & Cao, Y. (2012). Effects of arc-anhedral angle, airfoil and leading edge cut on parafoil aerodynamic performance. *Hangkong Xuebao/Acta Aeronautica et Astronautica Sinica*, 33, 7, 1189-1200

[16] Cao, Y. & Zhu, X. (2013). Effects of characteristic geometric parameters on parafoil lift and drag. *Aircraft Engineering and Aerospace Technology*, 85(4), 280–292. https://doi.org/10.1108/aeat-jun-2011-0096

[17] Hanke, K. & Schenk, S. (2014). Evaluating the geometric shape of a flying paraglider. *The International Archives of the Photogrammetry, Remote Sensing and Spatial Information Sciences*, XL–5, 265–272. https://doi.org/10.5194/isprsarchives-xl-5-265-2014

[18] Boffadossi, M. & Savorgnan, F. (2016). Analysis on aerodynamic characteristics of a paraglider airfoil. *Aerotecnica Missili & Spazio*, 95(4), 211–218. https://doi.org/10.1007/bf03404729

[19] Belloc, H., Chapin, V., Manara, F., Sgarbossa, F. & Forsting, A. M. (2016). Influence of the air inlet configuration on the performances of a paraglider open airfoil. *International Journal of Aerodynamics*, 5(2), 83. https://doi.org/10.1504/ijad.2016.080510

[20] Abdelqodus, A. A. & Kursakov, I. A. (2018). Optimal aerodynamic shape optimization of a paraglider airfoil based on the sharknose concept. *MATEC Web of Conferences*, 221, 05002. https://doi.org/10.1051/matecconf/201822105002

[21] Lolies, T., Gourdain, N., Charlotte, M., Belloc, H. & Goldsmith, B. (2019). Numerical methods for efficient fluid–structure interaction simulations of paragliders. *Aerotecnica Missili & Spazio*, 98(3), 221–229. https://doi.org/10.1007/s42496-019-00017-2

[22] Kulhánek, R. (2019). Identification of a degradation of aerodynamic characteristics of a paraglider due to its flexibility from flight test. *Aircraft Engineering and Aerospace Technology*, 91(6), 873–879. https://doi.org/10.1108/aeat-06-2018-0162

[23] Benedetti, D. M. & Veras, C. A. (2021). Wind-tunnel measurement of differential pressure on the surface of a dynamically inflatable wing cell. *Aerospace*, 8(2), 34. https://doi.org/10.3390/aerospace8020034

[24] He, X., Wang, X. & Tang, G. (2021). Wind tunnel testing of flexible wing model with aileron freeplay nonlinearity. *AIAA AVIATION 2021 FORUM*. https://doi.org/10.2514/6.2021-2534

[25] Kim, M. J., Hwang, H. G., Lee, J. H., Kim, J., Park, J. & Song, G. (2022). Aerodynamic design optimization for a canopy based on response surface methodology and a multi-objective genetic algorithm. *Journal of Mechanical Science and Technology*, 36, 9, 4509-4522. http://doi.org/10.1007/s12206-022-0815-1

[26] Geiger R. H. & Wailes W. K. (1990). *Advanced recovery systems wind tunnel test report* [microform]. Ames Research Center

[27] Matos, C., Mahalingam, R., Ottinger, G., Klapper, J., Funk, R. & Komerath, N. (1998). Wind tunnel measurements of parafoil geometry and Aerodynamics. *36th AIAA Aerospace Sciences Meeting and Exhibit*. https://doi.org/10.2514/6.1998-606

[28] Lingard, J. S. (1995). *Ram-air parachute Design*. *13th AIAA Aerodynamic Decelerator Systems Technology Conference and Seminar*

[29] Uddin, N. & Mashud, M. (2010) Wind tunnel test of a paraglider (flexible) wing canopy, *International Journal of Mechanical & Mechatronics Engineering IJMME-IJENS*, 10, 3. 7–13

[30] Pohl, L. (2011). *Aerodynamický výzkum leteckých profilů pro padákové kluzáky* [Aerodynamic Research of the Airfoils for the Paragliders] (dissertation). Faculty of Mechanical Engineering CTU in Prague

[31] Ovchinnikov, V. V., Petrov, Y. V. & Ganiev, S. F. (2021), Effect of paragliding wing dome shape on its aerodynamic characteristics, *Civil Aviation High Technologies*, 24, 6, 54-65. https://doi.org/10.26467/2079-0619-2021-24-6-54-65

[32] Maślanka, P. & Korycki, R. (2022). Sensitivity of aerodynamic characteristics of paraglider wing to properties of covering material. *Autex Research Journal*, 22(1), 64–72. https://doi.org/10.2478/aut-2020-0010

[33] Maślanka P. & Korycki R. (2019). Textile cover effect on aerodynamic characteristics of a paraglider wing. *Fibres & Textiles in Eastern Europe* 27, 1(133): 78-83. https://doi.org/ 10.5604/01.3001.0011.7511

[34] Lewin, M. (2007). *Handbook of Fiber Chemistry*. CRC Taylor & Francis

[35] EN ISO 9237:1995. Textiles — Determination of the permeability of fabrics to air

[36] PIA-C 44378. (1997) Parachute Industry Association – Commercial Specification. *Cloth, Parachute, Nylon, Air permeability*

[37] Maślanka, P., Aleksieiev, A., Korycki, R., Szafrańska, H. & Dąbrowska, A. (2022). Experimental and numerical determination of strength characteristics related to paraglider wing with Fourier transform infrared spectroscopy of applied materials. *Materials*, 15(20), 7291. https://doi.org/10.3390/ma15207291

[38] Peets, P., Kaupmees, K., Vahur, S. & Leito, I. (2019). Reflectance FT-IR spectroscopy as a viable option for textile fiber identification. *Heritage Science*, 7(1). https://doi.org/10.1186/s40494-019-0337-z

[39] Datta, J., Błażek, K., Włoch, M. & Bukowski, R. (2018). A new approach to chemical recycling of Polyamide 6.6 and synthesis of polyurethanes with recovered intermediates. *Journal of Polymers and the Environment*, 26(12), 4415–4429. https://doi.org/10.1007/s10924-018-1314-4

[40] Defeyt, C., Langenbacher, J., & Rivenc, R. (2017). Polyurethane coatings used in twentieth century outdoor painted sculptures. part I: Comparative study of various systems by means of ATR-FTIR spectroscopy. *Heritage Science*, 5(1). https://doi.org/10.1186/s40494-017-0124-7

[41] Cheval, N., Gindy, N., Flowkes, C. & Fahmi, A. (2012). Polyamide 66 microspheres metallised with in situ synthesised gold nanoparticles for a catalytic application. *Nanoscale Research Letters*, 7(1). https://doi.org/10.1186/1556-276x-7-182

[42] Johnson, L. M., Gao, L., Shields IV, C. W., Smith, M., Efimenko, K., Cushing, K., Genzer, J. & López, G. P. (2013). Elastomeric microparticles for acoustic mediated bioseparations. *Journal of Nanobiotechnology*, 11(1). https://doi.org/10.1186/1477-3155-11-22

[43] Lancastre, J. J. H., Fernandes, N., Margaça, F. M. A., Miranda Salvado, I. M., Ferreira, L. M., Falcão, A. N. & Casimiro, M. H. (2012). Study of PDMS conformation in PDMS-based hybrid materials prepared by gamma irradiation. *Radiation Physics and Chemistry*, 81(9), 1336–1340. https://doi.org/10.1016/j.radphyschem.2012.02.016

[44] Żurek, W & Kopias, K. (1983). *Struktura płaskich wyrobów włókienniczych* [Structure of flat textile products] . Wydawnictwa Naukowo-Techniczne

[45] Vassiliadis, S., Kallivretaki, A., Domvoglou, D. & Provatidis, C. (2011). Mechanical analysis of woven fabrics: the state of the art. *Advances in Modern Woven Fabrics Technology*. https://doi.org/10.5772/25255

[46] EN ISO 4892-3 Plastics – Methods of exposure to laboratory light sources

[47] EN ISO 7854. Rubber- or plastics-coated fabrics — Determination of resistance to damage by flexing

[48] EN ISO 105-J01. Textiles – Tests for color fastness

[49] Marzec, A., Szadkowski, B., Rogowski, J., Rybiński, P. & Maniukiewicz, W. (2021). Novel eco-friendly hybrid pigment with improved stability as a multifunctional additive for elastomer composites with reduced flammability and ph sensing properties. *Dyes and Pigments*, 186, 108965. https://doi.org/10.1016/j.dyepig.2020.108965

[50] Torchynska, T. V., Sheinkman, M. K., Korsunskaya, N. E., Khomenkovan, L. Y., Bulakh, B. M., Dzhumaev, B. R., Many, A., Goldstein, Y. & Savir, E. (1999). OH-related emitting centers in interface layer of porous silicon. *Physica B: Condensed Matter*, 273–274, 955–958. https://doi.org/10.1016/s0921-4526(99)00563-3

[51] Yu, L. (2015) *Tolerance Equivalency between ΔE*ab and ΔE00 Metrics* (thesis). Rochester Institute of Technology

[52] EN-ISO 13934. Textiles – Tensile properties of fabrics

[53] Vlad, D. & Oleksik, M. (2019). Research regarding uniaxial tensile strength of nylon woven fabrics, coated and uncoated with silicone. *MATEC Web of Conferences*, 290, 09003. https://doi.org/10.1051/matecconf/201929009003

[54] Danilecki, S. (2004). *Konstruowanie samolotów: wyznaczanie obciążeń*. Oficyna Wydawnicza Politechniki Wrocławskiej,

[55] Brnada, S., Šomođi, Ž. & Kovačević, S. (2019). A new method for determination of Poisson's ratio of woven fabric at higher stresses. *Journal of Engineered Fibers and Fabrics*, 14, 155892501985622. https://doi.org/10.1177/1558925019856225

[56] Maślanka, P., Korycki, R., & Szafrańska, H. (2022). Estimation of seams in Paraglider Wing. Autex Research Journal, 22(4), 383–390. https://doi.org/10.2478/aut-2020-0054

[57] ISO 4916:1991. Textiles – Seam types – Classification and terminology

[58] Independece. (2014) *Owner's manual Cruiser paraglider*

[59] cousin-trestec.com/en/categorie-produit/sport-en/cords-en-sport-en/

ANNEX 1 [58]

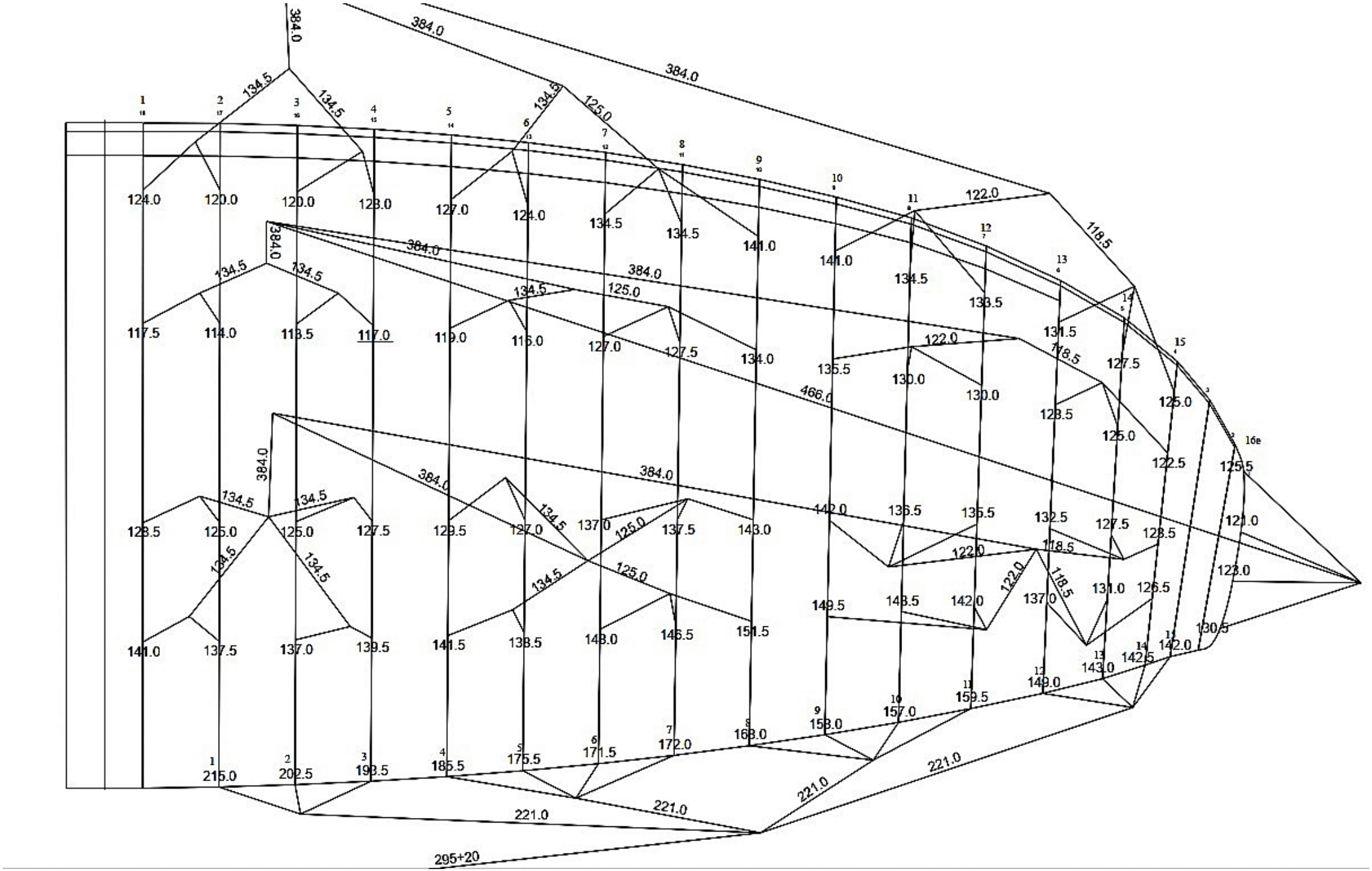
384.0
134.5
125.0
124.0
120.0
123.0
127.0
134.5
141.0
122.0
118.5
117.5
114.0
113.5
117.0
119.0
116.0
127.0
127.5
134.0
135.5
130.0
133.5
131.5
466.0
128.5
125.0
122.5
125.5
123.0
121.0
137.0
143.0
142.0
136.5
132.5
118.5
131.0
126.5
149.5
143.5
142.0
137.5
139.5
141.5
138.5
148.0
146.5
151.5
143.0
142.5
130.5
215.0
202.5
193.5
185.5
175.5
171.5
172.0
168.0
159.5
157.0
153.0
221.0
295+20

Type core	Braided	Twisted	Braided	Braided	Braided	Braided	Braided
Ø mm	0,95	1,1	1,3	1,4	1,5	1,9	2,1
Weight g/m	0,78	1	1,21	1,6	1,78	2,41	3,3
Effective breaking strength daN	**86**	**128**	**146**	**165**	**216**	**328**	**413**
Elongation at 5 daN (%)	0,1	0,1	0,05	0,05	0,05	0	0,05
Elongation at 10 daN (%)	0,2	0,2	0,2	0,15	0,1	0,05	0,1
Elongation at 15 daN (%)	0,4	0,4	0,3	0,3	0,2	0,1	0,15
Elongation at 20 daN (%)	0,6	0,5	0,5	0,35	0,3	0,15	0,15
Elongation at 25 daN (%)	0,7	0,7	0,6	0,55	0,4	0,2	0,3
Elongation at 50 daN (%)	1,7	1,2	1,2	0,95	0,6	0,4	0,35
Elongation at 75 daN (%)	2,55	2	1,8	1,35	1	0,55	0,5
Elongation at 100 daN (%)		2,6	2,4	1,75	1,3	0,8	0,7
Elongation at 125 daN (%)			3	2,4	1,6	0,95	0,85
Elongation at 150 daN (%)				2,9	2,1	1,2	1
Elongation at 175 daN (%)					2,45	1,5	1,2
Elongation at 200 daN (%)					2,8	1,75	1,45
Elongation at 225 daN (%)						2,2	1,55